Elucidating the Role of Protein Sulfenylation in Eukaryotic Signal Transduction

by

Candice Elaine Paulsen

A dissertation submitted in partial fulfillment
of the requirements for the degree of
Doctor of Philosophy
(Chemical Biology)
in The University of Michigan
2011

Doctoral Committee:

Associate Professor Kate S. Carroll, co-Chair
Professor Anna K. Mapp, co-Chair
Professor Stephen W. Ragsdale
Professor Janet L. Smith
Associate Professor Jason E. Gestwicki

Candice Elaine Paulsen

2011

For my family: Mom, Dad, Craig, and Katie, who are my voices of reason and pillars of strength. You all have been supportive of my being so far away for many years and have never lost faith in my dream, or me.

Acknowledgements

First, I would like to thank my mentor, Dr. Kate Carroll, for allowing me to join her lab, for providing me with unwavering support and guidance over my graduate career, and for having far more confidence in me than I have in myself. She has shared with me a wealth of knowledge and has provided me with endless opportunities for scientific development over the years, and while I am not enough of a wordsmith to adequately articulate my appreciation, know that I will be eternally grateful for all that Kate has done. Graduate school has certainly been more of an adventure than I ever dreamed it would be, and I can honestly not imagine having traversed the occasionally rocky terrain working with anyone else. I would also like to thank Kate for moving us to Florida as living near the beach has had the most amazing calming effect on me and, therefore, has significantly improved my personal happiness.

I would next like to thank all of the members of the Carroll lab for the countless helpful discussions over the years. I have been so fortunate to work alongside an amazing group of graduate students and post-docs who have all been so supportive of my research and me. Collectively, they have also taught me that family is not just something you are born into, but is also those amazing people you meet over the course of your life who change you for the better. To my fellow senior graduate students, Dr. Stephen Leonard (Sleonarz), who I had the pleasure of sitting next to every day after joining the Carroll lab until we relocated to Florida, Dr. Devayani Bhave (Tenacious D), and Jiyoung Hong (JAnnieH), I additionally thank you so very much for the amazing camaraderie and the many laughs and good times. I will treasure them and you all

always. I am grateful to Thu Truong (ThuPac), who started as my rotation student, for working with me on multiple projects, which has continuously renewed my excitement in my work, for being a wonderful and supportive friend, and for sharing (and, in many cases, fueling) my love of trashy TV and Chuckie D's. To Francisco Garcia (B-Cakes), I am additionally thankful for the extensive musical education, for tolerating the sometimes endless Twilight, Jersey Shore, Girls Next Door, and Jazzercise talk, and for being a fellow night owl. I would like to thank the post-docs Dr. Young Ho Seo, Dr. Vinayak Gupta, Dr. Hanumantharao Paritala, and Dr. Mauro LoConte for their support and the many helpful discussions and laughs. I also owe Vinayak many thanks for the numerous late night conversations about science, books and the like. Additionally, I would like to thank Dr. Khalilah Reddie (Special K) for the extensive questioning that always kept me on my toes, the lengthy scientific discussions over many a Potbelly's or Michigan League sandwich, for introducing me to fantastic literature including A Confederacy of Dunces and Elegance of the Hedgehog, and for having, along with Kate, taught me how to be the tough person that I am today.

Outside of lab, I would like to thank Dr. Jason Gestwicki, Dr. Stephen Ragsdale, and Dr. Janet Smith for serving as my thesis committee the past three years. They have all been very supportive of my work and of me, and have provided invaluable feedback and insight that has helped me design my future directions. Working with them has truly been a pleasure. I would also like to thank my college friend, Kelly O'Neal, who also went to graduate school for her camaraderie during this adventure.

I would next like to acknowledge and thank those who influenced my course of study and inspired me to apply to graduate school. The person to whom I can credit for having initially put the quest for a Ph.D. into my head, and who may not even know it, is my

Uncle Ansel. He was a professor of geophysics at Portland State University my whole life and, though I never saw his lab and my understanding of his work was as deep as knowing that he would be on the news anytime Portland experienced earthquake aftershocks or a mudslide, I could tell that he loved his job. To this day, whenever we go to his house, he is always working on something that challenges his mind such a puzzle and I've always thought to myself, "I want to do what he does". I would next like to thank my Uncle Arvid, who was a professor of geology at Purdue University, for having discouraged me from studying paleontology, the field that I was determined to dedicate my working life to because I've loved dinosaurs since I was a kid. His words of wisdom ultimately resulted in my reconsideration of a major. My Uncle Arvid also deserves many thanks for having encouraged me to get involved in undergraduate research. I thank my Uncle Roy, a retired OB/GYN, for dissuading each of his nieces and nephews from going to medical school and therefore having pushed the other "obvious" career path for a biology major out of my head long ago. Lastly, I want to thank my undergraduate research advisor Dr. Sergey Savinov and my graduate student mentor Dr. Olvia Colón for helping me fall in love with doing science.

Moving across the country at the beginning of my final year of graduate school was both incredibly exciting and daunting, and I am thankful to Karbstein lab members Melody Campbell, Bethany Strunk, and Crystal Young as well as fellow external graduate student Heather Rust for having become an amazing support group and a terrific bunch of friends. Additionally, I am grateful to Dr. Anna Mapp and Laura Howe for their support of my decision to move with the lab and their assistance with making the necessary arrangements for my defense from afar.

My graduate career has been full of countless late (occasionally never-ending) and lonely nights in lab, which would have been unbearable and impossible if not for Chevy Chase classics including Caddyshack and National Lampoon's Christmas Vacation, Eminem's "Lose Yourself", and All American Rejects' "Move Along". Additionally, I am thankful to J.K. Rowling for giving the world the wonderful Harry Potter series that has inspired and entertained me from high school through the end of graduate school, and I am grateful to Stephenie Meyer for having written the amazing Twilight Saga that succeeded, where all other attempts had failed, at returning me to my "chipper chicken" self and for instilling me with renewed hope.

Finally, I would like to thank my wonderful family for their endless support and encouragement over my undergraduate and graduate careers. My mom, who saw two of her own brothers go through graduate school, and my dad have been the most amazing support system I could ever have asked for. Any time the road got rough, I could always count on them for words of wisdom to help give me the strength to hold my head high and keep trucking through. I also want to thank my parents for the multiple care packages of jawbreakers I received while writing this thesis after I figured out that they helped keep me calm. I want to thank my big brother, Craig, for the many good times that we've had together when I've gone home in the winter, for inadvertently providing the Carroll lab with our how-to guide Sh*t My Dad Says, and to acknowledge him for continuing to be the most brilliant person I've ever known. Lastly, I owe oodles of thanks to my bestie and the sister I never had, Katie, for being the best and most loyal friend I could ever have dreamed of having and my #1 cheerleader. Katie has never wavered in her support and encouragement of me or of my dream, even when I first told her about it at the ripe young age of 18, and I look forward to returning the favor when she embarks on veterinary school.

Preface

This thesis is the compilation of published and unpublished work on the elucidation of the role of protein sulfenylation in eukaryotic redox signaling. Cysteine sulfenic acid forms upon reaction of a protein thiolate with hydrogen peroxide, which functions as an essential second messenger in a number of signaling pathways. Protein sulfenylation is a reversible modification that has emerged as a biologically important mechanism for dynamic modification and regulation of protein activity.

In Chapter 1, we discuss biological sources of reactive oxygen species, including hydrogen peroxide and current methods to detect their production. Additionally, we discuss protein sulfenylation within the broader context of cysteine oxidation, methods to detect each of these disparate modifications, and highlight recent examples from the literature to illustrate the diverse mechanisms by which hydrogen peroxide can regulate protein function. This work has been published as a review for which the citation is Paulsen C.E. and Carroll K.S., "Orchestrating redox signaling networks through regulatory cysteine switches," (2010) *ACS Chem Biol* 5: 47-62.

Chapter 2 focuses on the first direct demonstration of an essential role for sulfenic acid modification of the thiol peroxidase Gpx3 to communicate conditions of oxidative stress to the transcription factor Yap1 in *Saccharomyces cerevisiae*. The citation for this chapter is Paulsen C.E. and Carroll K.S., "Chemical dissection of an essential redox switch in yeast," (2009) *Chem Biol* 16: 217-225.

Chapter 3 outlines the characterization of methods to profile ROS production and to monitor the redox status of the cellular glutathione pool, as well as the development of a method to profile global protein sulfenylation in *Saccharomyces cerevisiae*. These methods were intended to be applied to study the effect of mutant huntingtin expression and aggregation on changes in the cellular redox status and in global protein oxidation, which would have provided insight into the role reactive oxygen species production plays in disease progression.

In Chapter 4, we present the development and application of an alkyne-based probe for sulfenic acids, DYn-2. DYn-2 was used to reveal dynamic changes in global protein sulfenylation in response to epidermal growth factor stimulation of the human epidermoid carcinoma A431 cell line. This study identified three protein tyrosine phosphatases and the epidermal growth factor receptor as direct protein targets of hydrogen peroxide produced for epidermal growth factor signaling. Additionally, oxidation of the epidermal growth factor receptor was shown to enhance inherent kinase activity. These data have been submitted for publication in *Nature Chemical Biology* as Paulsen C.E., Truong T.H., Garcia F.J., Homann, A., Gupta V., Leonard S.E., and Carroll K.S., "Protein sulfenylation goes global: probing intracellular targets of hydrogen peroxide produced for growth factor signaling."

Finally, Chapter 5 is a discussion of future directions for developing redox-based irreversible inhibitors for the epidermal growth factor receptor and for the continued study of redox regulation of protein tyrosine kinases that contain cysteine residues with structural homology to the epidermal growth factor receptor.

Table of Contents

List of Figures

List of Tables

List of Appendices

List of Abbreviations

ADP	Adenosine diphosphate
Ala	Alanine
AngII	Angiotensin II
Apaf-1	Apoptotic protease-activating factor 1
ASK1	Apoptotic signal-regulating kinase
ATP	Adenosine triphosphate
bFGF	Basic fibroblast growth factor
BSA	Bovine serum albumin
bZIP	Basic leucine zipper motif
CAN	Ceric (IV) ammonium nitrate
CBP	CREB binding protein
c-CRD	C-terminal cysteine rich domain
Cys	Cysteine
DAPI	4',6-diamidino-2-phenylindole
DAz-1	*N*-(3-azidopropyl)-3,5-dioxocyclohexandecarboxamide
DAz-2	4-(3-azidopropyl)cyclohexane-1,3-dione
DCF	Dichlorofluorescein
DCFH	2',7'-Dihydrodichlorofluorescein
DCM	Dichloromethane
DHE	Dihydroethidium
DHR	Dihydrorhodamine
Dimedone	5,5-dimethyl-1,3-cyclohexadione

DMEM	Dulbecco's modified Eagle medium
DMF	Dimethylformamide
DMSO	Dimethylsulfoxide
DPI	Diphenyleneiodonium
DTT	Dithiothreitol
EGF	Epidermal growth factor
EGFR	Epidermal growth factor receptor
ER	Endoplasmic reticulum
ERK	Extracellular signal-regulated kinases
ESI-MS	Electrospray ionization-mass spectrometry
ETC	Electron transport chain
EtOAc	Ethyl acetate
FBS	Fetal bovine serum
FAD	Flavin adenine dinucleotide
FGF	Fibroblast growth factor
GAPDH	Glyceraldehyde-3-phosphate dehydrogenase
GFP	Green fluorescent protein
GM-CSF	Granulocyte-macrophage colony-stimulating factor
GSH	Reduced glutathione
GSH/GSR	Glutathione/Glutathione reductase system
GSSG	Oxidized glutathione
H_2DCF-DA	2',7'-Dihydrodichlorofluorescein diacetate
H_2O_2	Hydrogen peroxide
HD	Huntington's disease
HDAC	Histone deacetylase
HMPA	Hexamethyl phosphoramide

Ht	Huntingtin protein
IAM	Iodoacetamide
ICAT	Isotope-coded affinity tag
ICDID	Isotope-coded dimedone and 2-iododimedone
IL	Interleukin
Imp	Importin α
IP	Immunoprecipitation
JNK	c-Jun N-terminal kinase
LC-MS/MS	Liquid chromatography-tandem mass spectrometry
LDA	Lithium diisopropylamide
L-NAME	γ-nitro-L-arginine-methyl ester
LPA	Lysophosphatidic acid
LPS	Lipopolysaccharide
MnSOD	Manganese superoxide dismutase
MS	Mass spectrometry
MT	Mitochondria
NAC	N-acetyl cysteine
NADPH	Nicotinamide adenine dinucleotide phosphate
n-CRD	N-terminal cysteine-rich domain
NEM	N-ethylmaleimide
NES	Nuclear export signal
NLS	Nuclear localization signal
NMR	Nuclear magnetic resonance spectroscopy
NO	Nitric oxide
$O_2\bullet^-$	Superoxide

•OH	Hydroxyl radical
pBiotin	Phosphine biotin
PBS	Phosphate buffered saline
PDGF	Platelet-derived growth factor
PEG	Polyethylene glycol
PI3K	Phosphoinositide 3-kinase
PIP3	Phosphatidylinositol-3,4,5-triphosphate
polyQ	Polyglutamine expansion
Prdx	Peroxiredoxin
Prx	Peroxiredoxin
PTEN	Phosphatase and tensin homolog
PTK	Protein tyrosine kinase
PTM	Post-translational modification
PTP	Protein tyrosine phosphatase
PTP1B	Protein tyrosine phosphatase 1B
RFK	Riboflavin kinase
ROS	Reactive oxygen species
RS^-	Thiolate anion
RSH	Reduced thiol
RSSR	Disulfide
RTK	Receptor tyrosine kinase
SDS-PAGE	Sodium dodecyl sulfate polyacrylamide gel electrophoresis
Ser	Serine
SH2	Src homology 2 domain
SHP2	SH2-containing protein tyrosine phosphatase 2
S-NO	S-nitrosothiol

SOD	Superoxide dismutase
SOH	Sulfenic acid
SO_2H	Sulfinic acid
SO_3H	Sulfonic acid
Strep-HRP	Streptavidin-conjugated horseradish peroxidase
TBP-2	Thioredoxin binding protein-2
TBST	Tris buffered saline with Tween-20
TBTA	Tris[(1-benzyl-1H-1,2,3-triazol-4-yl)methyl] amine
TCEP	Tris[2-carboxyethyl] phosphine
TGF-β1	Transforming growth factor-β1
THF	Tetrahydrofuran
TLC	Thin layer chromatography
TNFα	Tumor necrosis factor α
Trx/TrxR	Thioredoxin/thioredoxin reductase system
VEGF	Vascular endothelial growth factor
WB	Western blot
WT	Wild type

ABSTRACT

Elucidating the Role of Protein Sulfenylation in Eukaryotic Signal Transduction

By

Candice Elaine Paulsen

Co-Chair: Kate S. Carroll and Anna K. Mapp

H_2O_2 acts as a second messenger that can modulate intracellular signal transduction *via* chemoselective oxidation of cysteine residues in signaling proteins, however, the protein targets of H_2O_2 as well as how oxidation influences protein activity has remained largely unknown. In the present study, we present the first direct demonstration of an essential role for sulfenic acid modification of the thiol peroxidase Gpx3 to communicate conditions of oxidative stress to the transcription factor Yap1 in *Saccharomyces cerevisiae*. We then describe the characterization of methods to profile ROS production and to monitor the redox status of the cellular glutathione pool, as well as the development of a method to profile global protein sulfenylation in *Saccharomyces cerevisiae*. Next we present the development and application of an alkyne-based probe for sulfenic acids, DYn-2. This new probe was used to reveal dynamic changes in global protein sulfenylation in response to epidermal growth factor stimulation of the human epidermoid carcinoma A431 cell line. This study identified three protein tyrosine phosphatases and the epidermal growth factor receptor as direct protein targets of hydrogen peroxide produced for epidermal growth factor signaling. Additionally,

oxidation of the epidermal growth factor receptor was shown to enhance inherent kinase activity. Collectively, these results provide novel insight into how hydrogen peroxide can function as a second messenger to regulate eukaryotic signaling pathways and have broad implications for therapeutic development.

Chapter 1

Orchestrating redox signaling networks through regulatory cysteine switches

1.1 Abstract

Hydrogen peroxide (H_2O_2) acts as a second messenger that can mediate intracellular signal transduction via chemoselective oxidation of cysteine residues in signaling proteins. This Review presents current mechanistic insights into signal-mediated H_2O_2 production and highlights recent advances in methods to detect reactive oxygen species (ROS) and cysteine oxidation both *in vitro* and in cells. Selected examples from the recent literature are used to illustrate the diverse mechanisms by which H_2O_2 can regulate protein function. The continued development of methods to detect and quantify discrete cysteine oxoforms should further our mechanistic understanding of redox regulation of protein function and may lead to the development of new therapeutic strategies.

1.2 Introduction

Reactive oxygen species (ROS) including hydrogen peroxide (H_2O_2), superoxide ($O_2^{\cdot -}$), and the hydroxyl radical (·OH) are generally deemed toxic consequences of aerobic life that are swiftly eradicated to maintain cellular homeostasis. If left unchecked, ROS can indiscriminately damage biomolecules and contribute to aging and pathologies such as

cancer, diabetes, and neurodegenerative disorders[1-3]. However, studies performed over the past decade also indicate that a diverse array of external signals (**Table 1.1**)

Table 1.1 External Stimulants that Induce ROS Production.

Stimulant	Organism[a]	ROS Source[b]	Effect of Stimulant	Reference
Peptide Growth Factors				
Epidermal growth factor (EGF)	Hs,M,R	NOX[c]	Proliferation	4-7
Platelet-derived growth factor (PDGF)	Hs,M,R	NOX	Proliferation/Migration	7-10
Basic fibroblast growth factor (bFGF)	B	NOX	Proliferation	11
Vascular endothelial growth factor (VEGF)	P	L	Angiogenesis/Proliferation	12
Granulocyte-macrophage colony-stimulating factor (GM-CSF)	H	ND	Proliferation/Migration	13
Insulin	M,R	NOX	Glucose uptake/transport	14,15
Cytokines				
Lipopolysaccharide (LPS)	M	NOX	Induction of immune response	16-18
Interleukin-1β (IL-1β)	Hs,M	NOX,L	Induction of immune response	7,19
Interleukin-3 (IL-3)	Hs	ND	Induction of immune response	13
Interleukin-4 (IL-4)	Hs	NOX	Induction of immune response	20
CD28 stimulation	Hs	L	Induction of immune response/Proliferation	21
Tumor necrosis factor α (TNFα)	B,M,Hs	NOX	Apoptosis	7,11,22,23
Transforming growth factor-β1 (TGF-β1)	M	ND	Cell cycle arrest	24
Agonists of GPCRs[d]				
Angiotensin II (AngII)	R	NOX	Hypertrophy	25-28
Lysophosphatidic acid (LPA)	Hs	NOX,L	Proliferation	29,30
Thrombin	Hs	NOX	Proliferation	8
Serotonin	Ha	NOX	Proliferation	31
Other Stimulants				
Wounding	Z	NOX	Leukocyte recruitment	32
Oxidative stress	D	MT	Differentiation	33
Reoxygenation after hypoxia	R	MT	$O_2^{\cdot-}$ burst	34

[a] B, bovine; D, *Drosophila melanogaster*; Ha, hamster; Hs, human; M, mouse; P, pig; R, rat; Z, zebrafish.
[b] NOX, NADPH Oxidase; M, mitochondria; L, lipoxygenase; ND, not determined.
[c] For many of these cases, the specific NOX isoform activated is unknown. Each NOX isoform demonstrates disparate tissue expression and continued studies will be required to elucidate the regulation of each NOX isoform in response to diverse external signals.
[d] Guanosine triphosphate (GTP)-binding protein (G protein)-coupled receptors (GPCRs).

stimulate the controlled production of ROS in healthy cells and have uncovered a role for oxidants as essential second messengers in intracellular signaling pathways. An important cellular target or "sensor" of ROS is the thiol (RSH) functional group of the amino acid cysteine, which can exist in a number of oxidation states such as disulfides (RSSR) or sulfenic (SOH), sulfinic (SO_2H) and sulfonic (SO_3H) acids[35]. Such oxidative cysteine modifications can constitute a facile switch for modulating protein function, akin to phosphorylation. In this Review, we present current mechanistic insights into signal-mediated H_2O_2 production and highlight recent advances in methods to detect ROS and cysteine oxidation both *in vitro* and in cells. Selected examples from the recent literature of proteins that form disulfides, SOH, and SO_2H are discussed, underscoring the variety of mechanisms by which ROS can modulate protein function and signal transduction cascades.

1.3 H_2O_2 as a signaling molecule

$O_2{\cdot}^-$ spontaneously dismutates to H_2O_2, a process that is enhanced at least 1,000-fold by a class of enzymes known as superoxide dismutases (SOD) [36]. In the presence of metal ions (iron or copper), H_2O_2 can be decomposed through the Fenton reaction to form ·OH. Among these, H_2O_2 is the most abundant ROS (*in vivo* concentration of 10^{-7} M) with the longest half life ($t_{1/2} = 10^{-5}$ sec) [37,38]. The relative stability and uncharged nature of H_2O_2 permits its diffusion across long distances and membranes, though recent evidence indicates that $O_2{\cdot}^-$ may also cross membranes through anion channels [36]. Owing to its highly diffusible nature, H_2O_2 has been shown to act as a paracrine signal both in plant cell differentiation [39] and more recently in the recruitment of immune cells to wound sites in zebrafish larvae [32]. As will be discussed below, H_2O_2 can be quickly generated in cells, selectively perceived by downstream proteins, and undergo

degradation by cellular antioxidant defense systems. Collectively, these properties make H_2O_2 an ideal mediator of signal transduction processes.

1.4 Signal-mediated ROS production

The mitochondrial electron transport chain (ETC) funnels electrons from reduced matrix substrates through four protein complexes (I-IV) to molecular oxygen producing water and establishing a proton gradient across the inner mitochondrial membrane. The energy from this gradient is then harnessed to drive the production of the primary cellular energy source, adenosine triphosphate (ATP). The final complex in this pathway, complex IV delivers electrons to molecular oxygen to generate water; however, electrons can leak prematurely from the ETC upstream of complex IV to cause the univalent reduction of oxygen to $O_2{\cdot}^-$ [37]. The accidental production of $O_2{\cdot}^-$ by the ETC is thought to be the primary intracellular source of this oxidant, though cellular signals can also stimulate $O_2{\cdot}^-$ generation in the mitochondria. This process is strictly dependent upon the redox enzyme $p66^{Shc}$, which has been shown to be a genetic determinant of lifespan in mammals [40]. In response to signals that include growth factor deprivation, oxidative stress, or UV irradiation, $p66^{Shc}$ translocates to the mitochondria where it generates ROS (either H_2O_2 or $O_2{\cdot}^-$) by delivering electrons from the ETC to molecular oxygen (**Figure 1.1a**) [41,42].

$p66^{Shc}$-derived ROS can diffuse into the cytoplasm where it down-regulates the activity of FoxO3, a transcription factor implicated in the expression of mitochondrial antioxidant enzymes including manganese SOD (MnSOD) and catalase [43,44]. The resulting decrease in the mitochondrial antioxidant capacity renders the organelle more susceptible to oxidative stress. This may enhance the pro-apoptotic effect of $p66^{Shc}$ through increased permeability of the mitochondrial inner membrane, ultimately resulting

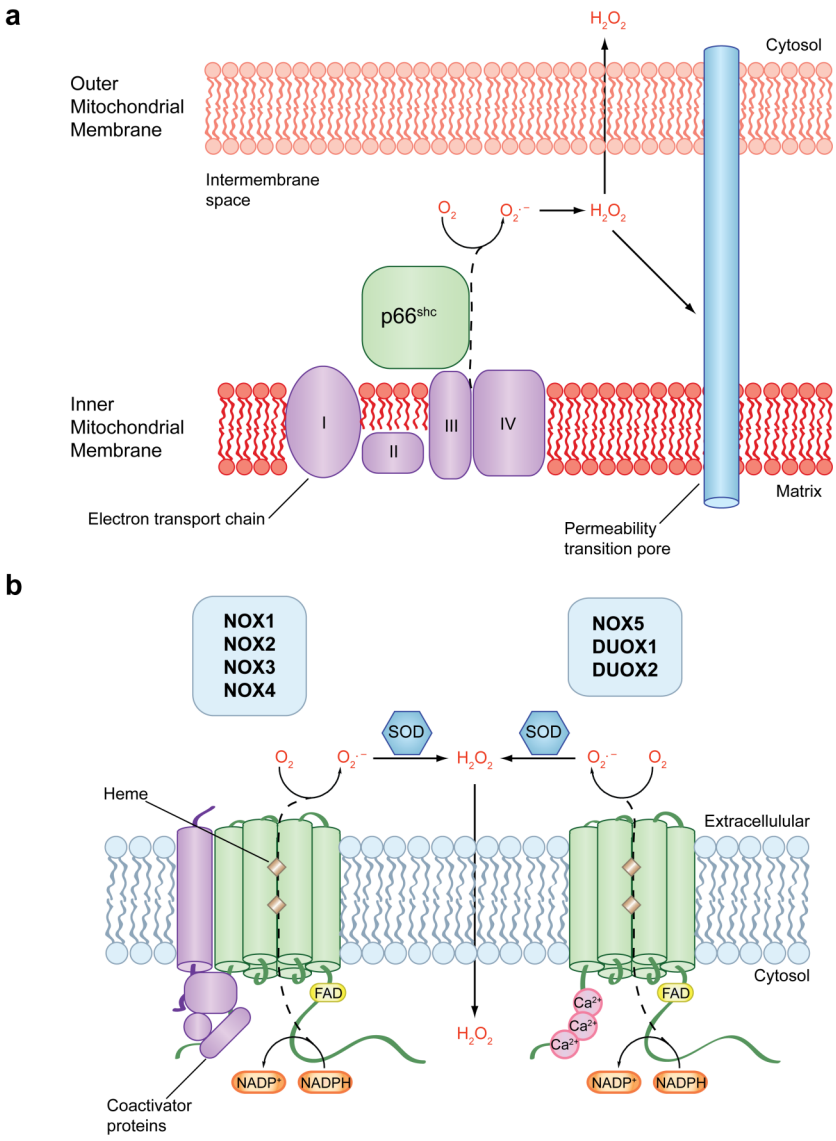

Figure 1.1. Signaling-derived sources of intracellular ROS. (a) $p66^{Shc}$ generates pro-apoptotic ROS in the mitochondria. In response to oxidative stress, UV irradiation, or growth factor deprivation, $p66^{Shc}$ localizes to the mitochondria where it generates ROS ($O_2^{\cdot -}$ or H_2O_2). H_2O_2 ultimately produced can diffuse across the outer mitochondrial membrane to the cytosol where it can modulate the activity of diverse proteins. $P66^{Shc}$-derived H_2O_2 also stimulates the opening of the permeability transition pore causing mitochondrial swelling and apoptosis. (b) NOX enzymes assemble at discrete locations in the cell such as the plasma membrane and at focal adhesions to generate ROS in response to diverse extracellular signals. The catalytic subunit of each NOX isoform (NOX1-5, DUOX1-2) has a conserved domain structure of six transmembrane a-helices and binding sites for two heme prosthetic groups. The C-terminal intracellular domain binds the FAD and NADPH cofactors and electrons from NADPH are translocated across the membrane through the heme prosthetic groups to generate $O_2^{\cdot -}$ (NOX1-5) or H_2O_2 (DUOX1-2). Full enzymatic activity of these enzymes requires the association of co-activator proteins (NOX1-4) or Ca^{2+} (NOX5, DUOX1-2) to the N-terminal intracellular domain. The $O_2^{\cdot -}$ produced is dismutated by SOD to H_2O_2, which can freely diffuse across the membrane to the cytosol to regulate protein activity and signaling cascades.

in apoptosis [45]. Mice lacking $p66^{Shc}$ accumulate significantly less ROS over time, exhibit extended life spans and reduced incidence of aging-associated degenerative diseases without an increase in tumor frequency [40,41,46-48]. Therefore, $p66^{Shc}$ has recently been deemed a potential therapeutic target for treating diseases such as neurodegenerative disorders that are associated with ROS accumulation and induction of apoptosis [37,49,50].

A variety of extracellular signals have also been shown to stimulate ROS production by activating NADPH oxidase (NOX) enzymes, which translocate an electron from reduced nicotinamide adenine dinucleotide phosphate (NAPDH) across the cell membrane to generate H_2O_2 (**Table 1.1**) [25,32,37,51,52]. ROS production by these enzymes requires a catalytic subunit, of which there are seven known isoforms (Nox1-5, Duox1 and Duox2) that show disparate cell- and tissue-specific expression patterns. Full activity of these multi-component enzymes also requires the binding of flavin adenine dinucleotide (FAD) and the association of either a distinct set of cytoplasmic coactivator proteins or calcium to the intracellular domain (**Figure 1.1b**) [53]. Recent work indicates that receptor-mediated NOX activation occurs through the recruitment of these additional proteins [20,22,54] and cofactors [20], though the precise mechanistic details appear to be pathway- and isoform-specific. For example, NOX1 and NOX2 activation by tumor necrosis factor (TNF) requires riboflavin kinase (RFK). This association may promote enzyme activation by increasing local levels of the FAD prosthetic group [23]. Future studies on the mechanism of NOX activation are likely to reveal additional biochemical features that could conceivably lead to the identification of potential therapeutic targets. Lastly, is important to note that intracellular and extracellular signals can also initiate ROS production through $p66^{Shc}$- and NOX-independent mechanisms (**Table 1.1**) [55-57].

Regardless of the specific cellular source, the H_2O_2 signal diffuses rapidly into the cytoplasm where it can induce distinct physiological responses including proliferation,

differentiation and apoptosis/necrosis [33,37,58,59]. However, the high diffusability of H_2O_2 also raises the specter of aberrant signaling. To circumvent this problem, NOX complexes appear to be targeted to distinct regions of the plasma membrane via lipid rafts [53] and assemble at focal adhesions [60] to direct H_2O_2 production to specific cellular microdomains. The precise mechanisms that prevent H_2O_2 diffusion from such microenvironments are unknown [61,62]. One possibility is that antioxidant enzymes including glutathione peroxidases, catalase, and peroxiredoxins co-localize with NOX complexes to limit extraneous ROS dissemination [53].

1.5 Cellular ROS detection

The subcellular location and relative ROS concentration produced in response to external signals can have a dramatic impact on the cellular outcome (*e.g.* proliferation or apoptosis). Chemical probes for oxidant detection have emerged as essential tools to probe signal-mediated ROS production in cells [63]. Compounds such as dihydrodichlorofluorescin (DCFH), dihydrorhodamine-123 (DHR), and more recently, dihydrocyanines [16] are routinely used to visualize intracellular ROS. Often times, however, these reagents exhibit high background fluorescence resulting from auto- and photo-oxidation. An innovative, new generation of reagents employs a caged boronate switch and provides chemoselective detection of cellular H_2O_2 [6]. Ratiometric sensors [64], nanoparticles [17], and protein-based [34] systems have also been developed for ROS detection. Continued improvement in the reaction kinetics and dynamic range of these reagents should facilitate detection of intracellular ROS at subcellular resolution [65].

1.6 Sensing H_2O_2 through cysteine oxidation

The reaction of H_2O_2 with biomolecules provides a mechanism for how cells can “sense” changes in redox balance. In proteins, the thiol side chain of the amino acid cysteine is

particularly sensitive to oxidation [66]. Some cysteines are more susceptible to oxidation than others and this provides a basis for specificity in ROS-mediated signaling. Thiolate anions (RS^-) are intrinsically better nucleophiles and show enhanced reactivity with H_2O_2, compared to the thiol form [67]. Thus, the pKa value of the thiol group can modulate cysteine reactivity. In proteins, a typical cysteine residue has a pKa of ~8.5. However, the presence of polar or positively charged amino acids can stabilize the thiolate form through electrostatic interactions and decrease the pKa to as low as 3.5 [66,68].

Other determinants of cysteine reactivity toward H_2O_2 include access of the oxidant to its target and the presence of specific binding sites. For example, peroxiredoxins have low pKa catalytic cysteines (4.5-5.9) [69-71] that react with H_2O_2 with second-order rate constants of 10^5-10^8 M^{-1} sec^{-1} [72,73]. The catalytic cysteine of protein tyrosine phosphatases (PTPs) is also characterized by a low pKa value (4.6-5.5) [74,75]. However, H_2O_2 reacts with PTPs at second-order rate constants between 10-160 M^{-1} sec^{-1} [67,76,77]. This difference in reactivity is likely due to the unique architecture of the peroxiredoxin active site and facilitates rapid reaction with low, endogenous levels of H_2O_2 [78]. Importantly, the decreased reactivity of non-peroxiredoxin thiolates with H_2O_2 provides a potential mechanism to modulate protein activity only after robust changes in oxidant concentration (*e.g.,* in response to external signals).

The initial reaction of a cysteine thiolate with H_2O_2 yields a sulfenic acid (SOH), which is implicated in a number of important biochemical transformations. Once formed, a SOH lies at a crossroad and can lead to formation of additional posttranslational modifications (PTMs) (**Figure 1.2**). The stability of a SOH is influenced, in part, by the presence of nearby cysteine residues and by the accessibility of the modification site to the low molecular weight thiol, glutathione (GSH) [35]. The reaction of SOH with either a

neighboring cysteine or GSH will generate a disulfide bond that, in the case of GSH, is known as *S*-glutathiolation [79]. Both disulfide products can be reduced back to the thiol by the action of either the GSH/glutathione reductase (GSH/GSR) or the thioredoxin/thioredoxin reductase (Trx/TrxR) systems [80]. Cysteine thiolates can also react with reactive nitrogen species (RNS) including nitric oxide (NO) to generate S-nitrosothiols (S-NO) that can hydrolyze to form SOH or react with a second cysteine to form a disulfide [81,82].

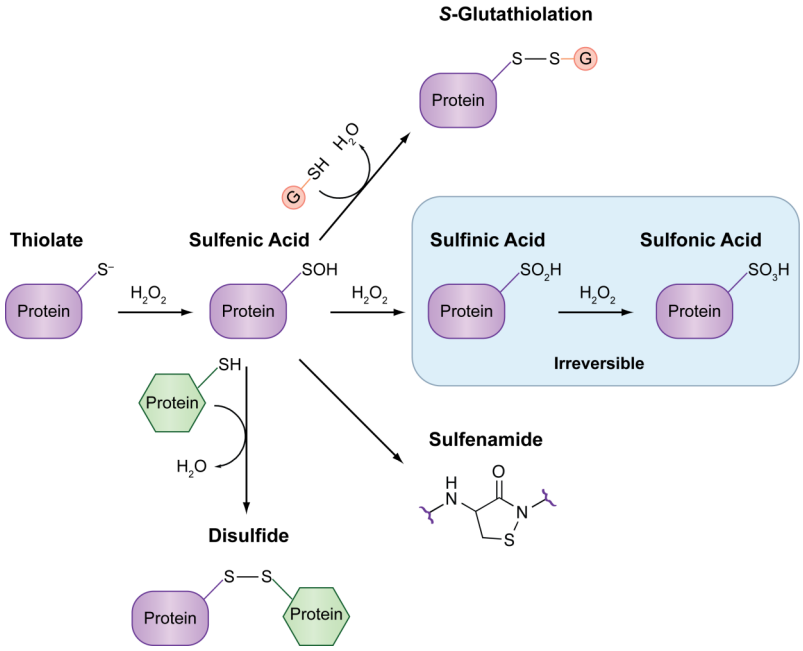

Figure 1.2. Oxidative modifications of protein cysteine residues. Low pKa cysteines are present in the cell as thiolates and form a SOH upon reaction with H_2O_2. Once formed, the SOH can react with a second cysteine either in the same or a second protein yields a disulfide. Alternatively, a SOH can react with the LMW thiol GSH (pink circle) to form a special disulfide known as *S*-glutathiolation. In the event that a neighboring cysteine or glutathione are absent, the amide nitrogen of the neighboring residue can attack the SOH to form a sulfenamide. Each of these oxoforms can be reduced by the GSH/GSR or Trx/TrxR systems to regenerate the thiols (not depicted). The SOH can also further react with H_2O_2 to generate the irreversible SO_2H and SO_3H oxoforms.

SOH can undergo further reaction with H_2O_2 to generate the SO_2H and SO_3H oxoforms (**Figure 1.2**), though the rate of these reactions is slower than observed for a thiolate [70]. With the exception of one protein family, both the SO_2H and SO_3H modifications are considered irreversible and the latter is deemed a hallmark of diseases such as cancer, diabetes, and neurodegenerative disorders that are associated with oxidative stress [1-3]. To prevent over-oxidation of critical cysteine residues, SOH may be converted to a disulfide or be *S*-glutathiolated. Sulfenamide [83-86]

and hypervalent sulfur [87] species also form through SOH intermediates and may also safeguard against over-oxidation (**Figure 1.2**).

The switch-like nature of the disulfide and SOH highlights their ability to function as a reversible means to regulate protein function, analogous to phosphorylation. The SO_2H oxoform has also emerged as an important PTM. For these reasons, efforts have been aimed at identifying proteins with redox-active cysteine residues and to elucidate the biological roles of these cysteine oxoforms. To highlight the progress in this area over the past few years, the remainder of this Review will focus on recent examples from the literature that demonstrate the diverse ways in which these PTMs regulate vital cellular processes.

1.7 Disulfide bonds

Disulfide bond formation in proteins is a widely recognized cysteine modification and, under normal conditions, occurs predominately in the endoplasmic reticulum (ER). This organelle provides an oxidizing environment to facilitate disulfide bond formation in nascent proteins destined for export to the extracellular milieu [88]. By contrast, the cytoplasm, nucleus, and mitochondrial matrix are reducing environments. In these compartments, cysteines are maintained in their thiol form by the combined activity of the GSH/GSR and Trx/TrxR systems [80,88], though protein disulfides can be generated by the action of the Erv family of sulfhydryl oxidases [89]. In response to external signals and under stress conditions the cytoplasm becomes more oxidizing, which allows protein disulfides to accumulate until redox balance is restored.

Disulfide bond formation can influence the catalytic activity, protein-protein interactions, and subcellular localization. Underscoring the importance of this oxoform, a number of

methods have been developed to identify proteins that undergo this modification [90,91]. These approaches are typically based on loss of reactivity with thiol-modifying reagents or restoration of labeling by reducing agents such as dithiothreitol (DTT) with subsequent analysis by mass spectrometry (MS). To enable quantitative analysis of redox-sensitive cysteines, Cohen and colleagues have employed isotope-coded affinity tag (ICAT) methodology [92]. This differential isotopic labeling method uses a subtractive approach to monitor fluctuations in levels of reduced protein thiols under different conditions (*e.g.* +/- oxidant). Jakob and coworkers have expanded the application of ICAT to develop a ratiometric labeling approach, termed OxICAT [93]. This approach permits direct identification and quantitative evaluation of proteins that form disulfides under different cellular conditions.

Global studies to identify proteins that undergo disulfide bond formation implicate this modification in the regulation of numerous biological processes including redox homeostasis, chaperone activity, metabolism, transcriptional regulation, and protein translation (**Table 1.2**) [93,94]. Once formed, a disulfide can have divergent effects on protein function, which are central to the ability of H_2O_2 to orchestrate cellular signaling events, which can lead to diverse biological outcomes (**Table 1.2**). For example, starvation-induced autophagy is associated with a temporary increase in ROS production that inactivates a key cysteine protease, Atg4 by forming a disulfide bond involving the catalytic cysteine [95]. In contrast, survival of bacteria such as *Escherichia coli* under conditions of both oxidative and heat stresses requires activation of the molecular chaperone Hsp33 via intramolecular disulfide bond formation [96].

H_2O_2 can also regulate the activity of protein tyrosine phosphatases (PTPs) by inducing intramolecular disulfide bond formation, which inactivates the phosphatases to permit

prolonged flux through the corresponding signaling pathways (**Table 1.2**). Protein kinases are also believed to undergo redox control; however, the evidence for this is less direct since increased activity may also be attributed to inhibition of the opposing phosphatase. Recently, the serine/threonine kinase, PKGIα was shown to undergo intermolecular disulfide formation between monomers and this modification appears to enhance its affinity for target proteins [97].

Table 1.2. Examples of Redox-Regulated Proteins and Complexes.

Protein	Oxoform[a,b]	Effect of Oxidation on Protein	Reference
Phosphatases			
LMW-PTPs	A,B	Inactivates	98
PTEN	A,B	Inactivates	99,100
Cdc25	A,B	Inactivates	77,101
PTP1B	A,B,C	Inactivates	84,85
PTP2a	A,B,C	Inactivates	86
SHP-1/SHP-2	A,B	Inactivates	102
Kinases			
Sty1/Tpx1	A	Activates	103
PKA RI	A	Activates	104
Src tyrosine kinase	A	Activates/Inactivates	105,106
PKG-1a	A	Enhances affinity for substrates	97
ASK1	A	Initiates oligomerization/Activates	107
Transcription factors			
AP-1 (Fos/Jun)	A	Inhibits DNA binding	108
Hsf1	A	Activates	109,110
Nrf-2/Keap-1	A	Enhances Nrf-2 stability	111
FoxO4/p300/CBP	A	Acetylates/Inactivates	112
OxyR	A,B	Activates	113,114
Yap1/Gpx3	A,B	Activates	115-117
OhrR	A,B	Inhibits DNA binding	83,118
SarZ	A,B	Inhibits DNA binding	119
Other			
Hsp33	A	Activates	96
HDAC4/DnaJb5	A	Inactivates/Inhibits complex formation	120
GDE2	A	Inactivates	121
DJ-1	D	Locates to mitochondria/Active as a cytoprotectant	122,123
MMP-7	D	Activates	124

[a] The significance of oxidation for many of these proteins in live cells remains to be determined.
[b] A, inter/intramolecular disulfide; B, sulfenic acid; C, sulfenamide; D, sulfinic acid.

The terminal targets of signal transduction cascades are transcription factors that regulate gene expression. Some transcription factors, such as AP-1 [108] and OxyR [113,114] appear to be regulated by direct oxidative modification (**Table 1.2**). The activity of transcription factors can also be regulated by changes in the accessibility of their target genes, for example, by PTM of histones. The class II histone deacetylases (HDACs) function as transcriptional corepressors of various developmental and differentiation processes. The activity of one isoform, HDAC4 is regulated by its interaction with the small molecular chaperone DnaJb5 [120]. This chaperone forms a multiprotein complex with thioredoxin (Trx1) and importin α (Imp), a component of the nuclear import machinery, through the adapter protein Trx binding protein-2 (TBP-2) (**Figure 1.3**) [125]. In a recent study, Sadoshima and colleagues demonstrated that cysteine residues in DnaJb5 can form a disulfide preventing its interaction with HDAC4. Dissociation from the DnaJb5 multiprotein complex coupled with disulfide bond formation in HDAC4 exposed the nuclear export signal (NES) resulting in cytoplasmic localization of HDAC4 and derepression of its target genes [120]. Sadoshima and coworkers proposed a model whereby Trx1 reduces intramolecular disulfides in DnaJb5 and HDAC to restore complex formation and nuclear accumulation (**Figure 1.3**). This

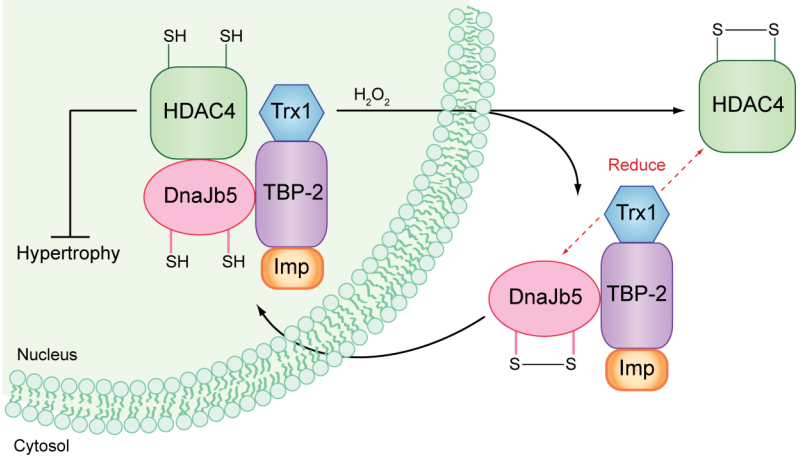

Figure 1.3. Model for redox-regulation of cardiac hypertrophy by HDAC4. The type-II histone deacetylase, HDAC4 normally modifies histones to repress the expression of genes involved in hypertrophy. Nuclear localization of HDAC4 is mediated by its association with importin α (Imp) through a multiprotein complex consisting of the molecular chaperone DnaJb5, TBP-2, and Trx1. In the presence of H_2O_2, intramolecular disulfide bonds form within HDCA4 and DnaJb5, which stimulates dissociation and nuclear export of the complex. Upon removal of H_2O_2, Trx1 reduces the disulfides in both HDAC4 and DnaJb5 to restore formation and nuclear localization of the complex.

model presents a mechanism for how signal-mediated H_2O_2 production may promote developmental defects such as cardiac hypertrophy and highlights this pathway as a potential target for therapeutic intervention.

Disulfide bond formation can also lead to additional PTM of oxidized proteins and represents another important mechanism to modulate activity. An example of such a regulatory mechanism was recently demonstrated for the FoxO4 transcription factor, which is inactivated by forming an intermolecular disulfide with either the p300 or CREB-binding protein (CBP) acetyltransferases [112]. Caspase-9, the initial caspase in the mitochondrial apoptotic cascade also appears to be regulated in this manner since formation of an intermolecular disulfide with apoptotic protease-activating factor 1 (Apaf-1) stimulates auto-cleavage of caspase-9 and initiation of the apoptotic cascade [126].

1.8 Sulfenic acids

Sulfenic acids are relatively unstable and reactive groups, which have traditionally been viewed as intermediates *en route* to other oxidation states (**Figure 1.2**). In recent years, however, stable SOH have been identified in a growing list of proteins and received intense interest for their roles in cell signaling (**Table 1.2**) [35,61,127]. Indeed, the appropriate protein microenvironment can lead to stable SOH formation. For example, SOH modification of human serum albumin can persist for hours [128] and has been observed in more than 40 crystal structures [68,119].

The PTP family of phosphatases is another commonly cited example of SOH-mediated regulation of activity [129-131]. In these enzymes, the low pKa catalytic cysteine can oxidize to SOH with concomitant inactivation. Crystal structures of PTP1B and PTPa demonstrate that the SOH modification can react with the backbone amide nitrogen of a

neighboring amino acid to form a cyclic sulfenamide [84-86]. However, the rate of sulfenamide formation is slow relative to reaction of the SOH intermediate with thiols such as GSH or cysteine [83]. Alternatively, the SOH intermediate in PTPs can condense with a proximal "backdoor" cysteine to generate an intramolecular disulfide, as has been observed for low molecular weight (LMW) [98], Cdc25 [77,101], and PTEN phosphatases [100]. Two members of the tandem Src homology 2 (SH2) domain-containing PTPs (SHPs) also undergo oxidative modification in activated T cells [132]. Interestingly, SHPs possess two "backdoor" cysteines that comprise a unique regulatory mechanism [102]. Sequential reaction of these proximal cysteines with the SOH intermediate and subsequent disulfide exchange generates a disulfide between the "backdoor" cysteines that inactivates the enzyme.

Peroxidases and peroxiredoxins also form SOH intermediates as part of their catalytic cycle [61]. The primary role of these enzymes is to metabolize peroxides and maintain the reducing environment of the cell. Recent studies, however, reveal additional regulatory functions for these antioxidant enzymes. For example, peroxiredoxin 1 (Prdx1) was shown to promote PTEN tumor suppressor activity by protecting against oxidative inactivation [99]. A molecular mechanism was not provided in this study, however, it is possible that Prdx1 either neutralizes local H_2O_2 to prevent PTEN oxidation or acts as a reductase to reduce the PTEN disulfide. The latter activity is analogous to the newly elucidated role for Prdx1 in promoting neuronal cell differentiation [121].

Small molecule probes that recognize specific cysteine oxoforms over similar species represent promising new tools for elucidating signaling pathways and regulatory mechanisms that involve redox signaling and thiol oxidation. To this end, approaches have been developed that allow for the detection of sulfenic acid modifications on

proteins that exploit the unique chemical reactivity of this species [133-138]. Although SOH are often metastable species, the direct detection of SOH formation has several advantages including the identification of the reactive site where the oxidation chemistry was initiated [61].

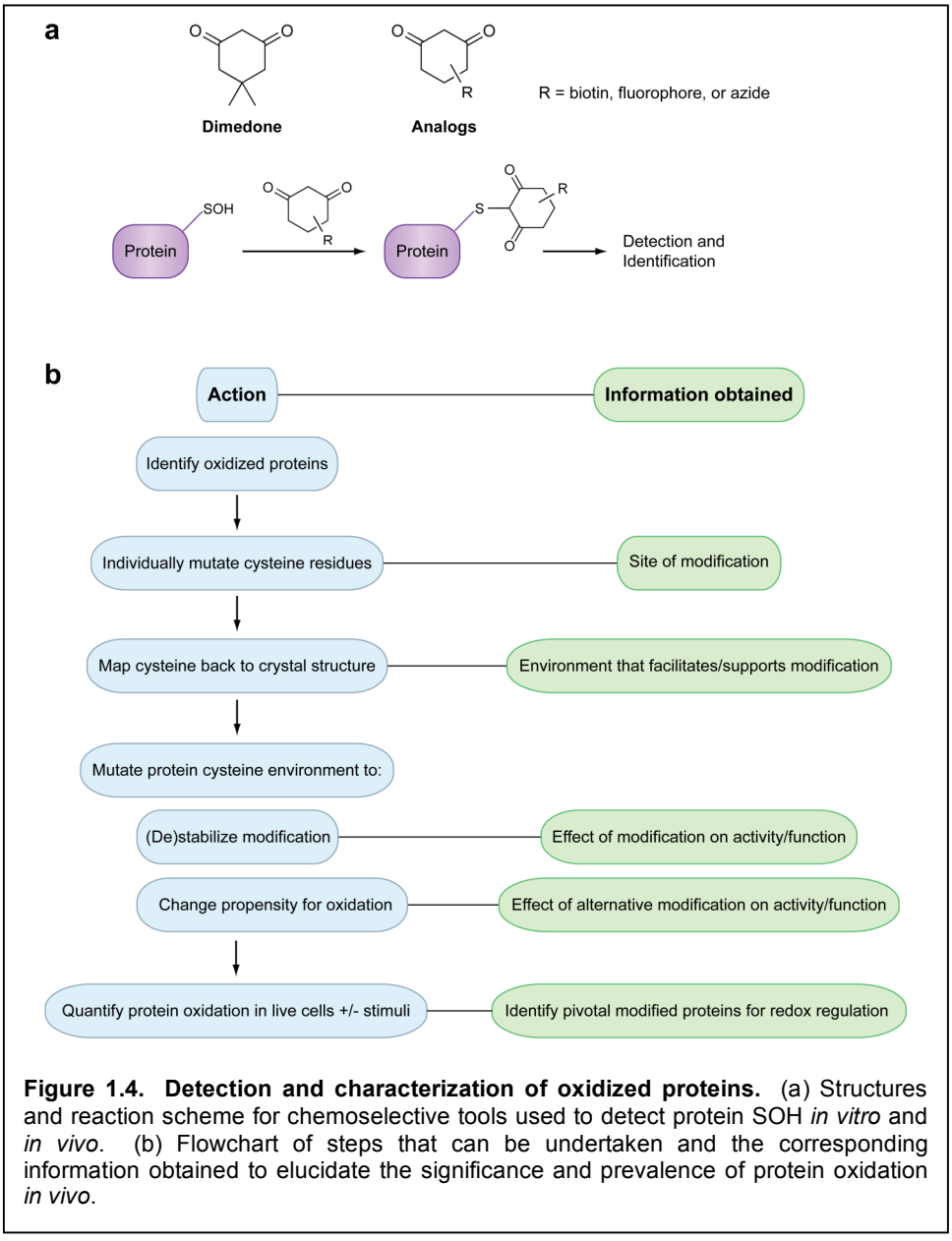

Figure 1.4. Detection and characterization of oxidized proteins. (a) Structures and reaction scheme for chemoselective tools used to detect protein SOH *in vitro* and *in vivo*. (b) Flowchart of steps that can be undertaken and the corresponding information obtained to elucidate the significance and prevalence of protein oxidation *in vivo*.

All recently developed reagents for sulfenic acid detection are based on 5,5-dimethyl-1,3-cyclohexanedione, also known as dimedone **(Figure 1.4a)**. The chemoselective

reaction between dimedone and a protein SOH was first reported by Benitez and Allison in 1974 [139,140]. Since then, this reaction has been exploited to detect SOH modifications by MS and through direct conjugation to fluorophores and biotin [133,135]. More recently, azide analogs of dimedone, known as DAz-1 [136,137] and DAz-2 [134], have been developed that can be used to label sulfenic acid-containing proteins in live cells, thereby minimizing the potential for oxidative artifacts during cell lysis. Proteins tagged by the azidodimedone analogs can be conjugated to biotin or fluorophores via chemical ligation techniques such as the Staudinger ligation or click chemistry (**Figure 1.4a**) [137,141]. Application of azidodimedone probes to discover protein targets of oxidation in human cell lines has shown that as many as 200 different cellular proteins undergo SOH modification [134]. The newly identified proteins have roles in signal transduction, DNA repair, metabolism, protein synthesis, redox homeostasis, nuclear transport, vesicle trafficking, and ER quality control. Azidodimedone probes have also been used to identify a functional role for SOH modifications in the yeast peroxide-sensing system comprising the peroxidase Gpx3 and the transcription factor Yap1 [117].

1.9 Sulfinic acids

The SO_2H modification has been best characterized in peroxiredoxins and forms through reaction of H_2O_2 with the SOH intermediate. Notably, only the eukaryotic homologues of the peroxiredoxins are susceptible to SO_2H formation [142,143]. For a subset of eukaryotic peroxiredoxins, the SO_2H modification can be reversed by an enzyme termed, sulfiredoxin [144]. Recent studies indicate that SO_2H repair proceeds through a sulfinic acid phosphoryl ester intermediate formed by the direct transfer of the γ-phosphate from ATP to peroxiredoxin [145-147]. The reversibility of SO_2H in peroxiredoxins suggests that this modification may also function as a controllable redox switch in proteins. Indeed, Poole and coworkers have proposed the floodgate model of signaling, which posits that SO_2H

modification of peroxiredoxin permits a temporary increase in cellular H_2O_2 [143]. In addition to peroxiredoxins, important biological functions for SO_2H modifications have been demonstrated in matrix metalloproteases [124] and the Parkinson's disease protein DJ-1 [122,123]. Although oxidation of cysteine to SO_2H is gaining acceptance as an important regulatory mechanism as well as a marker of protein damage, the full scope of these modifications remain unknown. The development of chemical tools for SO_2H detection may afford new opportunities to elucidate the role of this modification in human health and disease.

1.10 Regulation of protein signaling complexes

H_2O_2 can also influence protein activity through oxidative modification of regulatory protein complexes, as illustrated by the mammalian NRF2/KEAP1 system. NRF2 is a basic leucine zipper (bZIP) transcription factor that regulates the expression of enzymes involved in oxidant and xenobiotic detoxification [148]. This transcription factor has a nuclear localization sequence (NLS), however, it is held in the cytoplasm under non-stress conditions by KEAP1, which functions as a homodimer and interacts with the DLG and ETGE sites of NRF2 (**Figure 1.5a**) [149,150]. KEAP1 serves as an adaptor for an ubiquitin ligase complex and binding of KEAP1 to both the DLG and ETGE sites optimally orients NRF2 lysine residues for ubiquitination, which targets it for degradation [151]. Nuclear accumulation and activation of NRF2 in response to oxidative stress is associated with increased NRF2 stability and is dependent upon oxidative modification of three cysteine residues in KEAP1, which weakens its interaction with the DLG motif in NRF2 [149-152]. Until recently, it was not clear how KEAP1 oxidation enhances the stability of NRF2 since oxidized KEAP1 still interacts fully with the ETGE site and weakly with the DLG site. A new study demonstrated that $p21^{Cip1/WAF1}$, a protein involved in numerous cellular processes including cell-cycle arrest and apoptosis, could compete with KEAP1

for binding to the DLG site of NRF2. Displacement of KEAP1 by $p21^{CIP1/WAF1}$ inhibits KEAP1-mediated ubiquitination of NRF2 and provides a unique regulatory role for

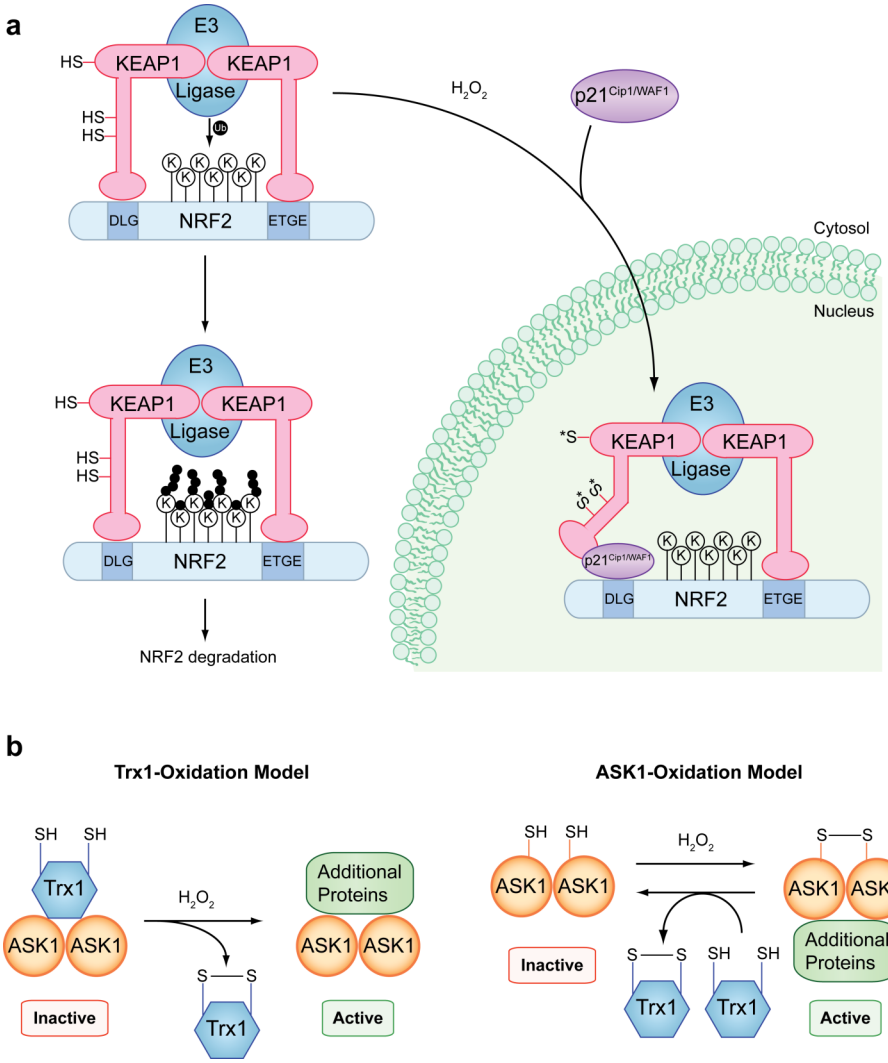

Figure 1.5. Redox-regulation of protein complexes influences gene transcription and signaling cascades. (a) Proposed mechanism for redox-regulation of NRF2 stability and activity by KEAP1 and $p21^{CIP1/WAF1}$. Binding of KEAP1 to the DLG and ETGE sites in NRF2 optimally orients lysine residues in NRF2 for ubiquitination (black circles) leading to degradation. In the presence of H_2O_2, three cysteine residues in KEAP1 are oxidatively modified (oxoform unknown, S*), which induces a conformational change in KEAP1 that decreases its affinity for the DLG site. Additionally, KEAP1 oxidation may mask its NES leading to nuclear accumulation of the complex and activation of NRF2. $p21^{CIP1/WAF1}$ can compete with oxidized KEAP1 for binding to the NRF2 DLG site to enhance the stability of the transcription factor. (b) Two proposed models for H_2O_2-mediated activation of ASK1. ASK1 assembles into multimers in the cell that interact with Trx1. Association of Trx1 with ASK1 sequesters the kinase in an inactive conformation. Upon oxidation of Trx1 by H_2O_2, ASK1 is released to interact with additional proteins forming the active signaling complex (Trx1-oxidation model). Alternatively, H_2O_2 induces intermolecular disulfide bond formation between ASK1 monomers to facilitate the interaction with additional proteins forming the activate kinase complex (ASK1-oxidation model). In this second model, Trx1 negatively regulates ASK1 by maintaining the kinase in a reduced and inactivate state.

$p21^{Cip1/WAF1}$ (**Figure 1.5a**) [111].

The apoptosis signal-regulating kinase (ASK1)/Trx1 system represents another H_2O_2-sensitive protein complex (**Figure 1.5b**). Two models have been proposed to explain H_2O_2-mediated activation of ASK1. One model posits that Trx1 sequesters ASK1 in an inactive complex and, upon treatment of cells with TNF or H_2O_2, undergoes intramolecular disulfide formation. In subsequent steps, ASK1 is released, which permits oligomerization to form the active kinase complex (**Figure 1.5b, left**) [153]. A recent study, however, demonstrated that stable ASK1 oligomerization and activation in response to H_2O_2 is mediated by disulfide bond formation between ASK1 monomers [107]. Hence, an alternative regulatory model was presented whereby Trx1 negatively regulates ASK1 signaling under resting conditions by maintaining it in a reduced state (**Figure 1.5b, right**). This alternative model is attractive since it is consistent with the known disulfide reductase activity of Trx1.

Prolonged activation of ASK1 by TNF signaling induces apoptosis, which is also associated with ROS production from the NOX1 complex [22]. ASK1 activates the Jun N-terminal kinase (JNK) and $p38^{MAPK}$-signaling pathways. The latter is required for induction of mitochondrial apoptosis during oxidative stress by enhancing the stability of p53 [154]. Interestingly, p53 regulates the expression of $p66^{Shc}$, which is required for stress-activated p53 to stimulate mitochondrial ROS production and apoptosis [49]. This apoptotic signaling pathway provides an attractive mechanistic link between NOX activation and the initiation of $p66^{Shc}$-dependent mitochondrial ROS production, though further studies will be required to evaluate this potential connection.

1.11 Cysteine oxidation in disease

To date, a number of proteins have been identified wherein chemoselective oxidation of cysteine residues serves as a mechanism to regulate normal cellular functions (**Table 1.2**). It is important to note, however, that excessive H_2O_2 production, either through aberrant receptor activation or mitochondrial dysfunction can lead to spurious modification and hyper-oxidation of cysteines. This would be expected, for example, in disease states that are associated with excessive ROS production such as cancer, diabetes, or neurodegenerative disorders [1-3]. Consistent with this proposal, a recent study found that SOH modification of proteins is enhanced in malignant breast cell lines using an antibody that recognizes the protein-dimedone adduct [138]. Although Trx/TrxR, GSH/GSR and the recently identified bacterial sulfenate reductase [155] can repair reversible forms of thiol oxidation, persistent oxidative stress can overpower these systems can lead to aberrant protein oxidation that may contribute to disease pathogenesis.

1.12 Future perspectives

The recent development of chemical tools to detect cellular ROS as well as mechanistic studies into NOX enzymes activation and $p66^{Shc}$ have greatly expanded our understanding of how ROS are produced in response to diverse external signals. Continued development of ROS-sensing reagents should facilitate the temporal and spatial resolution of signal-mediated ROS production. Once formed, ROS can modulate the activity of proteins and regulate signaling pathways involved in cell proliferation, cell differentiation, and apoptosis via chemoselective oxidation of cysteine residues. The recent development of methods to detect disulfides and SOH has expanded the inventory of protein cysteine residues known to undergo oxidation modifications, though probes for SO_2H are lacking. Such proteins targets of oxidation are implicated in a wide

array of cellular processes including signal transduction, DNA repair, metabolism, protein synthesis, redox homeostasis, nuclear transport, vesicle trafficking, and ER quality control. Though some reactive cysteines are susceptible to numerous modifications, the majority of thiols appear to undergo specific oxidative PTMs, which suggests that there are fundamental differences in the chemical and biological basis for target specificity [134].

Profiling oxidized proteins (*i.e.,* inventory mapping) serves as the first step to elucidating the biological roles of these cysteine PTMs (**Figure 1.4b**). Mapping sites of cysteine modification can be used to expand our understanding of features within a protein microenvironment that facilitate the oxidation process. The transition from inventory mapping to the mapping of functional cellular context will be greatly facilitated by genetic and biochemical experiments. For example, site-directed mutagenesis can be employed to remove the modified cysteine or alter the protein environment in order to influence the redox sensitivity, as in DJ-1 [122] and Gpx3 [116]. Another important step toward evaluating the physiological significance of oxidative cysteine modifications will be to quantify redox-dependent changes in the extent of protein oxidation. To this end, the OxICAT method [93] should facilitate such analysis for disulfide bond formation. Since increased H_2O_2 concentrations can lead to aberrant SOH formation [138], similar ratiometric methods should be developed for SOH to hone in on the modified proteins that are pivotal for regulation of cellular signaling.

Studies reported in the last three years have expanded our knowledge regarding mechanisms of signal-mediated ROS production and the means by which ROS regulate cellular signaling networks. The continued emergence of methods to detect and quantify

discrete cysteine oxoforms should further our mechanistic understanding of redox regulation of protein function and could lead to the development of new therapeutics.

Acknowledgements

We thank the CBI Training Program T32-GM-008597-13 to C.E.P. and the Life Sciences Institute and the American Heart Association Scientist Development Grant #0835419N to K.S.C. for support of this work.

Notes

This work has been published as “Orchestrating redox signaling networks through regulatory cysteine switches.” ACS Chemical Biology **2010** 5(1): 47-62. The manuscript was written by Candice E. Paulsen and Kate S. Carroll.

1.13 References

1 Andersen, J. K. Oxidative stress in neurodegeneration: cause or consequence? *Nat Med* **10 Suppl**, S18-25 (2004).

2 Klaunig, J. E. & Kamendulis, L. M. The role of oxidative stress in carcinogenesis. *Annu Rev Pharmacol Toxicol* **44**, 239-267 (2004).

3 Lowell, B. B. & Shulman, G. I. Mitochondrial dysfunction and type 2 diabetes. *Science* **307**, 384-387 (2005).

4 Bae, Y. S. *et al.* Epidermal growth factor (EGF)-induced generation of hydrogen peroxide. Role in EGF receptor-mediated tyrosine phosphorylation. *J Biol Chem* **272**, 217-221 (1997).

5 Goldman, R., Moshonov, S. & Zor, U. Generation of reactive oxygen species in a human keratinocyte cell line: role of calcium. *Arch Biochem Biophys* **350**, 10-18 (1998).

6 Miller, E. W., Tulyathan, O., Isacoff, E. Y. & Chang, C. J. Molecular imaging of hydrogen peroxide produced for cell signaling. *Nat Chem Biol* **3**, 263-267 (2007).

7 Sundaresan, M. *et al.* Regulation of reactive-oxygen-species generation in fibroblasts by Rac1. *Biochem J* **318 (Pt 2)**, 379-382 (1996).

8 Patterson, C. *et al.* Stimulation of a vascular smooth muscle cell NAD(P)H oxidase by thrombin. Evidence that p47(phox) may participate in forming this oxidase in vitro and in vivo. *J Biol Chem* **274**, 19814-19822 (1999).

9 Sundaresan, M., Yu, Z. X., Ferrans, V. J., Irani, K. & Finkel, T. Requirement for generation of H2O2 for platelet-derived growth factor signal transduction. *Science* **270**, 296-299 (1995).

10 Wang, Y. & Lou, M. F. The regulation of NADPH oxidase and its association with cell proliferation in human lens epithelial cells. *Invest Ophthalmol Vis Sci* **50**, 2291-2300 (2009).

11 Lo, Y. Y. & Cruz, T. F. Involvement of reactive oxygen species in cytokine and growth factor induction of c-fos expression in chondrocytes. *J Biol Chem* **270**, 11727-11730 (1995).

12 Colavitti, R. *et al.* Reactive oxygen species as downstream mediators of angiogenic signaling by vascular endothelial growth factor receptor-2/KDR. *J Biol Chem* **277**, 3101-3108 (2002).

13 Sattler, M. *et al.* Hematopoietic growth factors signal through the formation of reactive oxygen species. *Blood* **93**, 2928-2935 (1999).

14 Mahadev, K. *et al.* Hydrogen peroxide generated during cellular insulin stimulation is integral to activation of the distal insulin signaling cascade in 3T3-L1 adipocytes. *J Biol Chem* **276**, 48662-48669 (2001).

15 May, J. M. & de Haen, C. Insulin-stimulated intracellular hydrogen peroxide production in rat epididymal fat cells. *J Biol Chem* **254**, 2214-2220 (1979).

16 Kundu, K. *et al.* Hydrocyanines: a class of fluorescent sensors that can image reactive oxygen species in cell culture, tissue, and in vivo. *Angew Chem Int Ed Engl* **48**, 299-303 (2009).

17 Lee, D. *et al.* In vivo imaging of hydrogen peroxide with chemiluminescent nanoparticles. *Nat Mater* **6**, 765-769 (2007).

18 Matsuzawa, A. *et al.* ROS-dependent activation of the TRAF6-ASK1-p38 pathway is selectively required for TLR4-mediated innate immunity. *Nat Immunol* **6**, 587-592 (2005).

19 Bonizzi, G. *et al.* Reactive oxygen intermediate-dependent NF-kappaB activation by interleukin-1beta requires 5-lipoxygenase or NADPH oxidase activity. *Mol Cell Biol* **19**, 1950-1960 (1999).

20 Sharma, P. *et al.* Redox regulation of interleukin-4 signaling. *Immunity* **29**, 551-564 (2008).
21 Los, M. *et al.* IL-2 gene expression and NF-kappa B activation through CD28 requires reactive oxygen production by 5-lipoxygenase. *Embo J* **14**, 3731-3740 (1995).
22 Kim, Y. S., Morgan, M. J., Choksi, S. & Liu, Z. G. TNF-induced activation of the Nox1 NADPH oxidase and its role in the induction of necrotic cell death. *Mol Cell* **26**, 675-687 (2007).
23 Yazdanpanah, B. *et al.* Riboflavin kinase couples TNF receptor 1 to NADPH oxidase. *Nature* **460**, 1159-1163 (2009).
24 Ohba, M., Shibanuma, M., Kuroki, T. & Nose, K. Production of hydrogen peroxide by transforming growth factor-beta 1 and its involvement in induction of egr-1 in mouse osteoblastic cells. *J Cell Biol* **126**, 1079-1088 (1994).
25 Block, K. *et al.* Nox4 NAD(P)H oxidase mediates Src-dependent tyrosine phosphorylation of PDK-1 in response to angiotensin II: role in mesangial cell hypertrophy and fibronectin expression. *J Biol Chem* **283**, 24061-24076 (2008).
26 Lassegue, B. *et al.* Novel gp91(phox) homologues in vascular smooth muscle cells : nox1 mediates angiotensin II-induced superoxide formation and redox-sensitive signaling pathways. *Circ Res* **88**, 888-894 (2001).
27 Ushio-Fukai, M. *et al.* Reactive oxygen species mediate the activation of Akt/protein kinase B by angiotensin II in vascular smooth muscle cells. *J Biol Chem* **274**, 22699-22704 (1999).
28 Zafari, A. M. *et al.* Role of NADH/NADPH oxidase-derived H2O2 in angiotensin II-induced vascular hypertrophy. *Hypertension* **32**, 488-495 (1998).
29 Chen, Q., Olashaw, N. & Wu, J. Participation of reactive oxygen species in the lysophosphatidic acid-stimulated mitogen-activated protein kinase kinase activation pathway. *J Biol Chem* **270**, 28499-28502 (1995).
30 Sekharam, M., Cunnick, J. M. & Wu, J. Involvement of lipoxygenase in lysophosphatidic acid-stimulated hydrogen peroxide release in human HaCaT keratinocytes. *Biochem J* **346 Pt 3**, 751-758 (2000).
31 Mukhin, Y. V. *et al.* 5-Hydroxytryptamine1A receptor/Gibetagamma stimulates mitogen-activated protein kinase via NAD(P)H oxidase and reactive oxygen species upstream of src in chinese hamster ovary fibroblasts. *Biochem J* **347 Pt 1**, 61-67 (2000).
32 Niethammer, P., Grabher, C., Look, A. T. & Mitchison, T. J. A tissue-scale gradient of hydrogen peroxide mediates rapid wound detection in zebrafish. *Nature* **459**, 996-999 (2009).
33 Owusu-Ansah, E. & Banerjee, U. Reactive oxygen species prime Drosophila haematopoietic progenitors for differentiation. *Nature* **461**, 537-541 (2009).
34 Wang, W. *et al.* Superoxide flashes in single mitochondria. *Cell* **134**, 279-290 (2008).
35 Reddie, K. G. & Carroll, K. S. Expanding the functional diversity of proteins through cysteine oxidation. *Curr Opin Chem Biol* **12**, 746-754 (2008).
36 Mumbengegwi, D. R., Li, Q., Li, C., Bear, C. E. & Engelhardt, J. F. Evidence for a superoxide permeability pathway in endosomal membranes. *Mol Cell Biol* **28**, 3700-3712 (2008).
37 Giorgio, M., Trinei, M., Migliaccio, E. & Pelicci, P. G. Hydrogen peroxide: a metabolic by-product or a common mediator of ageing signals? *Nat Rev Mol Cell Biol* **8**, 722-728 (2007).
38 Halliwell, B. G., J.M.C. *Free Radicals in Biology and Medicine*. (Oxford University Press, 1999).

39 Bienert, G. P., Schjoerring, J. K. & Jahn, T. P. Membrane transport of hydrogen peroxide. *Biochim Biophys Acta* **1758**, 994-1003 (2006).

40 Migliaccio, E. *et al.* The p66shc adaptor protein controls oxidative stress response and life span in mammals. *Nature* **402**, 309-313 (1999).

41 Giorgio, M. *et al.* Electron transfer between cytochrome c and p66Shc generates reactive oxygen species that trigger mitochondrial apoptosis. *Cell* **122**, 221-233 (2005).

42 Orsini, F. *et al.* The life span determinant p66Shc localizes to mitochondria where it associates with mitochondrial heat shock protein 70 and regulates trans-membrane potential. *J Biol Chem* **279**, 25689-25695 (2004).

43 Guo, J., Gertsberg, Z., Ozgen, N. & Steinberg, S. F. p66Shc links alpha1-adrenergic receptors to a reactive oxygen species-dependent AKT-FOXO3A phosphorylation pathway in cardiomyocytes. *Circ Res* **104**, 660-669 (2009).

44 Nemoto, S. & Finkel, T. Redox regulation of forkhead proteins through a p66shc-dependent signaling pathway. *Science* **295**, 2450-2452 (2002).

45 Bernardi, P., Petronilli, V., Di Lisa, F. & Forte, M. A mitochondrial perspective on cell death. *Trends Biochem Sci* **26**, 112-117 (2001).

46 Francia, P. *et al.* Deletion of p66shc gene protects against age-related endothelial dysfunction. *Circulation* **110**, 2889-2895 (2004).

47 Menini, S. *et al.* Deletion of p66Shc longevity gene protects against experimental diabetic glomerulopathy by preventing diabetes-induced oxidative stress. *Diabetes* **55**, 1642-1650 (2006).

48 Rota, M. *et al.* Diabetes promotes cardiac stem cell aging and heart failure, which are prevented by deletion of the p66shc gene. *Circ Res* **99**, 42-52 (2006).

49 Pani, G., Koch, O. R. & Galeotti, T. The p53-p66shc-Manganese Superoxide Dismutase (MnSOD) network: a mitochondrial intrigue to generate reactive oxygen species. *Int J Biochem Cell Biol* **41**, 1002-1005 (2009).

50 Pinton, P. & Rizzuto, R. p66Shc, oxidative stress and aging: importing a lifespan determinant into mitochondria. *Cell Cycle* **7**, 304-308 (2008).

51 Ameziane-El-Hassani, R. *et al.* Dual oxidase-2 has an intrinsic Ca2+-dependent H2O2-generating activity. *J Biol Chem* **280**, 30046-30054 (2005).

52 Garrido, A. M. & Griendling, K. K. NADPH oxidases and angiotensin II receptor signaling. *Mol Cell Endocrinol* **302**, 148-158 (2009).

53 Chen, K., Craige, S. E. & Keaney, J. F., Jr. Downstream targets and intracellular compartmentalization in Nox signaling. *Antioxid Redox Signal* **11**, 2467-2480 (2009).

54 Choi, H. *et al.* Mechanism of angiotensin II-induced superoxide production in cells reconstituted with angiotensin type 1 receptor and the components of NADPH oxidase. *J Biol Chem* **283**, 255-267 (2008).

55 Ali, M. H., Mungai, P. T. & Schumacker, P. T. Stretch-induced phosphorylation of focal adhesion kinase in endothelial cells: role of mitochondrial oxidants. *Am J Physiol Lung Cell Mol Physiol* **291**, L38-45 (2006).

56 Fay, A. J., Qian, X., Jan, Y. N. & Jan, L. Y. SK channels mediate NADPH oxidase-independent reactive oxygen species production and apoptosis in granulocytes. *Proc Natl Acad Sci U S A* **103**, 17548-17553 (2006).

57 Handy, D. E. *et al.* Glutathione peroxidase-1 regulates mitochondrial function to modulate redox-dependent cellular responses. *J Biol Chem* **284**, 11913-11921 (2009).

58 Kwon, S. H., Pimentel, D. R., Remondino, A., Sawyer, D. B. & Colucci, W. S. H(2)O(2) regulates cardiac myocyte phenotype via concentration-dependent activation of distinct kinase pathways. *J Mol Cell Cardiol* **35**, 615-621 (2003).

59 Veal, E. A., Day, A. M. & Morgan, B. A. Hydrogen peroxide sensing and signaling. *Mol Cell* **26**, 1-14 (2007).
60 Wu, R. F. *et al.* Subcellular targeting of oxidants during endothelial cell migration. *J Cell Biol* **171**, 893-904 (2005).
61 Poole, L. B. & Nelson, K. J. Discovering mechanisms of signaling-mediated cysteine oxidation. *Curr Opin Chem Biol* **12**, 18-24 (2008).
62 Ushio-Fukai, M. Localizing NADPH oxidase-derived ROS. *Sci STKE* **2006**, re8 (2006).
63 Miller, E. W. & Chang, C. J. Fluorescent probes for nitric oxide and hydrogen peroxide in cell signaling. *Curr Opin Chem Biol* **11**, 620-625 (2007).
64 Srikun, D., Miller, E. W., Domaille, D. W. & Chang, C. J. An ICT-based approach to ratiometric fluorescence imaging of hydrogen peroxide produced in living cells. *J Am Chem Soc* **130**, 4596-4597 (2008).
65 Zhao, W. Lighting up H2O2: the molecule that is a "necessary evil" in the cell. *Angew Chem Int Ed Engl* **48**, 3022-3024 (2009).
66 Banerjee, R. (John Wiley & Sons, 2008).
67 Winterbourn, C. C. & Metodiewa, D. Reactivity of biologically important thiol compounds with superoxide and hydrogen peroxide. *Free Radic Biol Med* **27**, 322-328 (1999).
68 Salsbury, F. R., Jr., Knutson, S. T., Poole, L. B. & Fetrow, J. S. Functional site profiling and electrostatic analysis of cysteines modifiable to cysteine sulfenic acid. *Protein Sci* **17**, 299-312 (2008).
69 Bryk, R., Griffin, P. & Nathan, C. Peroxynitrite reductase activity of bacterial peroxiredoxins. *Nature* **407**, 211-215 (2000).
70 Hugo, M. *et al.* Thiol and sulfenic acid oxidation of AhpE, the one-cysteine peroxiredoxin from mycobacterium tuberculosis: kinetics, acidity constants, and conformational dynamics. *Biochemistry* **48**, 9416-9426 (2009).
71 Nelson, K. J., Parsonage, D., Hall, A., Karplus, P. A. & Poole, L. B. Cysteine pK(a) values for the bacterial peroxiredoxin AhpC. *Biochemistry* **47**, 12860-12868 (2008).
72 Parsonage, D., Karplus, P. A. & Poole, L. B. Substrate specificity and redox potential of AhpC, a bacterial peroxiredoxin. *Proc Natl Acad Sci U S A* **105**, 8209-8214 (2008).
73 Peskin, A. V. *et al.* The high reactivity of peroxiredoxin 2 with H(2)O(2) is not reflected in its reaction with other oxidants and thiol reagents. *J Biol Chem* **282**, 11885-11892 (2007).
74 Lohse, D. L., Denu, J. M., Santoro, N. & Dixon, J. E. Roles of aspartic acid-181 and serine-222 in intermediate formation and hydrolysis of the mammalian protein-tyrosine-phosphatase PTP1. *Biochemistry* **36**, 4568-4575 (1997).
75 Zhang, Z. Y. & Dixon, J. E. Active site labeling of the Yersinia protein tyrosine phosphatase: the determination of the pKa of the active site cysteine and the function of the conserved histidine 402. *Biochemistry* **32**, 9340-9345 (1993).
76 Denu, J. M. & Tanner, K. G. Specific and reversible inactivation of protein tyrosine phosphatases by hydrogen peroxide: evidence for a sulfenic acid intermediate and implications for redox regulation. *Biochemistry* **37**, 5633-5642 (1998).
77 Sohn, J. & Rudolph, J. Catalytic and chemical competence of regulation of cdc25 phosphatase by oxidation/reduction. *Biochemistry* **42**, 10060-10070 (2003).
78 Stone, J. R. & Yang, S. Hydrogen peroxide: a signaling messenger. *Antioxid Redox Signal* **8**, 243-270 (2006).

79 Mieyal, J. J., Gallogly, M. M., Qanungo, S., Sabens, E. A. & Shelton, M. D. Molecular mechanisms and clinical implications of reversible protein S-glutathionylation. *Antioxid Redox Signal* **10**, 1941-1988 (2008).
80 Berndt, C., Lillig, C. H. & Holmgren, A. Thiol-based mechanisms of the thioredoxin and glutaredoxin systems: implications for diseases in the cardiovascular system. *Am J Physiol Heart Circ Physiol* **292**, H1227-1236 (2007).
81 Forrester, M. T., Foster, M. W., Benhar, M. & Stamler, J. S. Detection of protein S-nitrosylation with the biotin-switch technique. *Free Radic Biol Med* **46**, 119-126 (2009).
82 Hess, D. T., Matsumoto, A., Kim, S. O., Marshall, H. E. & Stamler, J. S. Protein S-nitrosylation: purview and parameters. *Nat Rev Mol Cell Biol* **6**, 150-166 (2005).
83 Lee, J. W., Soonsanga, S. & Helmann, J. D. A complex thiolate switch regulates the Bacillus subtilis organic peroxide sensor OhrR. *Proc Natl Acad Sci U S A* **104**, 8743-8748 (2007).
84 Salmeen, A. *et al.* Redox regulation of protein tyrosine phosphatase 1B involves a sulphenyl-amide intermediate. *Nature* **423**, 769-773 (2003).
85 van Montfort, R. L., Congreve, M., Tisi, D., Carr, R. & Jhoti, H. Oxidation state of the active-site cysteine in protein tyrosine phosphatase 1B. *Nature* **423**, 773-777 (2003).
86 Yang, J. *et al.* Reversible oxidation of the membrane distal domain of receptor PTPalpha is mediated by a cyclic sulfenamide. *Biochemistry* **46**, 709-719 (2007).
87 Nakamura, T. *et al.* Oxidation of archaeal peroxiredoxin involves a hypervalent sulfur intermediate. *Proc Natl Acad Sci U S A* **105**, 6238-6242 (2008).
88 Go, Y. M. & Jones, D. P. Redox compartmentalization in eukaryotic cells. *Biochim Biophys Acta* **1780**, 1273-1290 (2008).
89 Fass, D. The Erv family of sulfhydryl oxidases. *Biochim Biophys Acta* **1783**, 557-566 (2008).
90 Hansen, R. E., Roth, D. & Winther, J. R. Quantifying the global cellular thiol-disulfide status. *Proc Natl Acad Sci U S A* **106**, 422-427 (2009).
91 Leichert, L. I. & Jakob, U. Global methods to monitor the thiol-disulfide state of proteins in vivo. *Antioxid Redox Signal* **8**, 763-772 (2006).
92 Sethuraman, M., McComb, M. E., Heibeck, T., Costello, C. E. & Cohen, R. A. Isotope-coded affinity tag approach to identify and quantify oxidant-sensitive protein thiols. *Mol Cell Proteomics* **3**, 273-278 (2004).
93 Leichert, L. I. *et al.* Quantifying changes in the thiol redox proteome upon oxidative stress in vivo. *Proc Natl Acad Sci U S A* **105**, 8197-8202 (2008).
94 Le Moan, N., Clement, G., Le Maout, S., Tacnet, F. & Toledano, M. B. The Saccharomyces cerevisiae proteome of oxidized protein thiols: contrasted functions for the thioredoxin and glutathione pathways. *J Biol Chem* **281**, 10420-10430 (2006).
95 Scherz-Shouval, R. *et al.* Reactive oxygen species are essential for autophagy and specifically regulate the activity of Atg4. *Embo J* **26**, 1749-1760 (2007).
96 Ilbert, M. *et al.* The redox-switch domain of Hsp33 functions as dual stress sensor. *Nat Struct Mol Biol* **14**, 556-563 (2007).
97 Burgoyne, J. R. *et al.* Cysteine redox sensor in PKGIa enables oxidant-induced activation. *Science* **317**, 1393-1397 (2007).
98 Chiarugi, P. The redox regulation of LMW-PTP during cell proliferation or growth inhibition. *IUBMB Life* **52**, 55-59 (2001).
99 Cao, J. *et al.* Prdx1 inhibits tumorigenesis via regulating PTEN/AKT activity. *Embo J* **28**, 1505-1517 (2009).

100 Kwon, J. *et al.* Reversible oxidation and inactivation of the tumor suppressor PTEN in cells stimulated with peptide growth factors. *Proc Natl Acad Sci U S A* **101**, 16419-16424 (2004).
101 Savitsky, P. A. & Finkel, T. Redox regulation of Cdc25C. *J Biol Chem* **277**, 20535-20540 (2002).
102 Chen, C. Y., Willard, D. & Rudolph, J. Redox regulation of SH2-domain-containing protein tyrosine phosphatases by two backdoor cysteines. *Biochemistry* **48**, 1399-1409 (2009).
103 Veal, E. A. *et al.* A 2-Cys peroxiredoxin regulates peroxide-induced oxidation and activation of a stress-activated MAP kinase. *Mol Cell* **15**, 129-139 (2004).
104 Brennan, J. P. *et al.* Oxidant-induced activation of type I protein kinase A is mediated by RI subunit interprotein disulfide bond formation. *J Biol Chem* **281**, 21827-21836 (2006).
105 Giannoni, E., Buricchi, F., Raugei, G., Ramponi, G. & Chiarugi, P. Intracellular reactive oxygen species activate Src tyrosine kinase during cell adhesion and anchorage-dependent cell growth. *Mol Cell Biol* **25**, 6391-6403 (2005).
106 Kemble, D. J. & Sun, G. Direct and specific inactivation of protein tyrosine kinases in the Src and FGFR families by reversible cysteine oxidation. *Proc Natl Acad Sci U S A* **106**, 5070-5075 (2009).
107 Nadeau, P. J., Charette, S. J., Toledano, M. B. & Landry, J. Disulfide Bond-mediated multimerization of Ask1 and its reduction by thioredoxin-1 regulate H(2)O(2)-induced c-Jun NH(2)-terminal kinase activation and apoptosis. *Mol Biol Cell* **18**, 3903-3913 (2007).
108 Abate, C., Patel, L., Rauscher, F. J., 3rd & Curran, T. Redox regulation of fos and jun DNA-binding activity in vitro. *Science* **249**, 1157-1161 (1990).
109 Ahn, S. G. & Thiele, D. J. Redox regulation of mammalian heat shock factor 1 is essential for Hsp gene activation and protection from stress. *Genes Dev* **17**, 516-528 (2003).
110 Manalo, D. J., Lin, Z. & Liu, A. Y. Redox-dependent regulation of the conformation and function of human heat shock factor 1. *Biochemistry* **41**, 2580-2588 (2002).
111 Chen, W. *et al.* Direct interaction between Nrf2 and p21(Cip1/WAF1) upregulates the Nrf2-mediated antioxidant response. *Mol Cell* **34**, 663-673 (2009).
112 Dansen, T. B. *et al.* Redox-sensitive cysteines bridge p300/CBP-mediated acetylation and FoxO4 activity. *Nat Chem Biol* **5**, 664-672 (2009).
113 Saurin, A. T., Neubert, H., Brennan, J. P. & Eaton, P. Widespread sulfenic acid formation in tissues in response to hydrogen peroxide. *Proc Natl Acad Sci U S A* **101**, 17982-17987 (2004).
114 Storz, G., Tartaglia, L. A. & Ames, B. N. Transcriptional regulator of oxidative stress-inducible genes: direct activation by oxidation. *Science* **248**, 189-194 (1990).
115 Delaunay, A., Pflieger, D., Barrault, M. B., Vinh, J. & Toledano, M. B. A thiol peroxidase is an H2O2 receptor and redox-transducer in gene activation. *Cell* **111**, 471-481 (2002).
116 Ma, L. H., Takanishi, C. L. & Wood, M. J. Molecular mechanism of oxidative stress perception by the Orp1 protein. *J Biol Chem* **282**, 31429-31436 (2007).
117 Paulsen, C. E. & Carroll, K. S. Chemical dissection of an essential redox switch in yeast. *Chem Biol* **16**, 217-225 (2009).
118 Fuangthong, M. & Helmann, J. D. The OhrR repressor senses organic hydroperoxides by reversible formation of a cysteine-sulfenic acid derivative. *Proc Natl Acad Sci U S A* **99**, 6690-6695 (2002).

119 Poor, C. B., Chen, P. R., Duguid, E., Rice, P. A. & He, C. Crystal structures of the reduced, sulfenic acid, and mixed disulfide forms of SarZ, a redox active global regulator in Staphylococcus aureus. *J Biol Chem* **284**, 23517-23524 (2009).
120 Ago, T. *et al.* A redox-dependent pathway for regulating class II HDACs and cardiac hypertrophy. *Cell* **133**, 978-993 (2008).
121 Yan, Y., Sabharwal, P., Rao, M. & Sockanathan, S. The antioxidant enzyme Prdx1 controls neuronal differentiation by thiol-redox-dependent activation of GDE2. *Cell* **138**, 1209-1221 (2009).
122 Blackinton, J. *et al.* Formation of a stabilized cysteine sulfinic acid is critical for the mitochondrial function of the parkinsonism protein DJ-1. *J Biol Chem* **284**, 6476-6485 (2009).
123 Canet-Aviles, R. M. *et al.* The Parkinson's disease protein DJ-1 is neuroprotective due to cysteine-sulfinic acid-driven mitochondrial localization. *Proc Natl Acad Sci U S A* **101**, 9103-9108 (2004).
124 Fu, X., Kassim, S. Y., Parks, W. C. & Heinecke, J. W. Hypochlorous acid oxygenates the cysteine switch domain of pro-matrilysin (MMP-7). A mechanism for matrix metalloproteinase activation and atherosclerotic plaque rupture by myeloperoxidase. *J Biol Chem* **276**, 41279-41287 (2001).
125 Nishinaka, Y. *et al.* Importin alpha1 (Rch1) mediates nuclear translocation of thioredoxin-binding protein-2/vitamin D(3)-up-regulated protein 1. *J Biol Chem* **279**, 37559-37565 (2004).
126 Zuo, Y. *et al.* Oxidative modification of caspase-9 facilitates its activation via disulfide-mediated interaction with Apaf-1. *Cell Res* **19**, 449-457 (2009).
127 D'Autreaux, B. & Toledano, M. B. ROS as signalling molecules: mechanisms that generate specificity in ROS homeostasis. *Nat Rev Mol Cell Biol* **8**, 813-824 (2007).
128 Turell, L. *et al.* Reactivity of sulfenic acid in human serum albumin. *Biochemistry* **47**, 358-367 (2008).
129 Tonks, N. K. Redox redux: revisiting PTPs and the control of cell signaling. *Cell* **121**, 667-670 (2005).
130 Tonks, N. K. Protein tyrosine phosphatases: from genes, to function, to disease. *Nat Rev Mol Cell Biol* **7**, 833-846 (2006).
131 Xu, D., Rovira, II & Finkel, T. Oxidants painting the cysteine chapel: redox regulation of PTPs. *Dev Cell* **2**, 251-252 (2002).
132 Michalek, R. D. *et al.* The requirement of reversible cysteine sulfenic acid formation for T cell activation and function. *J Immunol* **179**, 6456-6467 (2007).
133 Charles, R. L. *et al.* Protein sulfenation as a redox sensor: proteomics studies using a novel biotinylated dimedone analogue. *Mol Cell Proteomics* **6**, 1473-1484 (2007).
134 Leonard, S. E., Reddie, K. G. & Carroll, K. S. Mining the thiol proteome for sulfenic acid modifications reveals new targets for oxidation in cells. *ACS Chem Biol* **4**, 783-799 (2009).
135 Poole, L. B. *et al.* Fluorescent and affinity-based tools to detect cysteine sulfenic acid formation in proteins. *Bioconjug Chem* **18**, 2004-2017 (2007).
136 Reddie, K. G., Seo, Y. H., Muse III, W. B., Leonard, S. E. & Carroll, K. S. A chemical approach for detecting sulfenic acid-modified proteins in living cells. *Mol Biosyst* **4**, 521-531 (2008).
137 Seo, Y. H. & Carroll, K. S. Facile synthesis and biological evaluation of a cell-permeable probe to detect redox-regulated proteins. *Bioorg Med Chem Lett* **19**, 356-359 (2009).

138 Seo, Y. H. & Carroll, K. S. Profiling protein thiol oxidation in tumor cells using sulfenic acid-specific antibodies. *Proc Natl Acad Sci U S A* **106**, 16163-16168 (2009).
139 Allison, W. S. Formation and reactions of sulfenic acids in proteins. *Acc. Chem. Res.* **9**, 293-299 (1976).
140 Benitez, L. V. & Allison, W. S. The inactivation of the acyl phosphatase activity catalyzed by the sulfenic acid form of glyceraldehyde 3-phosphate dehydrogenase by dimedone and olefins. *J Biol Chem* **249**, 6234-6243 (1974).
141 Agard, N. J., Baskin, J. M., Prescher, J. A., Lo, A. & Bertozzi, C. R. A comparative study of bioorthogonal reactions with azides. *ACS Chem Biol* **1**, 644-648 (2006).
142 Karplus, P. A. & Hall, A. Structural survey of the peroxiredoxins. *Subcell Biochem* **44**, 41-60 (2007).
143 Wood, Z. A., Poole, L. B. & Karplus, P. A. Peroxiredoxin evolution and the regulation of hydrogen peroxide signaling. *Science* **300**, 650-653 (2003).
144 Biteau, B., Labarre, J. & Toledano, M. B. ATP-dependent reduction of cysteine-sulphinic acid by S. cerevisiae sulphiredoxin. *Nature* **425**, 980-984 (2003).
145 Jonsson, T. J., Johnson, L. C. & Lowther, W. T. Structure of the sulphiredoxin-peroxiredoxin complex reveals an essential repair embrace. *Nature* **451**, 98-101 (2008).
146 Jonsson, T. J., Johnson, L. C. & Lowther, W. T. Protein engineering of the quaternary sulfiredoxin-peroxiredoxin enzyme-substrate complex reveals the molecular basis for cysteine sulfinic acid phosphorylation. *J Biol Chem* (2009).
147 Roussel, X., Kriznik, A., Richard, C., Rahuel-Clermont, S. & Branlant, G. The catalytic mechanism of Sulfiredoxin from Saccharomyces cerevisiae passes through an oxidized disulfide Sulfiredoxin intermediate that is reduced by thioredoxin. *J Biol Chem* (2009).
148 Kensler, T. W., Wakabayashi, N. & Biswal, S. Cell survival responses to environmental stresses via the Keap1-Nrf2-ARE pathway. *Annu Rev Pharmacol Toxicol* **47**, 89-116 (2007).
149 Tong, K. I. *et al.* Keap1 recruits Neh2 through binding to ETGE and DLG motifs: characterization of the two-site molecular recognition model. *Mol Cell Biol* **26**, 2887-2900 (2006).
150 Tong, K. I. *et al.* Different electrostatic potentials define ETGE and DLG motifs as hinge and latch in oxidative stress response. *Mol Cell Biol* **27**, 7511-7521 (2007).
151 McMahon, M., Thomas, N., Itoh, K., Yamamoto, M. & Hayes, J. D. Dimerization of substrate adaptors can facilitate cullin-mediated ubiquitylation of proteins by a "tethering" mechanism: a two-site interaction model for the Nrf2-Keap1 complex. *J Biol Chem* **281**, 24756-24768 (2006).
152 Velichkova, M. & Hasson, T. Keap1 regulates the oxidation-sensitive shuttling of Nrf2 into and out of the nucleus via a Crm1-dependent nuclear export mechanism. *Mol Cell Biol* **25**, 4501-4513 (2005).
153 Matsuzawa, A. & Ichijo, H. Redox control of cell fate by MAP kinase: physiological roles of ASK1-MAP kinase pathway in stress signaling. *Biochim Biophys Acta* **1780**, 1325-1336 (2008).
154 Piccirillo, S., Filomeni, G., Brune, B., Rotilio, G. & Ciriolo, M. R. Redox mechanisms involved in the selective activation of Nrf2-mediated resistance versus p53-dependent apoptosis in adenocarcinoma cells. *J Biol Chem* **284**, 27721-27733 (2009).

155 Depuydt, M. L., S.E.; Vertommen, D.; Denoncin, K.; Morsomme, P; Wahni, K.; Messens, J.; Carroll, K.S.; Collet, J-F. A periplasmic reducing system protects single cysteine residues from oxidation. *Science* **326**, 1109-1111 (2009).

Chapter 2

Chemical dissection of an essential redox switch in yeast

2.1 Abstract

Saccharomyces cerevisiae responds to elevated levels of hydrogen peroxide in its environment *via* a redox relay system that is comprised of the thiol peroxidase Gpx3 and transcription factor Yap1. In this signaling pathway, a central question that has not been resolved is whether cysteine sulfenic acid (Cys-SOH) modification of Gpx3 is required for the Yap1 activation in cells. Here we report that cell-permeable chemical probes, which are selective for sulfenic acid, inhibit peroxide-dependent nuclear accumulation of Yap1, trap the Gpx3 sulfenic acid intermediate, and block formation of the Yap1-Gpx3 intermolecular disulfide directly in cells. In addition, we present electrostatic calculations that show cysteine oxidation is accompanied by significant changes in charge distribution, which may facilitate essential conformational rearrangements in Gpx3 during catalysis and intermolecular disulfide formation with Yap1. Collectively, these studies constitute the first direct demonstration that oxidation of the catalytic cysteine in Gpx3 to sulfenic acid is essential for oxidative stress sensing in budding yeast and highlight the growing roles of sulfenic acid modifications in biology.

2.2 Introduction

All organisms have evolved cellular responses to monitor and adapt to adverse and changing environmental conditions. In most cases, the stress response is initiated at the genetic level and ultimately, involves the synthesis of proteins that serve a protective

function [1-5]. One type of response mechanism is triggered by reactive oxygen species (ROS), including hydrogen peroxide (H_2O_2), superoxide ($O_2\bullet^-$), and hydroxyl radical (•OH), which are toxic due to their ability to damage DNA and proteins [6]. As a result, aerobic organisms have defense mechanisms to protect against ROS. The oxidative stress response has been well characterized in *Escherichia coli* and *Salmonella typhimurium* where transcription factors such as OxyR [7-12] and SoxR/SoxS [13-16] up-regulate the expression of genes involved in ROS metabolism. Genetic screens have also enabled the identification of transcription factors that regulate antioxidant systems in yeast [17,18].

In *Saccharomyces cerevisiae* the transcription factor Yap1 is a central regulator for the oxidative stress response [13,19]. Yap1 is a basic leucine zipper (bZIP) transcription factor and its DNA-binding domain exhibits homology to members of the mammalian Jun family of proteins [20,21]. Yap1 contains a non-canonical leucine-rich nuclear export signal (NES) embedded within its C-terminal, cysteine-rich domain (c-CRD) comprised of residues Cys598, Cys620, and Cys629 [22]. A second cysteine-rich domain in Yap1 is located within the N-terminal region (n-CRD) and is comprised of residues Cys303, Cys310, and Cys315 [22]. Yap1 is essential for yeast survival under conditions of oxidative stress [17,18] as well as for cellular resistance to diamide, electrophiles and cadmium [17,23-26]. In response to hydrogen peroxide, Yap1 stimulates the expression of ~100 genes including the *TRX2* gene which encodes thioredoxin, *GSH1* which encodes γ-glutamylcysteine synthetase involved in glutathione biosynthesis, and *GLR1* which encodes glutathione reductase [4,27].

Responding to changes in cellular ROS is critical for cell viability and, as a result, there has been significant interest in elucidating the molecular mechanism(s) of transcription

factor activation by oxidative stress [9-11,28,29]. In 1997, Kuge and colleagues reported that oxidative stress caused Yap1 to translocate from the cytosol to the nucleus, and that localization was mediated by conserved cysteine residues in the c-CRD [30]. *In vitro* studies reported by Delaunay *et al.* demonstrated that peroxide stress triggered disulfide formation between Cys303 and Cys598 [22,30]. The structural basis of Yap1 activation was revealed in a solution structure, which showed that in its active, oxidized form the nuclear export signal (NES) in the c-CRD of Yap1 was masked by disulfide-mediated interactions [31]. Additional studies demonstrated that a second protein was required for peroxide-induced Yap1 activation, which was identified as the non-heme peroxide-scavenging enzyme Gpx3 [32]. Notably, a yeast mutant with substitution of Gpx3 Cys36 to serine could not activate Yap1 and that expression of Yap1 Cys303Ala from a centromeric low-copy number plasmid stabilized a disulfide-linked complex with Gpx3 [32].

From these collective studies, Delaunay *et al.* proposed the mechanism for Gpx3-mediated Yap1 activation that is summarized in **Figure 2.1** [29,32]. In this model, the Gpx3 active site cysteine (Cys36) is oxidized to a sulfenic acid, which can react with the resolving cysteine in Gpx3 (Cys82) or with Yap1 Cys598 to form an intra- or intermolecular disulfide, respectively. In the latter pathway, thiol-disulfide exchange leads to a disulfide between Cys303 and Cys598 in Yap1 and nuclear accumulation of the transcription factor. Although a cysteine sulfenic acid modification is central to these competing pathways, it has yet not been determined whether this posttranslational modification is essential for Yap1 activation in cells or how Gpx3 Cys36 and Cys82, which are predicted to be separated by >13 Å in the reduced state, come into proximity to form a disulfide [19,33].

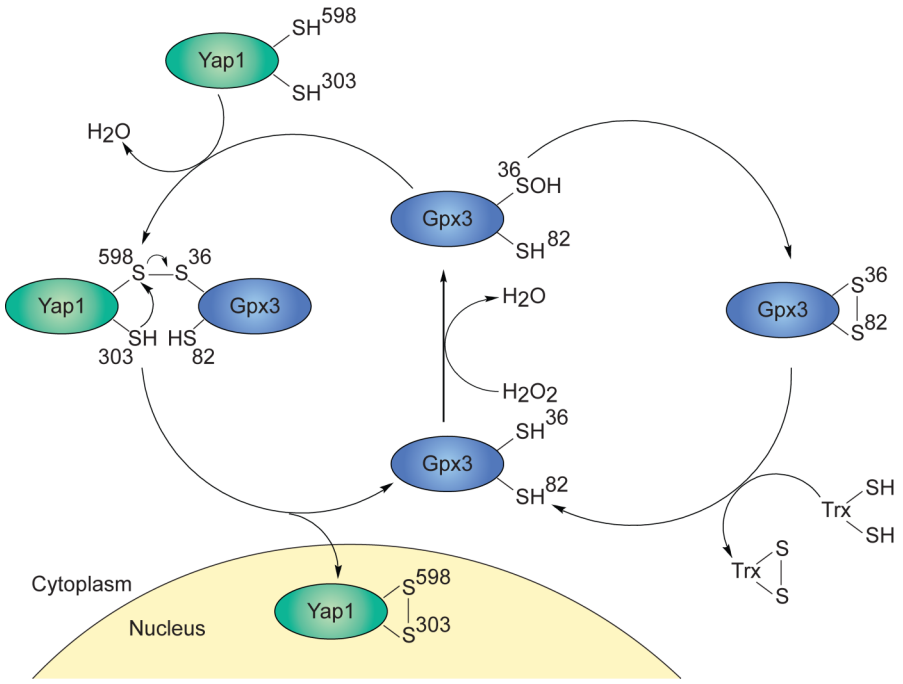

Figure 2.1. Proposed molecular mechanism for the Yap1-Gpx3 redox relay. Gpx3 is hypothesized to transmit a stress signal to Yap1 through oxidation of its catalytic cysteine (Cys36) to sulfenic acid. Next, the Gpx3 Cys36 sulfenic acid condenses with Cys598 in Yap1 to form the Yap1-Gpx3 intermolecular disulfide. Thiol-disulfide exchange with Yap1 Cys303 generates the Cys303-Cys598 intramolecular disulfide in Yap1. Formation of this disulfide masks the nuclear export signal and results in nuclear accumulation of the transcription factor. Figure adapted from D'Autreaux *et al.* **2008**.

In this report, we take a chemical biology approach to address the role of cysteine sulfenic acid modification in Yap1 activation. Here, we present four key results. First, we demonstrate that cell-permeable chemical probes, which covalently modify sulfenic acids, intercept the Yap1-Gpx3 redox relay and inhibit peroxide-induced nuclear localization of Yap1. Second, we show that disruption of the Yap1-Gpx3 relay is associated with peroxide-dependent labeling of the sulfenic acid intermediate in wild-type Gpx3, *in vitro* and directly in cells. Third, we demonstrate that a probe for sulfenic acid inhibits formation of the Yap1-Gpx3 intermolecular disulfide *in vivo*. Taken together, these studies demonstrate the essential role of sulfenic acid posttranslational modification in the Yap1-Gpx3 redox relay. Finally, electrostatic calculations indicate

that cysteine oxidation is accompanied by a significant amount of negative charge localization to the sulfenate oxygen, which could be exploited by Gpx3 to carry out the conformational change required for intramolecular disulfide formation during catalysis as well as intermolecular disulfide formation with Yap1.

2.3 Results and discussion

2.3.1 Sulfenic acid-specific chemical probes inhibit Yap1 nuclear localization

The mechanism outlined in **Figure 2.1** predicts that the sulfenic acid intermediate, which forms at Gpx3 Cys36, during the catalytic cycle is essential for Yap1 activation and nuclear localization. To test this model we reasoned that a small-molecule, which is cell-permeable and chemically selective for sulfenic acid could trap the Gpx3 sulfenic acid modification. Therefore, if the Gpx3 sulfenic acid modification is essential for Yap1 nuclear localization, yeast treated with a sulfenic acid-specific probe should not exhibit peroxide-induced nuclear localization of the transcription factor. Alternatively, if the Gpx3 sulfenic acid intermediate is not essential, the probe should not inhibit nuclear localization of Yap1.

To distinguish between these models, we used a green fluorescent protein (GFP)-tagged Yap1 yeast strain [34] and fluorescence microscopy to monitor the effect of sulfenic acid reactive probes on Yap1 localization. In untreated samples of logarithmically growing yeast cells, Yap1 showed primarily cytosolic localization (**Figure 2.2a** and **b**). After hydrogen peroxide stimulation, Yap1 accumulated in the nucleus, reaching maximal nuclear translocation within 5 min of peroxide treatment (**Figure 2.2a** and **b**). After ~30 min, fluorescently labeled protein moved back to the cytosol (**Figure 2.2a** and

b). These kinetics are consistent with published data describing peroxide-dependent Yap1 nuclear translocation [22,30].

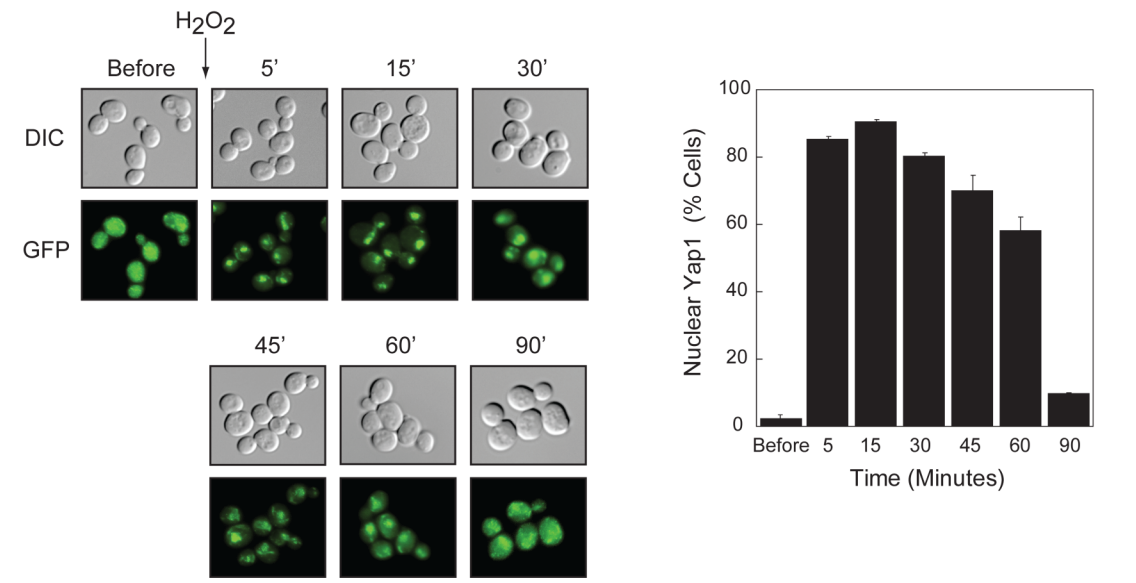

Figure 2.2. Analysis of Yap1-GFP cellular localization upon activation by hydrogen peroxide. a) Exponentially growing yeast with a chromosomal copy of Yap1 fused to GFP (Yap1-GFP) were treated with hydrogen peroxide (400 μM) during the indicated period and analyzed for GFP staining. b) Kinetics of Yap1-GFP nuclear localization. Cells (n = 200 –300) from (a) were scored for nuclear accumulation of Yap1-GFP.

To trap the sulfenic acid modification in Gpx3 in cells and prevent thiol-disulfide exchange with Yap1, we used dimedone (5,5-dimethyl-1,3-cyclohexadione), a cell-permeable and nucleophilic small-molecule that is chemically selective for sulfenic acids [35-40]. In this reaction, dimedone reacts with the electrophilic sulfur atom in sulfenic acid to form a stable thioether bond (**Figure 2.3a**). Dimedone alone had no effect on Yap1 distribution in nonstimulated cells (data not shown), but completely blocked its nuclear translocation in peroxide-treated cells (**Figure 2.3b** and **c**). Peroxide-dependent nuclear localization of Yap1 could be completely restored by diluting dimedone-treated yeast in fresh medium lacking inhibitor and culturing cells for 16 hours (**Appendix 2.6.1**). Since the protein-dimedone adduct is irreversible, these data suggest that the redox relay is

restored by degrading modified Gpx3 and biosynthesis of new thiol peroxidase. The rate of turnover for Gpx3 protein has not been reported, however, the half-life for Gpx2 in budding yeast is 168 minutes [41]. Based on this estimate, complete degradation (*e.g.,* five-half lives) of modified Gpx3 would take approximately 14 hours, consistent with our observations. Taken together these data demonstrate that a sulfenic acid modification is required for peroxide-induced Yap1 nuclear accumulation, directly in living cells.

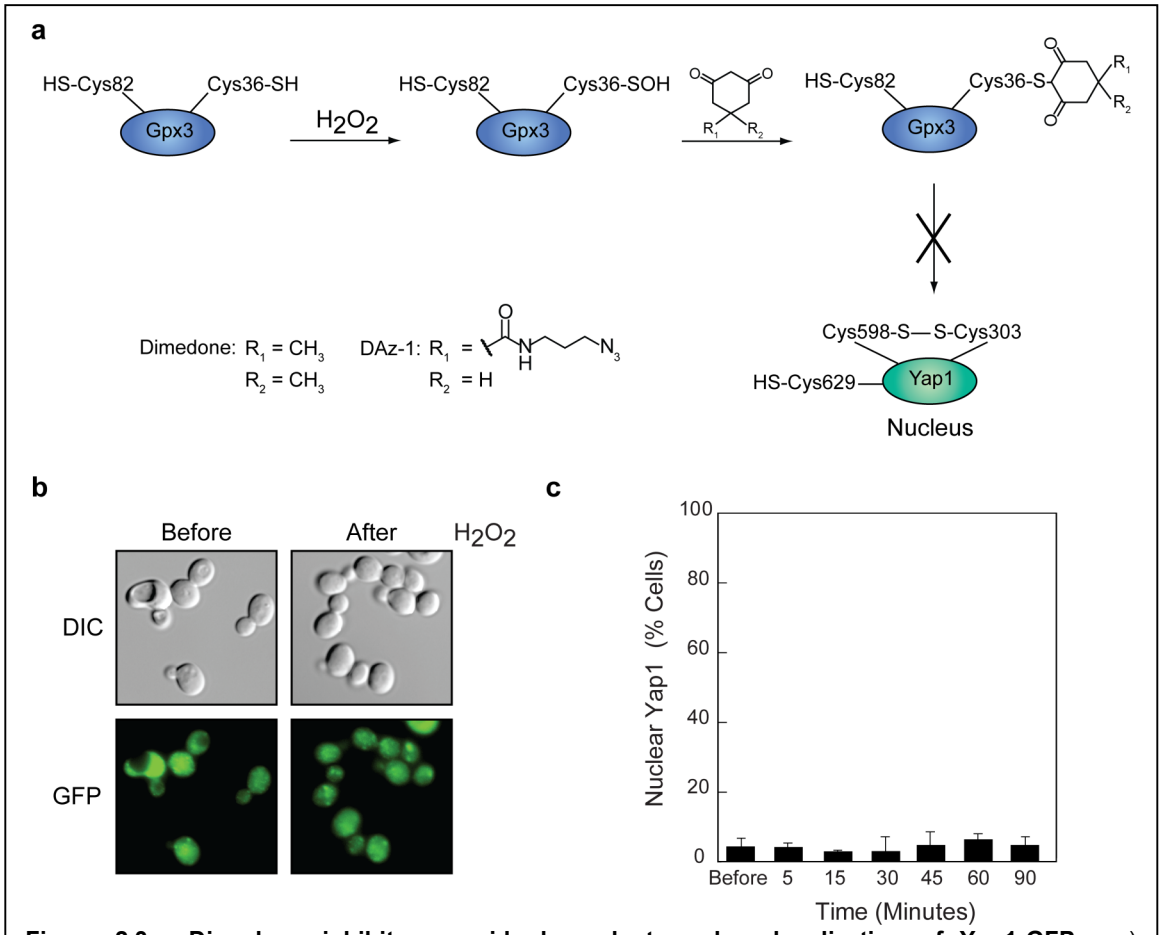

Figure 2.3. Dimedone inhibits peroxide-dependent nuclear localization of Yap1-GFP. a) Dimedone and DAz-1 selectively modify sulfenic acids. Reaction of either probe with Gpx3 Cys36 sulfenic acid will form a stable adduct and, based on the model in Figure 2.1, is predicted to inhibit peroxide-dependent nuclear localization of Yap1. b) Yap1-GFP remains in the cytoplasm when cells are exposed to dimedone. Exponentially growing yeast were treated with dimedone (50 mM) and hydrogen peroxide (400 μM) for 15 min at 30 °C and analyzed for GFP staining. c) Kinetics of Yap1-GFP nuclear localization in yeast exposed to dimedone. Cells (n = 200 –300) from (b) were scored as in Figure 2.2b.

2.3.2 Trapping the Gpx3 sulfenic acid modification *in vivo*

The above results are consistent with the model proposed in **Figure 2.1**. However, the data presented in **Figure 2.3** do not indicate whether Gpx3 is modified by sulfenic acid-specific probes in peroxide-treated cells. To show that inhibition of Yap1 nuclear localization is accompanied by peroxide-dependent tagging of Gpx3 in cells we used a sulfenic acid-specific probe that we have recently developed in our lab, known as DAz-1 (**Figure 2.3a**) [35,40]. Based on the dimedone scaffold, this probe is also functionalized with an azide chemical handle that can be selectively detected with phosphine or alkyne-based reagents *via* the Staudinger ligation or click chemistry for detection of modified proteins[42] (**Figure 2.4a**). Peroxide-dependent Yap1 nuclear accumulation was also suppressed in DAz-1 treated cells, as expected (data not shown).

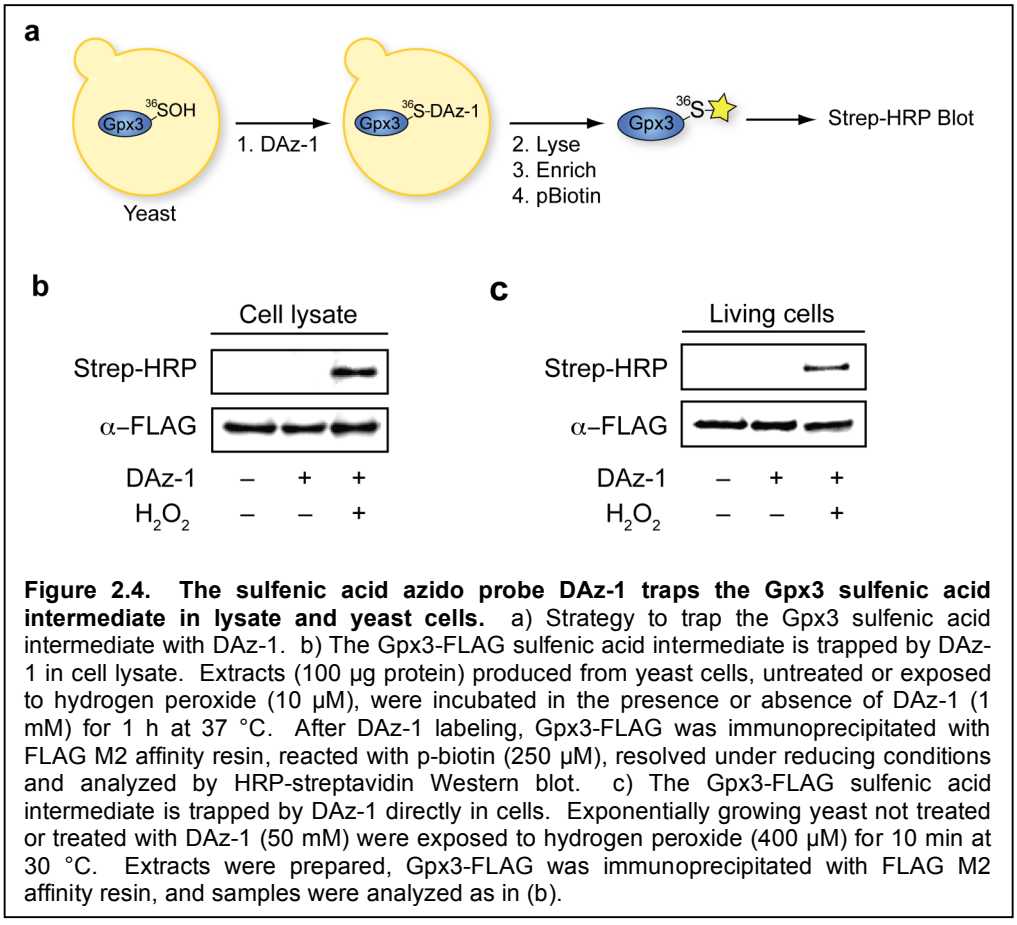

Figure 2.4. The sulfenic acid azido probe DAz-1 traps the Gpx3 sulfenic acid intermediate in lysate and yeast cells. a) Strategy to trap the Gpx3 sulfenic acid intermediate with DAz-1. b) The Gpx3-FLAG sulfenic acid intermediate is trapped by DAz-1 in cell lysate. Extracts (100 µg protein) produced from yeast cells, untreated or exposed to hydrogen peroxide (10 µM), were incubated in the presence or absence of DAz-1 (1 mM) for 1 h at 37 °C. After DAz-1 labeling, Gpx3-FLAG was immunoprecipitated with FLAG M2 affinity resin, reacted with p-biotin (250 µM), resolved under reducing conditions and analyzed by HRP-streptavidin Western blot. c) The Gpx3-FLAG sulfenic acid intermediate is trapped by DAz-1 directly in cells. Exponentially growing yeast not treated or treated with DAz-1 (50 mM) were exposed to hydrogen peroxide (400 µM) for 10 min at 30 °C. Extracts were prepared, Gpx3-FLAG was immunoprecipitated with FLAG M2 affinity resin, and samples were analyzed as in (b).

To facilitate enrichment of Gpx3, a relatively low abundance protein, we inserted the FLAG epitope into chromosomal Gpx3 (**Appendix 2.6.2a**). Control experiments verified that the tag did not disrupt the Yap1-Gpx3 redox relay (**Appendix 2.6.2b** and **c**) or the ability of sulfenic acid-specific chemical probes to inhibit peroxide-induced Yap1 nuclear accumulation (**Appendix 2.6.2d** and **e**). To probe for sulfenic acid modification of Gpx3 *in vitro*, whole cell yeast lysate was not treated or treated with DAz-1, in the presence or absence of hydrogen peroxide. Subsequently, Gpx3 was immunoprecipitated and conjugated to phosphine-biotin (pBiotin). Samples were analyzed under reducing conditions and DAz-1 labeling was detected by streptavidin-HRP Western blot (**Figure 2.4a**). Gpx3 showed peroxide-dependent labeling by DAz-1 (**Figure 2.4b**). Control reactions carried out in the absence of DAz-1 or hydrogen peroxide showed no labeling, as expected (**Figure 2.4b**). Next we investigated whether DAz-1 could trap the Gpx3 sulfenic acid intermediate directly in cells. For these experiments, cells were not treated or treated with DAz-1, in the presence or absence of hydrogen peroxide. Gpx3 showed peroxide-dependent labeling by DAz-1 (**Figure 2.4c**). As before, no signal was observed in the absence of DAz-1 or hydrogen peroxide (**Figure 2.4c**). Collectively, these data show that DAz-1 can trap the Gpx3-sulfenic acid intermediate in lysate and directly in cells.

The sulfenic acid intermediate has been detected at the active site in thiol peroxidases when the resolving cysteine is not present to generate the disulfide bond [38,43]. To our knowledge, however, chemical trapping of the sulfenic acid intermediate in a wild-type thiol peroxidase has not yet been reported. To provide additional evidence that dimedone can trap the reactive sulfenic acid intermediate in Gpx3 we investigated peroxide-dependent disulfide formation in recombinant his-tagged Gpx3, in the presence or absence of dimedone. For these experiments, we analyzed Gpx3 under nonreducing

conditions, which permit the oxidized and reduced forms of Gpx3 to be distinguished by their electrophoretic mobility [22,32]. Treatment with hydrogen peroxide converted Gpx3 from its reduced to its oxidized form (**Figure 2.5a**, lanes 1 and 2). However, in the presence of dimedone, the majority of Gpx3 remained in the reduced state (**Figure 2.5a**, lane 3). This observation is consistent with covalent modification of the Gpx3 Cys36 sulfenic acid intermediate by dimedone and inhibition of intramolecular disulfide formation between Cys36 and Cys82.

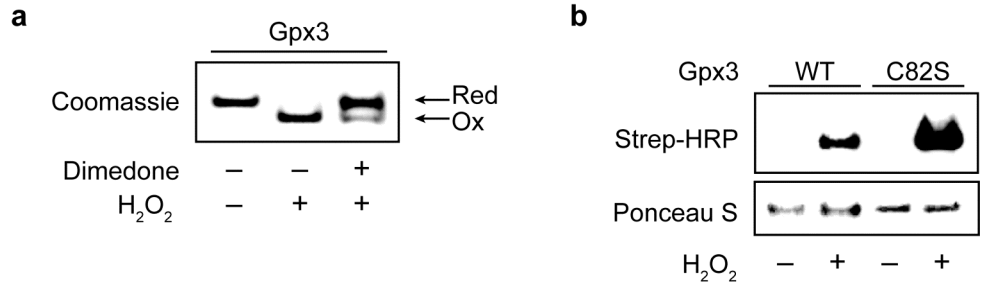

Figure 2.5. Dimedone treatment inhibits formation of the intramolecular disulfide in recombinant wild-type and or Cys82Ser Gpx3. a) Analysis of the *in vitro* redox state of recombinant Gpx3. Recombinant wild-type Gpx3 (60 µM), untreated or exposed to hydrogen peroxide (60 µM) was incubated in the presence or absence of dimedone (50 mM). Samples were resolved under non-reducing conditions and visualized by Coomassie blue stain. The oxidized and reduced forms of Gpx3 are indicated by arrows. b) DAz-1 traps the sulfenic acid intermediate in wild-type and mutant Gpx3. Wild-type or Cys82Ser Gpx3 (50 µM), untreated or exposed to hydrogen peroxide (100 µM), were incubated in the presence or absence of DAz-1 (10 mM) for 15 min at 37 °C. After DAz-1 labeling, samples were treated with p-biotin (250 µM), resolved under reducing conditions and analyzed by HRP-streptavidin Western blot.

Next, we investigated whether DAz-1 could trap the sulfenic acid intermediate in recombinant wild-type and mutant Gpx3 protein. Peroxide-dependent DAz-1 labeling of wild-type Gpx3 was observed (**Figure 2.5b**, lanes 1 and 2), analogous to results obtained with Gpx3-FLAG in yeast lysate and cells. Additional studies carried out with Gpx3 Cys36Ser and Gpx3 Cys36Ser Cys64Ser (**Appendix 2.6.3**) also indicate that DAz-1 labels the active site Cys36, consistent with previous results obtained using NBD-Cl [43]. Finally, the intensity of DAz-1 labeling was increased in the Gpx3 Cys82Ser mutant, as expected (**Figure 2.5b**, lanes 3 and 4).

In a previous study, Poole and coworkers investigated sulfenic acid formation in the bacterial thiol peroxidase AhpC, but failed to observe reactivity with dimedone during the catalytic cycle [44]. In these experiments, it is possible that the sulfenic acid in wild-type AhpC was not trapped by dimedone due to the low concentration of probe employed in these experiments [44]. Moreover, a more recent study reported by Poole and coworkers shows that the sulfenic acid intermediate in AhpC Cys165Ser reacts more slowly with a dimedone analog, relative to an oxidized cysteine protease [38]. Hence, rates of covalent modification may depend on the surrounding microenvironment of the sulfenic acid and vary from protein to protein.

2.3.3 Dimedone blocks formation of the Yap1-Gpx3 intermolecular disulfide *in vivo*

Previously, Toledano and coworkers demonstrated that expression of Yap1 Cys303Ala stabilized a disulfide-linked complex with Gpx3 [32]. Given this finding and the data presented in **Figures 2.2 – 2.5**, we reasoned that covalent modification of the Gpx3 sulfenic acid intermediate by dimedone should inhibit formation of the Yap1-Gpx3 intermolecular disulfide *in vivo*. To test this hypothesis, we generated a plasmid encoding Yap1 Cys303Ala with an N-terminal Myc epitope and transformed this construct into yeast. In subsequent steps, we challenged yeast with hydrogen peroxide, in the presence or absence of dimedone. After processing, cellular proteins were resolved under nonreducing conditions and Yap1-Gpx3 complex formation was monitored by Western blot (**Figure 2.6** and **Appendix 2.6.4**).

In the absence of hydrogen peroxide or at a low concentration of the oxidant (200 μM), the Western blot showed only a single band corresponding to Yap1 Cys303Ala (**Figure 2.6**, lanes 1 and 2). However, as the concentration of hydrogen peroxide was raised (400 μM – 800 μM) we observed a second band in the Western blot, which increased in

intensity and migrated approximately 25 kDa higher than Yap1 Cys303Ala (**Figure 2.6**, lanes 3 – 5). As predicted for the Yap1-Gpx3 complex, the higher molecular weight species disappeared when samples were analyzed under reducing conditions (data not shown) and was not observed in a gpx3 null strain (**Appendix 2.6.4**). To test whether dimedone could inhibit formation of the Yap1-Gpx3 complex, we conducted side-by-side experiments in the presence of the chemical probe. Notably, the higher molecular weight Yap1-Gpx3 complex was not observed in dimedone-treated cells (**Figure 2.6**, lanes 6 – 10). Likewise, the Yap1 Cys303Ala-Gpx3 complex could be selectively immunoprecipitated from peroxide-treated cells, but was not formed in dimedone-treated samples (**Appendix 2.6.5**). Together, these data show that dimedone inhibits the formation of the Yap1-Gpx3 intermolecular disulfide *in vivo*.

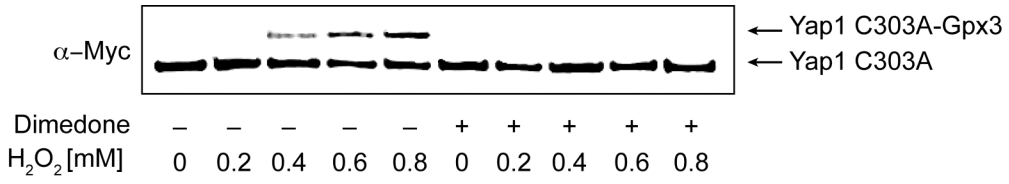

Figure 2.6. Dimedone inhibits formation of the Yap1-Gpx3 intermolecular disulfide *in vivo*. Exponentially growing yeast, carrying Myc-Yap1 Cys303Ala, untreated or exposed to dimedone (50 mM) were treated with hydrogen peroxide at the concentrations indicated for 2 min. NEM-blocked extracts were prepared as described in methods, resolved by non-reducing SDS-PAGE and analyzed by Western blot using antibodies against the Myc epitope. Myc-Yap1 Cys303Ala and the Myc-Yap1 Cys303Ala-Gpx3 mixed disulfide are indicated by arrows.

2.3.4 Sulfenic acid formation: a general mechanism for conformational change

A recent crystal structure of the peroxidase Gpx5 from *Populus trichocarpa x deltoids* (PtGPX5) determined that the catalytic and resolving cysteines are located 21 Å apart in the reduced enzyme [29]. Likewise, structure homology modeling predicts that Cys36 and Cys82 in Gpx3 are separated by 13 Å [33]. Therefore, the transition between the reduced and oxidized states is accompanied by significant conformational changes in this family of peroxidases. In their analysis of the PtGpx5 structures, Koh and colleagues propose

that during the catalytic cycle, deprotonation of Cys92 to form the thiolate anion destabilizes adjacent structural elements and thereby, facilitates conformational change [29]. However, since the catalytic cysteine in the peroxidase is characterized by a low pK_a [33] this residue is constitutively deprotonated at physiological pH. Therefore, it seems unlikely that the thiolate mediates conformational change during the catalytic cycle. Rather, we hypothesize that oxidation of the thiolate to the sulfenic acid, which is also expected to be deprotonated at physiological pH [45], is responsible for accelerating the rate of intramolecular disulfide formation.

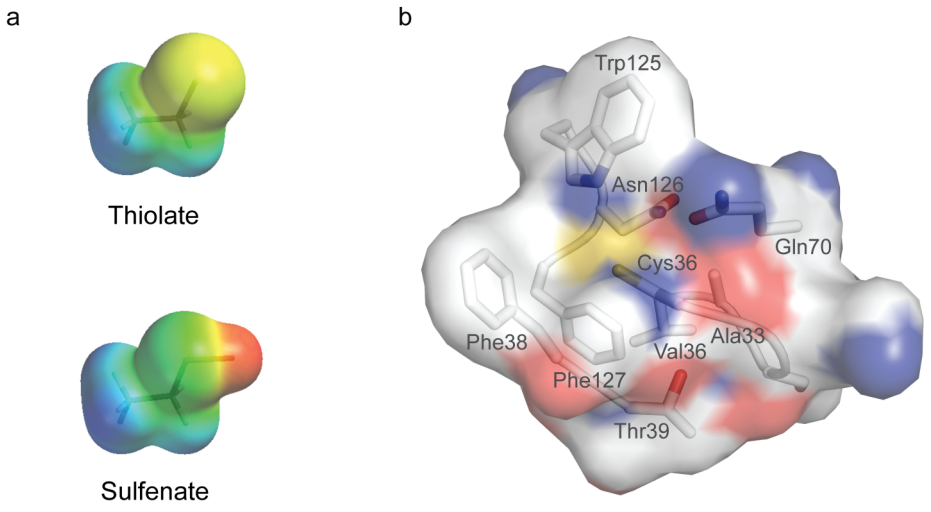

Figure 2.7. Cysteine oxidation to sulfenic acid as a mechanism for conformational change. a) Electrostatic potential surface of cysteine in the thiolate and sulfenate forms. The surfaces depict the highly delocalized negative charge of a nucleophilic thiolate and the accumulation of negative charge on the sulfenate oxygen atom. Electrostatic potential surfaces were generated using Spartan 06 (Wavefunction, Inc.). Color gradient: red corresponds to most negative and blue corresponds to most positive. b) Structure homology-based model of the yeast Gpx3 active site depicted with negative (red) and positive (blue) electrostatic surface potentials. Hydrophobic residues Ala33, Val34, Phe38, Trp125 and Phe127 surround the sulfur atom of Cys36 (yellow). The thiol functional group is also in proximity to amide functional groups from Gln70 and Asn126. This model was generated using the Swiss Model program with human Gpx3 (pdb 2r37), related to yeast Gpx3 by ~36% identify, as the structural template. The electrostatic surface potential and figure were generated in Pymol (http://pymol.sourceforge.net).

To investigate changes in charge-density distribution that occur when a thiolate is oxidized to a sulfenate we generated potential energy surfaces for these functional

groups (**Figure 2.7a**). These calculations show that the charge-density distribution differs dramatically between these states. Notably, cysteine oxidation is accompanied by a significant localization of negative charge to the sulfenate oxygen atom. Therefore, when surrounded by hydrophobic and electronegative residues (**Figure 2.7b**) formation of the sulfenate anion in the Gpx3 active site may promote conformational rearrangement *via* electrostatic repulsion, which is required for intramolecular disulfide formation during catalysis and for intermolecular disulfide formation with Yap1.

2.4 Conclusions

Reduction and oxidation comprise an important class of posttranslational modifications. In this context, the thiol side chain of cysteine is most sensitive to redox transformations and can occur in a variety of oxidation states. Among these, the thiol and the disulfide are best known, but oxygen derivatives such as sulfenic (RSOH), sulfinic (RSO_2H), and sulfonic (RSO_3H) acid are observed in a growing number of proteins, and are proposed to regulate a wide variety of phenomena such as catalysis, metal binding, protein turnover and signal transduction [37,46]. This study constitutes the first direct evidence that cysteine oxidation to sulfenic acid in the thiol peroxidase Gpx3 is essential for yeast to sense oxidative stress and, more broadly, sheds light on the growing roles of sulfenic acid modifications in biology. From a chemical perspective, this work highlights the utility of cell-permeable, small-molecule probes to investigate redox-regulated signal transduction in living cells [6]. Finally, this work also contributes to our molecular understanding of how oxidative cysteine modification and accompanying changes in electrostatic charge distribution may be exploited to facilitate conformational change in proteins.

2.5 Experimental Procedures

2.5.1 Strains and growth conditions

The *S. cerevisiae* strain ATCC-201388 (*MATa his3Δ1 leu2Δ0 met15Δ0 ura3Δ0*) containing GFP-modified Yap1 were used in all experiments, with the exception of the Δgpx3, which is in BY4742 (*MATα his3Δ1 leu2Δ0 lys2Δ0 ura3Δ0 can1-100*). Cells were grown at 30 °C in YPD [1% yeast extracts, 2% bactopeptone, and 2% glucose] or SC – Ura media containing 2% glucose. The Gpx3-FLAG strain was derived from the Yap1-GFP strain. The FLAG epitope was appended to Gpx3 in the yeast chromosome as described [47]. In brief, primers 5'-AAACCTTCTTCGTTGTCCGAAACCATCGAAGAACT TTTGAAAGAGGTGGAAAGGGAACAAAAGCTGGAG-3' and 5'-AAATATAAAAGAAAAC TAAGCTTTACCTAACTTCAAAAGAAGAAGACCTGCCTATAGGGCGAATTGGGT-3' were used to amplify a 3xFLAG/Kan cassette with regions of homology to Gpx3 from the p3FLAG-KanMX plasmid. The PCR-amplified product was transformed into the Yap1-GFP yeast strain [48,49]. Transformants were selected on YP-Gal plates supplemented with G418 (200 mg mL^{-1}). Chromosomal tagging was verified by PCR and anti-FLAG Western blot.

2.5.2 Cloning, expression, and purification of recombinant Gpx3

Yeast genomic DNA was isolated from the Yap1-GFP yeast strain as described [50]. Gpx3 was amplified by PCR from yeast genomic DNA using the following primers: 5'-TTTATCGGATCCATGTCAGAATTCTATAAGCTAGCACCT-3' and 5'-ACCTGCCTCGA GCTATTCCACCTCTTTCAAAAGTTCTTC-3'. pRSETa-6xHis-Gpx3 was constructed by subcloning Gpx3 into the BamHI and XhoI sites of pRSETa (Invitrogen). pRSETa-6xHis-Gpx3 Cys36Ser, pRSETa-6xHis-Gpx3 Cys82Ser, and pRSETa-6xHis-Gpx3 Cys36Ser Cys64Ser were generated using site-directed PCR mutagenesis. Wild-type, Cys82Ser,

Cys36Ser, and Cys36Ser Cys64Ser Gpx3 were purified from *Escherichia coli* strain BL21(DE3) pLysS as previously described [43].

2.5.3 Construction of Myc-Yap1 Cys303Ala

Yap1 was amplified by PCR from yeast genomic DNA using the following primers: 5'-TAAACCTCTAGAATGAGTGTGTCTACCGCCAAGAGGTC-3' and 5'-CCCGCTCTCG AGTTAGTTCATATGCTTATTCAAAGCTA–3'. Yap1 was then subcloned into pCR4 (Invitrogen). pCR4-Yap1 Cys303Ala was generated by site-directed PCR mutagenesis. Myc-Yap1 Cys303Ala was generated in two steps by PCR. The first PCR product was generated from the pCR4-Yap1 Cys303Ala template using the following primers: 5'-GATTTCCGAAGAAGACCTCATGAGTGTGTCTACCGCC-3' and 5'-GTTCATATGCTT ATTCAAAGCTAATTGAACGTCTTCTGC-3'. The product of this reaction was then used to generate the complete Myc-Yap1 Cys303Ala fragment using the following primers: 5'-AAGCTTATGGAACAGAAGTTGATTTCCGAAGAAGACCTC-3' and 5'-GTTCATATGC TTATTCAAAGCTAATTGAACGTCTTCTGC-3'. Finally, the Myc-Yap1 Cys303Ala PCR product was digested with HindIII and XhoI and subcloned into the multiple cloning region of p416-TEF [51].

2.5.4 Stock solutions of sulfenic acid probes

Dimedone was prepared in DMSO at a final concentration of 1.1 M. DAz-1 was synthesized as previously described [40] and prepared as a 50:50 mixture of DMSO and 0.1 M Bis-Tris HCl pH 7.0 at a final concentration of 0.25 M. Chemical probes were added directly to culture or reactions *in vitro*.

2.5.5 Yeast culture with sulfenic acid probes

Exponentially growing yeast were treated with dimedone or DAz-1 (50 – 100 mM) and cultured for 30 – 60 min prior to treatment with hydrogen peroxide (400 μM). At the indicated times, cells were fixed by incubating for 15 min at rt with 4% (w/v) paraformaldehyde with rocking. To restore peroxide-dependent nuclear localization of Yap1, dimedone-treated cells were diluted 10,000-fold in fresh media lacking probe, grown to saturation (16 hrs) and re-challenged with hydrogen peroxide (400 μM). Samples were fixed and analyzed as described above.

2.5.6 Fluorescence microscopy

Exponentially growing yeast (1 mL) were harvested and washed twice with 0.1 M KH_2PO_4, pH 6.6 and stored at 4 °C in the same buffer. For oxidized samples, exponentially growing yeast (1 mL) were exposed to hydrogen peroxide (400 μM) and samples were fixed at various time points, as described above. Yap1-GFP nucleocytoplasmic localization was analyzed with a Nikon Eclipse 80i fluorescent microscope equipped with a Photometrics CoolSnap ES^2 cooled CCD camera and MetaMorph software.

2.5.7 Kinetics of Yap1-GFP nucleocytoplasmic localization

Exponentially growing yeast were exposed to hydrogen peroxide (400 μM) only or dimedone (50 mM) and then hydrogen peroxide (400 μM). Samples were fixed before and after peroxide treatment as described above. At each time point, cells (n = 200 – 300) were scored for subcellular localization of Yap1-GFP. Nuclear localization of Yap1-GFP was verified by co-localization with DAPI stain (**Appendix 2.6.2**). Experiments

were performed in duplicate and data is presented as the average of the two trials and are presented with corresponding standard deviations.

2.5.8 Immunoprecipitation of Gpx3-FLAG from *S. cerevisiae*

Cells from the Yap1-GFP/Gpx3-FLAG strain (4 x 10^8 for *in vitro* studies, 1.25 x 10^8 for *in vivo* studies) were harvested, resuspended in lysis buffer [25 mM HEPES, pH 7.5, 35 mM NaCl, 2 mM EDTA, 1x yeast protease inhibitor cocktail, 40 μM chymostatin], and lysed by mechanical disruption using glass beads. Gpx3-FLAG was immunoprecipitated from lysate with EZView Red ANTI-FLAG M2 affinity gel (Sigma) for 1 – 4 h at 4 °C. The resin was collected at 8,200 *g* for 30 s and washed three times with 25 volumes of wash buffer [50 mM Tris HCl, 150 mM NaCl, pH 7.4]. Gpx3 was eluted with three volumes of elution buffer 1 [50 mM Tris HCl, pH 7.5, 150 mM NaCl, 1 mg mL^{-1} 1xFLAG peptide or 0.5 mg mL^{-1} 3xFLAG peptide].

2.5.9 Analysis of Gpx3 intramolecular disulfide formation *in vitro*

Recombinant wild-type Gpx3 was reduced with DTT (50 mM) for 1.5 h at rt. Reducing agent was removed by gel filtration using p-30 micro Bio-Spin columns (BioRad). Wild-type Gpx3 (60 μM) was then treated with dimedone (50 mM) or DMSO in the presence of hydrogen peroxide (50 μM) for 10 min at rt. Reactions were then incubated with iodoacetamide (300 mM) for 10 min at rt, resolved by non-reducing SDS-PAGE on 4-12% Bis-Tris gels (Invitrogen) and visualized by Coomassie blue staining.

2.5.10 DAz-1 labeling of recombinant Gpx3 and Gpx3-FLAG

Recombinant wild-type, Cys36Ser, Cys82Ser and Cys36Ser Cys64Ser Gpx3 were reduced with DTT (50 mM) for 1.5 h at rt. Reducing agent was removed by gel filtration

using p-30 micro Bio-Spin columns (BioRad). Wild-type Gpx3 and mutants (0 – 50 μM) were then treated with DAz-1 (10 mM) or DMSO in the presence of hydrogen peroxide (50 μM) for 15 min at 37 °C. Small-molecules were separated from the reaction by ultrafiltration with Amicon Ultra Filters (10 KD, Millipore). Reactions were then diluted with an equal volume of Buffer D and concentrated by ultrafiltration. Azide-modified Gpx3 was biotinylated and analyzed as described below. For Gpx3-FLAG, protein was immunoprecipitated from yeast lysate (100 μg total protein) and treated with DAz-1 (1 mM) or DMSO followed by the addition of hydrogen peroxide (0 – 25 μM). Reactions were incubated at rt for 1 h. Alternatively, yeast lysate (100 μg) was exposed to hydrogen peroxide (10 μM) and incubated at rt for 10 min prior to the addition of DMSO or DAz-1 (1 mM). Gpx3-FLAG was then immunoprecipitated as described above. For in vivo labeling of Gpx3-FLAG exponentially growing yeast were treated with DAz-1 (50 mM) for 20 min prior to peroxide treatment. Cells were exposed to hydrogen peroxide (400 μM) and grown at 30 °C for 10 min. Cells were harvested, washed and Gpx3 was enriched from the lysate (200 μg) as described above.

2.5.11 Biotinylation of Gpx3 and Western blot analysis

Azide-tagged Gpx3 was conjugated to biotin *via* Staudinger ligation with phosphine biotin (p-Biotin; 100 – 250 μM) for 2 – 4 h at 37 °C [52,53]. The resulting samples were subjected to SDS-PAGE and Western blot analyses as previously described [35] with the following modifications. Biotinylated proteins were detected by incubating PVDF membrane with 1:5,000 – 1:10,000 streptavidin-HRP (GE Healthcare) in Tris-buffered saline Tween-20 (TBST) or phosphate-buffered saline Tween-20 (PBST). For recombinant Gpx3 studies, 6xHis-Gpx3 was detected by incubating the PVDF membrane with 1:50,000 – 1:100,000 HisProbe-HRP (Pierce). For yeast studies, Gpx3-

3xFLAG was detected by incubating the PVDF membrane with 1:2,000 – 1:10,000 Anti-FLAG M2 (Stratagene) in TBST, washed in TBST (2 x 10 min) and then incubated with 1:10,000-1:50,000 Goat Anti-Mouse- HRP (Pierce). Western blots were developed with chemiluminescence (GE Healthcare ECL Plus Western Blot Detection System) and imaged on a Typhoon 9410 or by film.

2.5.12 Analysis of Yap1-Gpx3 intermolecular disulfide formation *in vivo*

Exponentially growing yeast carrying p416-TEF-Myc-Yap1 Cys303Ala were treated with dimedone (50 mM), hydrogen peroxide was added to yeast cultures (0 – 1 mM) and cells were grown at 30 °C for 2 min. Cultures were lysed with TCA (20% v/v) and protein precipitates were resuspended in NEM buffer [100 mM Tris HCl, pH 8.0, 1 mM EDTA, 1% SDS, 150 mM NEM, 1x yeast protease inhibitor cocktail, 40 mM chymostatin]. The pH was neutralized with sodium hydroxide and the alkylation reaction proceeded at rt for 15 min. For immunoprecipitation, the Yap1 Cys303Ala-Gpx3-FLAG complex was isolated from cell extracts as described above. Proteins were then resolved by non-reducing or reducing SDS-PAGE using NuPAGE 4-12% or 8% Bis-Tris gels (Invitrogen) in NuPAGE MES running buffer, transferred to PVDF membrane and blocked with 5% bovine serum albumin (BSA) in PBST overnight at 4 ^{o}C or 1 h at rt. The membrane was washed in PBST (2 x 10 min) and the Myc epitope was detected by incubation with 1:1,000 Anti-Myc monoclonal antibody (Covance) at 4 ^{o}C overnight, washed in PBST, followed by 1:10,000 Goat Anti-Mouse-HRP (Pierce). Alternatively, the Myc epitope was detected by incubating the PVDF membrane with 1:1,000 Anti-Yap1 polyclonal antibody (Santa Cruz Biotechnology) at 4 °C overnight, washed in PBST, followed by 1:25,000 Goat Anti-Rabbit-HRP (Calbiochem).

2.6 Appendices

2.6.1 Restoration of peroxide-dependent Yap1 nuclear localization. After dimedone treatment (100 mM) and peroxide exposure (400 μM), yeast cells were diluted 10,000-fold into dimedone-free media and cultured to saturation (16 hrs). Subsequently, cells were exposed to H_2O_2 (400 μM) for 15 min at 30 °C and analyzed for GFP staining.

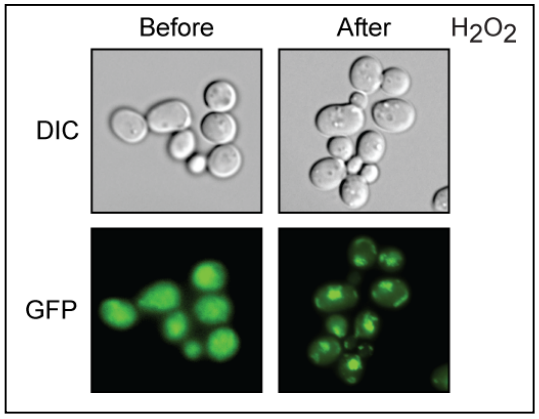

2.6.2 The FLAG epitope tag does not alter Gpx3 function in the Yap1-Gpx3 redox relay. a) Immunoprecipitation of Gpx3-FLAG from yeast. Gpx3 was immunoprecipitated from lysates produced from the Yap1-GFP and Yap1-GFP/Gpx3-FLAG yeast strains. The protein extract was incubated with M2 anti-FLAG resin for 1 h at 4 °C, washed, and eluted with the FLAG peptide (1 mg mL^{-1}). Samples were resolved under reducing conditions and analyzed by Western blot with M2 anti-FLAG, followed by HRP-goat anti-mouse. b) Peroxide-dependent nuclear localization of Yap1 in Yap1-GFP/Gpx3-FLAG yeast strain. Exponentially growing yeast culture was exposed to hydrogen peroxide (400 μM) for the times indicated and then analyzed for GFP staining. c) Kinetics of Yap1 nuclear localization in Yap1-GFP/Gpx3-FLAG yeast strain. Cells (n = 200 – 300) from (b) were scored for Yap1-GFP nuclear localization at the indicated time after hydrogen peroxide exposure. d) Dimedone inhibits peroxide-dependent Yap1 nuclear localization in the Yap1-GFP/Gpx3-FLAG strain. Exponentially growing yeast

culture was exposed to dimedone (50 mM), incubated for 30 min at 30 °C, treated with hydrogen peroxide (400 μM) for 15 min, and analyzed for GFP staining. e) Kinetics of peroxide-dependent nuclear localization of Yap1 in the presence of dimedone. Cells (n = 200 – 300) from (d) were scored for Yap1-GFP nuclear localization for the time indicated after H_2O_2 challenge.

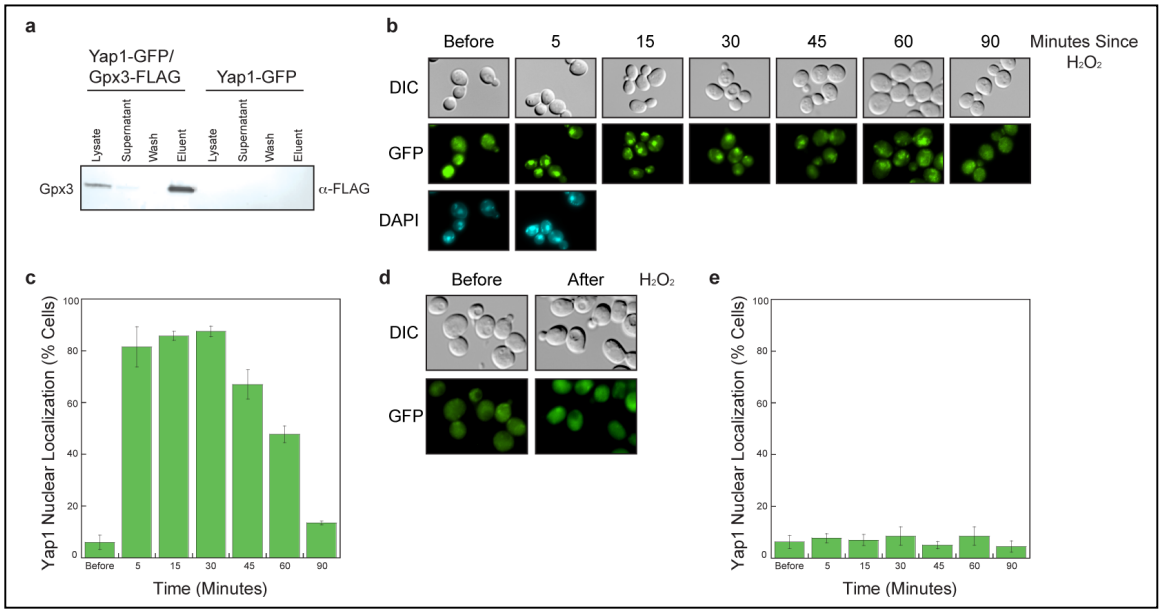

2.6.3 DAz-2 labeling of recombinant Gpx3. Wild-type, Gpx3 Cys36Ser or Gpx3 Cys36Ser Cys64Ser (50 μM) were incubated with or without DAz-1 (10 mM), in the presence or absence of hydrogen peroxide (50 μM) for 15 min at 37 °C. DAz-1 was removed by ultrafiltration and reactions were labeled with p-biotin (250 μM). Proteins were resolved under reducing conditions and analyzed by HRP-Streptavidin Western blot. Slight labeling of Gpx3 Cys36Ser is observed in these experiments (**Left panel**). Possible sites of sulfenic acid formation in the Gpx3 Cys36Ser mutant are Cys64 and Cys82. Since Cys82 has a high pKa [54] we hypothesized that Cys64 was the site of sulfenic acid formation in the mutant Gpx3 Cys36Ser protein. To this hypothesis, we probed the Gpx3 Cys36Ser Cys64Ser mutant for sulfenic acid formation, in the presence or absence of hydrogen peroxide (**Right panel**). The disappearance of label in these

experiments suggests that, in the context of the Gpx3 Cys36Ser mutant, Cys64 is the site of sulfenic acid formation. Since Cys64 oxidation is not observed in the wild-type protein it is possible that the Cys36Ser mutation alters the protein microenvironment surrounding Cys64, thereby enhancing its susceptibility to oxidation. Further, we note that the faint labeling observed for the Gpx3 Cys36Ser mutant, in the absence of exogenously added hydrogen peroxide, likely results from oxidation of the mutant protein during the gel filtration step, which is carried to remove reducing agent. Consistent with this proposal, we do not observe DAz-1 labeling of Gpx3 Cys36Ser in the presence of reducing agent (data not shown). Finally, we note that Gpx3 Cys64 is completely dispensable for the Yap1-Gpx3 redox relay [32,55].

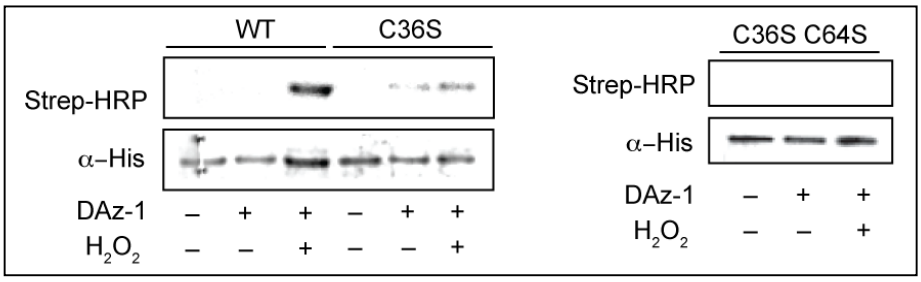

2.6.4 The Yap1-Gpx3 intermolecular disulfide is not observed in ΔGpx3 cells. Exponentially growing ΔGpx3 yeast strain carrying p416-TEF-Myc-Yap1 Cys303Ala was exposed to H_2O_2 (400 μM) for 2 min. Samples were processed as described in Figure 2.6, resolved under non-reducing conditions and analyzed by Western blot using antibodies against Yap1 (top). Ponceau S stain of membrane (bottom).

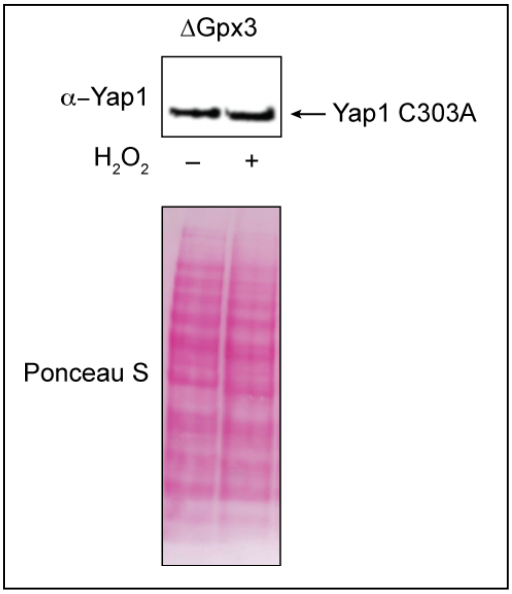

2.6.5 The Yap1-Gpx3 complex is immunoprecipitated via the FLAG epitope and is not formed in dimedone-treated cells. Exponentially growing yeast carrying p416-TEF-Myc-Yap1 Cys303Ala was exposed to H_2O_2 (400 μM) for 2 min. The Yap1 Cys303Ala-Gpx3-FLAG complex was immunoprecipitated as in Figure 2.4b, resolved under reducing conditions and analyzed by Western blot using antibodies against the Myc epitope.

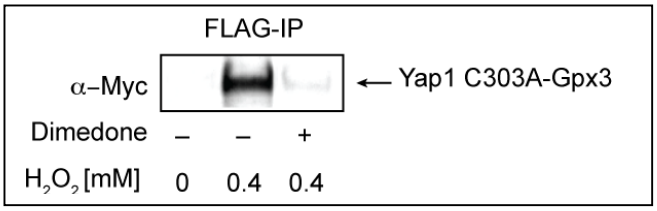

Acknowledgements

We thank the Life Sciences Institute, the Leukemia & Lymphoma Society Special Fellows Award #3100-07 and the American Heart Association Scientist Development Grant #0835419N to K.S.C. for support of this work. We also thank Prof. Lois Weisman for the Yap1-GFP yeast strain and Profs. Katrin Karbstein and Anuj Kumar for helpful discussions and Thu H. Truong for her assistance with recombinant Gpx3 studies.

Notes

This work has been published as "Chemical dissection of an essential redox switch in yeast." Chemistry & Biology **2009** 16: 217-225. Candice E. Paulsen and Kate S. Carroll designed the experiments. Candice E. Paulsen performed all experiments with assistance from Thu H. Truong on recombinant Gpx3 DAz-1 labeling studies and from Kate S. Carroll on generation of the Myc-Yap1 Cys303Ala construct. Candice E. Paulsen and Kate S. Carroll wrote the manuscript.

2.7 References

1 Prasad, S., Zhang, X., Ozkan, C. S. & Ozkan, M. Neuron-based microarray sensors for environmental sensing. *Electrophoresis* **25**, 3746-3760 (2004).

2 Paulding, W. R. *et al.* Regulation of gene expression for neurotransmitters during adaptation to hypoxia in oxygen-sensitive neuroendocrine cells. *Microsc Res Tech* **59**, 178-187 (2002).

3 Hua, Q., Yang, C., Oshima, T., Mori, H. & Shimizu, K. Analysis of gene expression in Escherichia coli in response to changes of growth-limiting nutrient in chemostat cultures. *Appl Environ Microbiol* **70**, 2354-2366 (2004).

4 Gasch, A. P. *et al.* Genomic expression programs in the response of yeast cells to environmental changes. *Mol. Biol. Cell* **11**, 4241-4257 (2000).

5 Amundson, S. A. *et al.* Fluorescent cDNA microarray hybridization reveals complexity and heterogeneity of cellular genotoxic stress responses. *Oncogene* **18**, 3666-3672 (1999).

6 Miller, E. W. & Chang, C. J. Fluorescent probes for nitric oxide and hydrogen peroxide in cell signaling. *Curr Opin Chem Biol* **11**, 620-625 (2007).

7 Christman, M. F., Morgan, R. W., Jacobson, F. S. & Ames, B. N. Positive control of a regulon for defenses against oxidative stress and some heat-shock proteins in Salmonella typhimurium. *Cell* **41**, 753-762 (1985).

8 Kim, S. O. *et al.* OxyR: a molecular code for redox-related signaling. *Cell* **109**, 383-396 (2002).

9 Lee, C. *et al.* Redox regulation of OxyR requires specific disulfide bond formation involving a rapid kinetic reaction path. *Nature Structural & Molecular Biology* **11**, 1179-1185 (2004).

10 Storz, G., Tartaglia, L. A. & Ames, B. N. Transcriptional regulator of oxidative stress-inducible genes: direct activation by oxidation. *Science* **248**, 189-194 (1990).

11 Zheng, M., Aslund, F. & Storz, G. Activation of the OxyR transcription factor by reversible disulfide bond formation. *Science* **279**, 1718-1721 (1998).

12 Zheng, M. *et al.* DNA microarray-mediated transcriptional profiling of the Escherichia coli response to hydrogen peroxide. *Journal of Bacteriology* **183**, 4562-4570 (2001).

13 D'Autreaux, B. & Toledano, M. B. ROS as signaling molecules: mechanisms that generate specificity in ROS homeostasis. *Nat. Rev. Mol. Cell Biol.* **8**, 813-824 (2007).

14 Nunoshiba, T., Hidalgo, E., Amabile Cuevas, C. F. & Demple, B. Two-stage control of an oxidative stress regulon: the Escherichia coli SoxR protein triggers redox-inducible expression of the soxS regulatory gene. *Journal of Bacteriology* **174**, 6054-6060 (1992).

15 Tsaneva, I. R. & Weiss, B. soxR, a locus governing a superoxide response regulon in Escherichia coli K-12. *Journal of Bacteriology* **172**, 4197-4205 (1990).

16 Wu, J. & Weiss, B. Two divergently transcribed genes, soxR and soxS, control a superoxide response regulon of Escherichia coli. *Journal of Bacteriology* **173**, 2864-2871 (1991).

17 Schnell, N. & Entian, K. D. Identification and characterization of a Saccharomyces cerevisiae gene (PAR1) conferring resistance to iron chelators. *European Journal of Biochemistry* **200**, 487-493 (1991).

18 Krems, B., Charizanis, C. & Entian, K. D. Mutants of Saccharomyces cerevisiae sensitive to oxidative and osmotic stress. *Current Genetics* **27**, 427-434 (1995).

19 Stone, J. R. & Yang, S. Hydrogen Peroxide: A Signaling Messenger. *Antioxidants & Redox Signaling* **8**, 243-270 (2006).
20 Harshman, K. D., Moye-Rowley, W. S. & Parker, C. S. Transcriptional activation by the SV40 AP-1 recognition element in yeast is mediated by a factor similar to AP-1 that is distinct from GCN4. *Cell* **53**, 321-330 (1988).
21 Moye-Rowley, W. S., Harshman, K. D. & Parker, C. S. Yeast YAP1 encodes a novel form of the jun family of transcriptional activator proteins. *Genes & Development* **3**, 283-292 (1989).
22 Delaunay, A., Isnard, A. D. & Toledano, M. B. H2O2 sensing through oxidation of the Yap1 transcription factor. *EMBO Journal* **19**, 5157-5166 (2000).
23 Azevedo, D., Tacnet, F., Delaunay, A., Rodrigues-Pousada, C. & Toledano, M. B. Two redox centers within Yap1 for H2O2 and thiol-reactive chemicals signaling. *Free Radic. Biol. Med.* **35**, 889-900 (2003).
24 Coleman, S. T., Epping, E. A., Steggerda, S. M. & Moye-Rowley, W. S. Yap1p activates gene transcription in an oxidant-specific fashion. *Molecular and Cellular Biology* **19**, 8302-8313 (1999).
25 Wu, A. *et al.* Yeast bZip proteins mediate pleiotropic drug and metal resistance. *Journal of Biological Chemistry* **268**, 18850-18858 (1993).
26 Wemmie, J. A., Wu, A. L., Harshman, K. D., Parker, C. S. & Moye-Rowley, W. S. Transcriptional activation mediated by the yeast AP-1 protein is required for normal cadmium tolerance. *Journal of Biological Chemistry* **269**, 14690-14697 (1994).
27 Kuge, S. & Jones, N. YAP1 dependent activation of TRX2 is essential for the response of Saccharomyces cerevisiae to oxidative stress by hydroperoxides. *EMBO Journal* **13**, 655-664 (1994).
28 Lee, J.-W., Soonsanga, S. & Helmann, J. D. A complex thiolate switch regulates the Bacillus subtilis organic peroxide sensor OhrR. *Proceedings of the National Academy of Sciences of the United States of America* **104**, 8743-8748 (2007).
29 Koh, C. S. *et al.* Crystal Structures of a Poplar Thioredoxin Peroxidase that Exhibits the Structure of Glutathione Peroxidases: Insights into Redox-driven Conformational Changes. *Journal of Molecular Biology* **370**, 512-529 (2007).
30 Kuge, S., Jones, N. & Nomoto, A. Regulation of yAP-1 nuclear localization in response to oxidative stress. *EMBO Journal* **16**, 1710-1720 (1997).
31 Wood, M. J., Storz, G. & Tjandra, N. Structural basis for redox regulation of Yap1 transcription factor localization. *Nature* **430**, 917-921 (2004).
32 Delaunay, A., Pflieger, D., Barrault, M.-B., Vinh, J. & Toledano, M. B. A thiol peroxidase is an H2O2 receptor and redox-transducer in gene activation. *Cell* **111**, 471-481 (2002).
33 Poole, L. B., Karplus, P. A. & Claiborne, A. Protein sulfenic acids in redox signaling. *Annual Review of Pharmacology and Toxicology* **44**, 325-347 (2004).
34 Huh, W.-K. *et al.* Global analysis of protein localization in budding yeast. *Nature* **425**, 686-691 (2003).
35 Reddie, K. G., Seo, Y. H., Muse, W. B., III, Leonard, S. E. & Carroll, K. S. A chemical approach for detecting sulfenic acid-modified proteins in living cells. *Molecular BioSystems* **4**, 521-531 (2008).
36 Poole, L. B., Zeng, B. B., Knaggs, S. A., Yakubu, M. & King, S. B. Synthesis of chemical probes to map sulfenic acid modifications on proteins. *Bioconjug Chem* **16**, 1624-1628 (2005).
37 Poole, L. B. & Nelson, K. J. Discovering mechanisms of signaling-mediated cysteine oxidation. *Curr Opin Chem Biol* **12**, 18-24 (2008).

38 Poole, L. B. *et al.* Fluorescent and affinity-based tools to detect cysteine sulfenic acid formation in proteins. *Bioconjug Chem* **18**, 2004-2017 (2007).
39 Allison, W. S. Formation and reactions of sulfenic acids in proteins. *Acc. Chem. Res.* **9**, 293 (1976).
40 Seo, Y. H. & Carroll, K. S. Facile synthesis and biological evaluation of a cell-permeable probe to detect redox-regulated proteins. *Bioorg Med Chem Lett* **19**, 356-359 (2009).
41 Belle, A., Tanay, A., Bitincka, L., Shamir, R. & O'Shea, E. K. Quantification of protein half-lives in the budding yeast proteome. *Proc Natl Acad Sci U S A* **103**, 13004-13009 (2006).
42 Agard, N. J., Baskin, J. M., Prescher, J. A., Lo, A. & Bertozzi, C. R. A comparative study of bioorthogonal reactions with azides. *ACS Chemical Biology* **1**, 644-648 (2006).
43 Ma, L.-H., Takanishi, C. L. & Wood, M. J. Molecular Mechanism of Oxidative Stress Perception by the Orp1 Protein. *Journal of Biological Chemistry* **282**, 31429-31436 (2007).
44 Ellis, H. R. & Poole, L. B. Novel application of 7-chloro-4-nitrobenzo-2-oxa-1,3-diazole to identify cysteine sulfenic acid in the AhpC component of alkyl hydroperoxide reductase. *Biochemistry* **36**, 15013-15018 (1997).
45 Poole, L. B. & Ellis, H. R. Identification of cysteine sulfenic acid in AhpC of alkyl hydroperoxide reductase. *Methods in Enzymology* **348**, 122-136 (2002).
46 Reddie, K. G. & Carroll, K. S. Expanding the functional diversity of proteins through cysteine oxidation. *Curr Opin Chem Biol* **12**, 746-754 (2008).
47 Gelbart, M. E., Rechsteiner, T., Richmond, T. J. & Tsukiyama, T. Interactions of Isw2 chromatin remodeling complex with nucleosomal arrays: analyses using recombinant yeast histones and immobilized templates. *Mol Cell Biol* **21**, 2098-2106 (2001).
48 Gietz, R. D. & Schiestl, R. H. Applications of high efficiency lithium acetate transformation of intact yeast cells using single-stranded nucleic acids as carrier. *Yeast* **7**, 253-263 (1991).
49 Gietz, R. D. & Woods, R. A. Genetic transformation of yeast. *Biotechniques* **30**, 816-820, 822-816, 828 passim (2001).
50 Rose, M. D., Winston, F., Hieter, P. . *Methods in Yeast Genetics: A Laboratory Course Manual*. (Cold Spring Harbor Laboratory Press, 1990).
51 Mumberg, D., Muller, R. & Funk, M. Yeast vectors for the controlled expression of heterologous proteins in different genetic backgrounds. *Gene* **156**, 119-122 (1995).
52 Saxon, E. & Bertozzi, C. R. Cell surface engineering by a modified Staudinger reaction. *Science* **287**, 2007-2010 (2000).
53 Vocadlo, D. J., Hang, H. C., Kim, E.-J., Hanover, J. A. & Bertozzi, C. R. A chemical approach for identifying O-GlcNAc-modified proteins in cells. *Proceedings of the National Academy of Sciences of the United States of America* **100**, 9116-9121 (2003).
54 Ma, L. H., Takanishi, C. L. & Wood, M. J. Molecular mechanism of oxidative stress perception by the Orp1 protein. *J Biol Chem* **282**, 31429-31436 (2007).
55 Inoue, Y., Matsuda, T., Sugiyama, K., Izawa, S. & Kimura, A. Genetic analysis of glutathione peroxidase in oxidative stress response of Saccharomyces cerevisiae. *Journal of Biological Chemistry* **274**, 27002-27009 (1999).

Chapter 3

Determining the contribution of reactive oxygen species production to huntingtin (Ht) pathogenesis in yeast

3.1 Abstract

Neurodegenerative diseases, including Huntington's disease (HD), are characterized by protein aggregation and are associated with mitochondrial dysfunction and oxidative stress due to increased reactive oxygen species (ROS) production. Little is known, however, about the role that ROS play in disease pathogenesis. To characterize the interplay between mutant huntingtin protein (Ht) expression/aggregation and changes to the cellular redox status, we employed a yeast model of HD. Herein, we present initial studies to develop and optimize methods to detect ROS production, changes in the redox status of the cellular glutathione pool, and global protein oxidation in yeast. Ultimately, the low level of global protein oxidation detected and challenges with reproducibility resulted in the discontinuation of these studies.

3.2 Introduction

ROS including hydrogen peroxide (H_2O_2), superoxide ($O_2\bullet^-$), and the hydroxyl radical ($\bullet OH$) have been deemed toxic byproducts of aerobic existence. More recently, ROS have also been shown to function as necessary second messengers in a number of eukaryotic signaling cascades [1-4]. Nontheless, unchecked ROS production can result in indiscriminate oxidative damage to important biomolecules including proteins, lipids and

DNA, and can contribute to aging and pathologies such as cancer, diabetes, and neurodegenerative disorders [5-7].

HD is a progressive neurodegenerative disorder that is caused by a glutamine CAG expansion in the N-terminal portion of exon I of the huntingtin gene [8]. The wild type (WT) Ht is a large (~348 KDa), predominantly cytoplasmic, protein of complex albeit largely uncharacterized function that is known to interact with a number of proteins involved in vesicle transport, cytoskeletal anchoring, clathrin-mediated endocytosis, neuronal transport and/or postsynaptic signaling [9]. Mutant Ht is cleaved into a number of polyglutamine (polyQ)-containing fragments that misfold and form soluble and insoluble protein aggregates containing co-associating proteins. Accumulation of these soluble and insoluble Ht aggregates has been shown to result in mitochondrial toxicity and dysfunction due to reduced activity of electron transport chain (ETC) enzymes in mouse and yeast models of HD [10,11]. Additionally, decreased expression of ETC enzymes has been detected in post-mortem samples of affected brain regions [12]. The ETC funnels electrons from reduced matrix substrates through four protein complexes to molecular oxygen producing water and establishing a proton gradient across the inner mitochondrial membrane that drives ATP synthesis. Electrons can leak prematurely from these enzyme complexes, however, to result in $O_2\bullet^-$ production and, as expected, mitochondrial dysfunction is associated with increased ROS production [13]. Consistent with observations of mitochondrial dysfunction in HD, signs of irreversible oxidative damage to lipids and proteins is observed in post-mortem brain slices and in the plasma of HD patients [14,15].

A long-standing question in the redox biology field is whether ROS are produced as a toxic byproduct of protein aggregation in neurodegenerative disorders or whether the

ROS produced function to initiate and/or promote pathogenesis [16]. Moreover, identifying the protein targets of oxidative stress would shed light on how oxidative modification of proteins may be contributing to disease progression. Yeast models of HD have been developed wherein yeast express Ht constructs containing polyQ expansions of varying lengths conjugated to green fluorescent protein (GFP) to facilitate visualization of Ht aggregation as a function of polyQ length (**Figure 3.1a**) [17,18]. Ht constructs containing smaller polyQ expansions such as Q25 exhibit diffuse fluorescence (**Figure 3.1b**) whereas increasing length of the polyQ expansion results in increased protein aggregation (**Figure 3.1b**). Importantly, expression of the longest mutant Ht polyQ expansion protein, Q103 has been shown to induce mitochondrial dysfunction and ROS production in yeast [11]. These observations validate the use of this model to study the correlation between Ht expression/aggregation and changes in the cellular redox balance. Herein, we present initial studies that were performed to develop and optimize methods to detect ROS production, changes in the redox status of the cellular glutathione pool, and global protein oxidation in yeast. Ultimately, the low level of protein oxidation detected and issues with reproducibility resulted in the discontinuation of these studies.

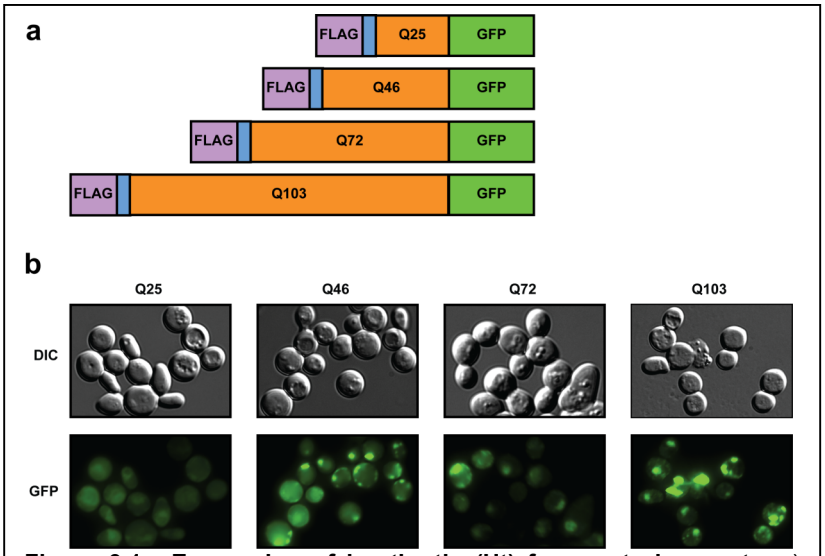

Figure 3.1. Expression of huntingtin (Ht) fragments in yeast. a) Schematic representation of the Ht exon I proteins with increasing polyQ expansion regions (orange), GFP (green), and FLAG (purple) tags. b) Expression of Ht proteins with various polyQ expansions was induced by growing exponentially growing yeast in media containing galactose for 25 h and analyzed for GFP staining.

3.3 Results and discussion

3.3.1 Exploration of methods to characterize the redox status of yeast

Our ultimate goal was to characterize the interplay between mutant Ht expression/aggregation and changes to cellular ROS production and protein oxidation. Changes in the cellular redox balance are routinely monitored by using fluorescent probes that report on ROS production, including 2',7'-dihydrodichlorofluorescein diacetate (H_2DCF-DA, **Figure 3.2a**) and dihydroethidium (DHE, **Figure 3.2b**) and by measuring fluctuations in the redox status of glutathione, a high abundance cellular antioxidant. Indeed, Barrientos and colleagues have previously demonstrated that Q103 Ht expression in yeast results in enhanced ROS production compared to yeast expressing Q25 Ht; however, the full panel of polyQ expansion proteins were not examined [11].

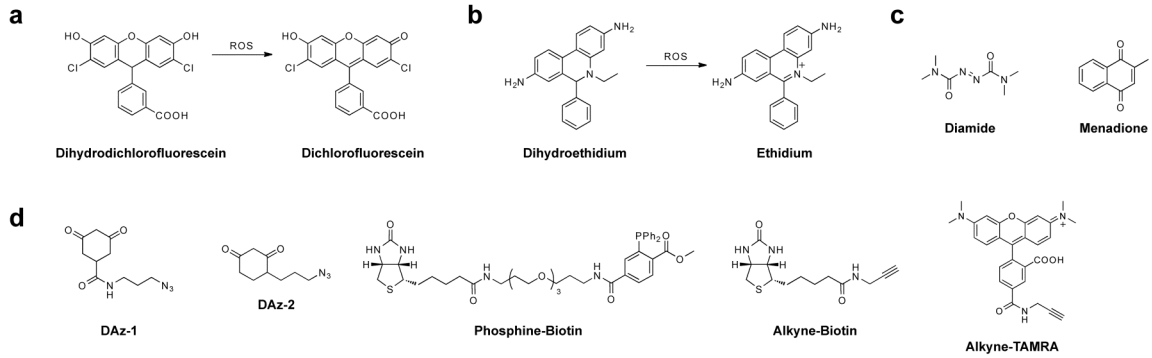

Figure 3.2. Compounds used in this study. Detection of intracellular ROS by oxidation of a) dihydrodichlorofluorescein (H_2DCF) to the fluorescent dichlorofluorescein (DCF), or b) dihydroethidium (DHE) to the fluorescent ethidium. c) Redox modulating compounds. Diamide oxidizes the cellular glutathione pool. Menadione induces redox cycling in the mitochondria resulting in $O_2^{\bullet-}$ formation. d) DAz-1 and DAz-2, sulfenic acid probes; phosphine-biotin (pBiotin) and alkyne-biotin, biotinylation reagents; alkyne-TAMRA, TAMRA-conjugating reagent.

As preliminary experiments, we first sought to demonstrate the utility of H_2DCF-DA and DHE in revealing differences in ROS content of WT versus Vma2Δ yeast under normal growth conditions and as a function of H_2O_2 or menadione treatment (**Figure 3.3**).

Vma2 is a vacuolar proton-translocating ATPase in yeast and its deletion has been shown to result in chronic oxidative stress [19]. Initially, we monitored changes in cellular ROS content with H_2DCF-DA, which is an oxidant-sensitive probe that is converted to the fluorescent product DCF by reaction with various ROS (**Figure 3.2a**). **Figure 3.3a** shows that while H_2DCF-DA detected a significant change in intracellular ROS content in cells treated with H_2O_2. However, inconsistent with literature, no significant difference in ROS content was revealed between WT and Vma2Δ yeast [19].

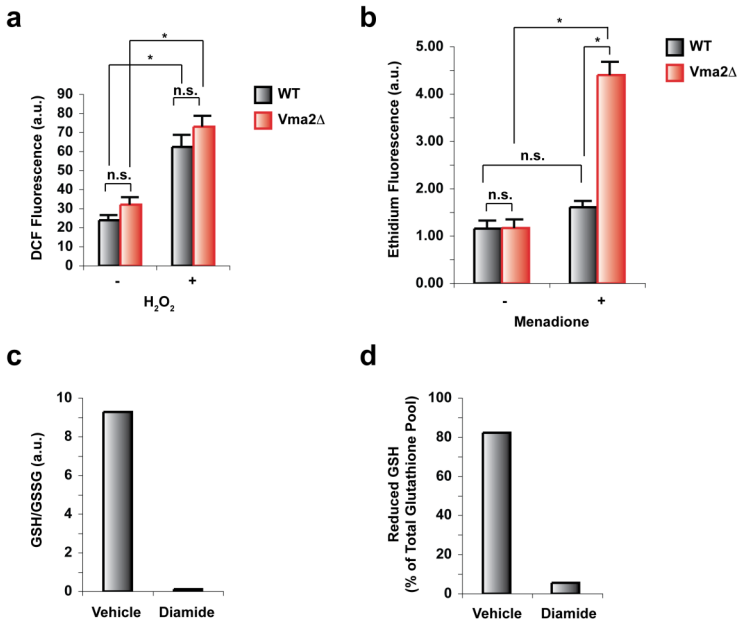

Figure 3.3. Characterization of the cellular redox status of WT and Vma2Δ yeast. a) Exponentially growing WT and Vma2Δ yeast were pre-loaded with 10 μM H_2DCF-DA for 15 min, stimulated with 1 mM H_2O_2 or vehicle control for 30 min at rt and intracellular ROS was measured by DCF fluorescence. b) Exponentially growing WT and Vma2Δ were incubated with 5 μM DHE and 1 mM menadione or vehicle control for 30 min at 37 °C and intracellular ROS was measured by ethidium fluorescence. Error bars represent s.e.m. of four readings. Statistical significance was determined by two-tailed Student's T-test with a $p < 0.05$ cutoff. n.s., not significant; *, $p < 0.001$. c and d) Exponentially growing WT yeast were incubated with 1.5 mM diamide or vehicle for 30 min at 30 °C and analyzed for c) GSH/GSSG or d) reduced GSH as a percentage of the total glutathione pool.

Because Q103 Ht expression in yeast induces mitochondrial dysfunction, we hypothesized that $O_2^{\bullet -}$ levels would increase [19]. While H_2DCF-DA exhibits broad reactivity with radical- and non radical-based ROS, DHE is an oxidant-sensitive probe that is converted to the fluorescent ethidium product primarily by reaction with radical-based ROS such as $O_2^{\bullet -}$ (**Figure 3.2b**) [20]. We, therefore, explored the utility of DHE to

detect changes in ROS content between WT and Vma2Δ yeast that have been untreated or treated with menadione, a compound that induces redox cycling in the mitochondria resulting in increased levels of $O_2\bullet^-$ (**Figure 3.2c**). While DHE did not reveal differences in basal ROS content among untreated, menadione-treated WT, and untreated Vma2Δ yeast, menadione treatment induced a significant increase in DHE oxidation in Vma2Δ cells (**Figure 3.3b**). Thus neither H_2DCF-DA nor DHE revealed differences in basal ROS content between WT and Vma2Δ yeast. This suggests either that these probes are insufficiently sensitive to monitor fluctuations in ROS production unless the changes are similar to those induced by exogenous H_2O_2 or menadione treatment, or that Vma2 deletion is not associated with a significant change in ROS.

In addition to monitoring changes in ROS production, fluctuations in the cellular redox balance can also be observed by characterizing the redox status of the cellular glutathione pool. Treatment of WT yeast with diamide, a compound that oxidizes the cellular glutathione pool (**Figure 3.2c**), resulted in a substantial decrease in the ratio of reduced to oxidized glutathione (GSH/GSSG, **Figure 3.3c**) and in the percentage of reduced glutathione (**Figure 3.3d**). Having demonstrated that the cellular redox status of pharmacologically treated yeast could be characterized by monitoring ROS production and determining the redox status of the cellular glutathione pool, we next sought to establish a protocol for profiling global protein oxidation in yeast.

3.3.2 Development of a method to profile global protein sulfenylation in yeast

Genetic and biochemical studies implicate protein cysteine thiols as the primary targets of intracellular ROS [2,21-25]. Given that Q103 Ht expression has been shown to stimulate ROS production in yeast [19], mutant Ht expression could potentially stimulate changes in

global protein oxidation that could contribute to disease progression. Interestingly, the N terminus of Ht contains several cysteine residues in addition to the polyQ expansion region, entertaining the possibility of direct redox modulation of Ht function or its propensity for aggregation [26,27]. Furthermore, N-terminal fragments of Ht have been shown to interact with and chemically reduce copper (II) to copper (I) [28]. Copper (I) can then react with molecular oxygen to generate $O_2\bullet^-$ that rapidly dismutates to H_2O_2. However, the relative contribution of Ht-bound copper versus mitochondrial dysfunction to $O_2\bullet^-$ generation in neurodegenerative disorders remains unknown. Nonetheless, both copper (I) and copper (II) can react with H_2O_2 to generate •OH and •OOH, respectively *via* Fenton-like chemistry that can ultimately result in protein oxidation [29]. If Cu-bound Ht serves as a significant source of intracellular ROS, then it is possible that proteins associating with Ht could be direct targets of this ROS. To address these collective possibilities we sought to develop a method to profile global protein oxidation in mutant Ht-expressing yeast that could also be applied to characterization of the oxidation status of mutant Ht and its co-associating proteins.

The initial reaction product of a protein thiol with ROS such as H_2O_2 is sulfenic acid, which is detected with high selectivity by reaction with the 1,3-cyclohexadione compound dimedone (**Figure 3.4a**). The selective reaction of dimedone with protein sulfenic acids has been exploited to detect oxidized proteins in cell lysates by conjugating the 1,3-cyclohexadione warhead to biotin or fluorophores [30,31]. Our lab has recently demonstrated the functionalization of 1,3-cyclohexadiones with azide chemical handles to facilitate labeling of protein sulfenic acids directly in cells [32-34]. The first of these probes, DAz-1 (**Figure 3.2d**), was used to demonstrate requirement for sulfenic acid modification of Gpx3 in the Yap1-Gpx3 redox relay in yeast [35]. In our study, a substantial amount of DAz-1 was required (50 μM) due to its low reactivity, the relatively

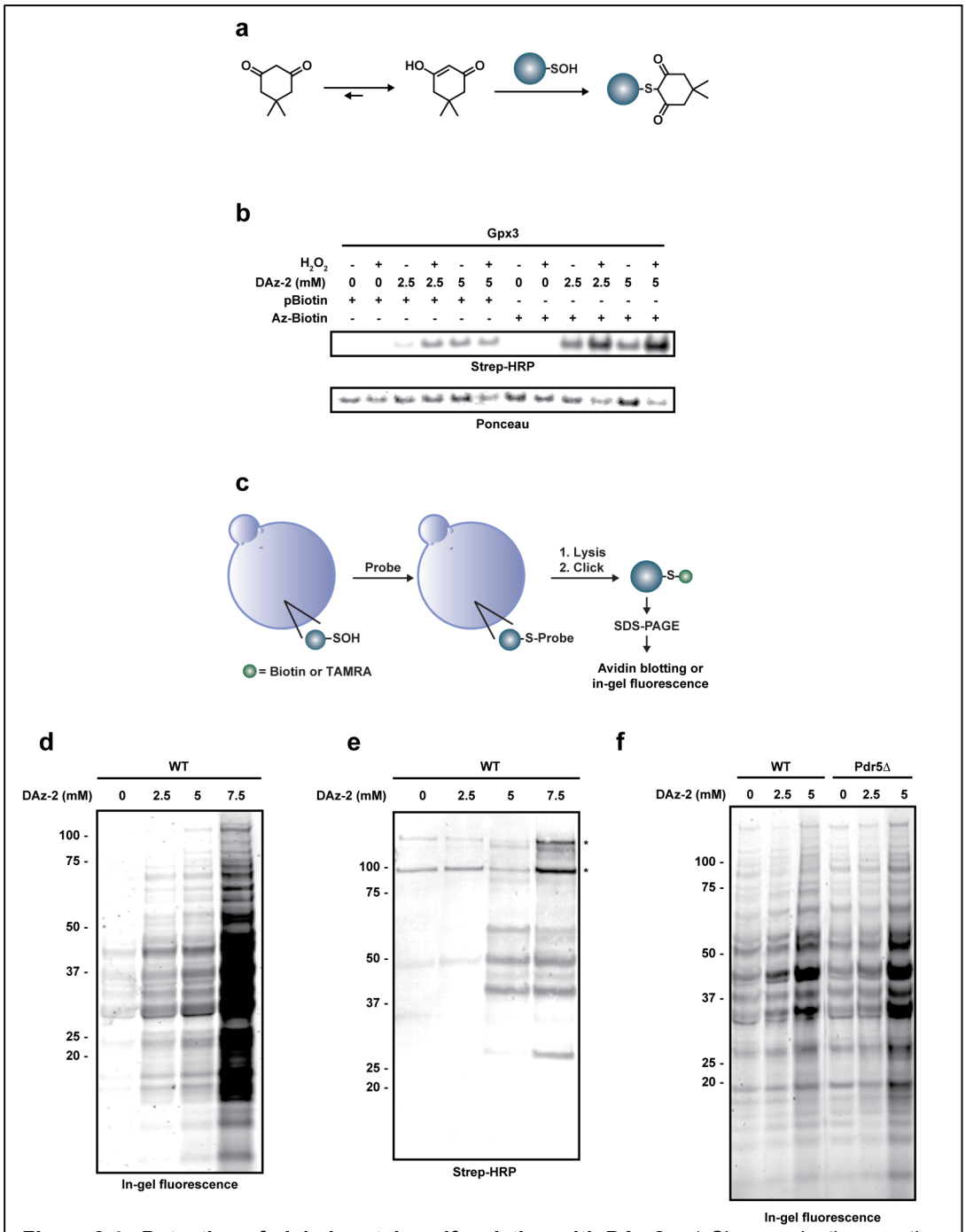

Figure 3.4. Detection of global protein sulfenylation with DAz-2. a) Chemoselective reaction of dimedone with protein sulfenic acids yields a covalent adduct. b) Click chemistry is more efficient than Staudinger ligation. Recombinant Cys82Ser Gpx3 (50 µM), untreated or exposed to 100 µM H_2O_2, was incubated with the indicated concentrations of DAz-2 or vehicle control for 15 min at rt. After DAz-2 labeling, samples were treated with pBiotin (250 µM) or alkyne-biotin (100 µM) and analyzed by streptavidin-HRP western blot. Protein loading was assessed by ponceau S stain. c) Decoupled strategy to label protein sulfenic acids with DAz-2 in yeast. d and e) Exponentially growing WT yeast were incubated with the indicated concentrations of DAz-2 for 2 h at 37 ^{o}C. Excess probe was washed away, extracts were prepared, and DAz-2 modified proteins were conjugated with d) alkyne-TAMRA or e) alkyne-biotin and analyzed by d) in-gel fluorescence or e) streptavidin-HRP blot. f) Exponentially growing WT and Pdr5Δ were incubated with the indicated concentrations of DAz-2 for 2 h at 37 ^{o}C and processed as in (d).

low expression of endogenous Gpx3, and the inefficiency of the Staudinger ligation reaction. Our second azido-dimedone probe, DAz-2, is more reactive than DAz-1 [34]. Therefore, we employed DAz-2 to develop a method that was more feasible for the detailed investigation of global protein sulfenylation to enhance sensitivity and lessen the amount of probe required. As an additional means to increase detection sensitivity, we also used click chemistry to append biotin or TAMRA tags as it is more efficient than Staudinger ligation (**Figure 3.4b**).

DAz-2 and alkyne-biotin or alkyne-TAMRA were used to establish a protocol to profile global protein sulfenylation in WT yeast (**Figure 3.4c**). We found that DAz-2 detected global protein sulfenylation in a dose-dependent manner in WT yeast as monitored by in-gel fluorescence (**Figure 3.4d**) and streptavidin-HRP Western blot (**Figure 3.4e**). The labeling efficiency, however, was far lower than what was routinely detected with mammalian cells (*e.g.* 1:30,000 streptavidin-HRP was required for detection in yeast cells whereas 1:50,000 – 1:80,000 is used for mammalian cells) and the results were insufficiently reproducible (data not shown). We additionally assessed the effect of exogenous H_2O_2 and redox modulating compounds on global protein sulfenylation, however reproducible increases in protein oxidation were not observed (data not shown). One possible reason for the decreased labeling of protein sulfenic acids in yeast and the complications with reproducibility could be due to insufficient probe retention. *S. cerevisiae* expresses xenobiotic export channels that could be expected to influence probe retention [36]. To determine the effect of the exportin channels on the observed level of global protein sulfenylation, we used a Pdr5 deletion yeast strain that is lacking Pdr5, a multidrug transporter that is involved in the pleiotropic drug response [36,37]. Unfortunately, deletion of Pdr5 did not appear to have a significant effect on the extent of global protein sulfenylation observed with DAz-2 (**Figure 3.4f**) and also failed

to increase the reproducibility of labeling results, suggesting that Pdr5 deletion had no effect on probe retention (data not shown). These collective results show that global protein sulfenylation can be detected in yeast using DAz-2. However, the extent of labeling and reproducibility is quite low, which could suggest that protein sulfenylation is not a common mechanism for protein regulation in this organism. Alternatively, and perhaps more likely, sulfenic acid probes with enhanced reactivity may be required to detect global protein sulfenylation in this organism.

3.4 Conclusion

The goal of this study was to characterize the redox status of yeast and to profile global and targeted protein sulfenylation in response to mutant Ht expression as a function of polyQ expansion size. These studies would have marked the first investigation into a correlation between mutant Ht-induced ROS production and protein oxidation in cells. To begin these studies, we first needed to establish methods that would allow us to characterize ROS production, changes in the redox status of the cellular glutathione pool and to reproducibly detect global protein sulfenylation. We have demonstrated that H_2DCF-DA and DHE can detect large increases in cellular ROS due to exogenous application of ROS or redox modulating compounds. However, whether H_2DCF-DA or DHE are sensitive enough to detect the changes in ROS content that are associated with expression of mutant Ht of differing polyQ expansions in yeast is unknown. Additionally, we were able to establish a protocol to profile global protein sulfenylation in yeast, but issues with reproducibility and sensitivity ultimately resulted in the discontinuation of these studies. Since the cessation of this project, a report by Hersch and colleagues has demonstrated that cysteine residues in the N-terminal portion of Ht are susceptible to oxidative modification when expressed in mammalian cell culture. While the specific cysteine oxoform was not identified, oxidation of this N-terminal

fragment was shown to delay clearance of soluble Ht protein, which is believed to be the toxic species [26]. In this way, cysteine oxidation of Ht appears to increase the burden of soluble mutant protein, which could contribute to disease progression.

3.5 Experimental procedures

3.5.1 Strains and growth conditions

The *S. cerevisiae* strains WT, Vma2Δ, and Pdr5Δ, which were kind gifts from Prof. Anuj Kumar (University of Michigan), are in the BY4742 (MATα his3Δ1 leu2Δ0 lys2Δ0 ura3Δ0 can1-100) background and were used in all experiments, with the exception of the Q25, Q46, Q72, and Q103 Ht-expressing strains, which were a generous gift from Prof. Jason Gestwicki (University of Michigan). WT, Vma2Δ and Pdr5Δ were grown at 30 ^{o}C in YPD (1% yeast extracts, 2% bactopeptone, and 2% glucose). Ht-expressing yeast were grown at 30 ^{o}C in SC – His media containing 2% glucose. Induction of Ht protein expression for fluorescence microscopy was achieved by growing yeast cultures in selective media containing 2% raffinose as the sole carbon source overnight followed by growth in SC – His media containing 2% galactose for 25 h.

3.5.2 Fluorescence microscopy

Yeast were fixed and analyzed by fluorescence microscopy for GFP-tagged Ht proteins as previously described [35].

3.5.3 Stock preparation

All stocks were freshly prepared, unless otherwise indicated. Dihydrodichlorofluorescein-diacetate (Sigma) was prepared at 1 mM in DMSO. Dihydroethidium (Sigma) was prepared at 100 μM in acetonitrile. Diamide, a gift from

Prof. Ursula Jakob (University of Michigan), was prepared at 1 M in distilled water. Menadione (AnaSpec) was prepared at 100 mM in methanol. DAz-2 and phosphine-biotin were synthesized and purified as previously described [34]. Alkyne-biotin was synthesized according to established literature procedures [38]. DAz-2 was prepared in DMSO at 250 mM. Phosphine-biotin (pBiotin) and alkyne-biotin were prepared in DMSO and alkyne-TAMRA (Invitrogen) was prepared in dimethylformamide at 5 mM. pBiotin stocks were stored in a dessicator at -80 ^{o}C whereas DAz-2, alkyne-biotin, and alkyne-TAMRA stocks were stored at -20 ^{o}C.

3.5.4 Intracellular ROS detection with DCF

Intracellular ROS were measured in a 96-well plate using the fluorescent probe DCF (the intracellular product of H_2DCF-DA that fluoresces in the presence of ROS, including H_2O_2). Exponentially growing yeast were resuspended in 50 mM HEPES pH 7.4 and 10^5 cells were apportioned to each well. The cells were pre-loaded with 10 µM H_2DCF-DA for 15 min at rt and then stimulated with 1 mM H_2O_2 or vehicle control and incubated for an additional 30 min at rt. After incubation, the intensity of fluorescence was measured at 488 nm (excitation) and 525 nm (emission) using a SpectraMax M5 microplate reader (Molecular Devices).

3.5.5 Intracellular ROS detection with DHE

Intracellular ROS were measured in a 96-well plate using the fluorescent probe ethidium (the intracellular product of DHE that fluoresces in the presence of radical-based ROS). Exponentially growing WT and Vma2Δ yeast (10^7 cells) were washed with PBS (x 2), resuspended in PBS (500 µl) and incubated with 5 µM DHE at 37 ^{o}C for 30 min in the presence of 1 mM menadione or vehicle control. Afterwards, the cells were washed with PBS (x 2), resuspended in PBS (90 µl), and apportioned to 3 wells. The intensity of

fluorescence was measured at 510 nm (excitation) and 580 nm (emission) using a SpectraMax M5 microplate reader (Molecular Devices).

3.5.6 Quantification of glutathione in WT yeast cells.

Exponentially growing WT yeast were treated with 1.5 mM diamide or vehicle at 30 ^{o}C for 30 min. The cells were then harvested in 5% sulfosalicylic acid and lysed by mechanical disruption with glass beads. Levels of total, reduced, and oxidized glutathione were measured using the Glutathione Fluorescent Detection kit (Luminos) according to the manufacturer's instructions.

3.5.7 Expression, purification, and labeling of sulfenylated Gpx3

Cys82Ser Gpx3 was expressed and purified as previously described [35]. Cys82Ser Gpx3 was previously stored in 50 mM Tris HCl pH 7.4, 300 mM NaCl, 10% glycerol, and 5 mM DTT. DTT was removed from Cys82Ser Gpx3 *via* spin filtration using P-30 micro BioSpin columns (BioRad) pre-equilibrated with Gpx3 buffer (50 mM Tris HCl pH 7.4, 300 mM NaCl). 50 µM Cys82Ser Gpx3 was treated with 0, 2.5, or 5 mM DAz-2 in the presence or absence of 100 µM H_2O_2 at rt for 15 min. Excess probe was removed by spin filtration as above and DAz-2 modified Cys82Ser Gpx3 was biotinylated and analyzed as described below. After bioorthogonal reactions, the samples were quenched by addition of SDS loading dye.

3.5.8 Yeast culture with DAz-2

Exponentially growing yeast were incubated with DAz-2 (2.5 – 7.5 mM) or DMSO vehicle control at 30 ^{o}C for 2 h with periodic gentle agitation. Following treatment, cells were collected, and washed with PBS. Cells were resuspended in triethanolamine lysis buffer (50 mM triethanolamine pH 7.4, 150 mM NaCl, 1x yeast protease inhibitor cocktail

(Sigma), 40 μM chymostatin) and lysates were generated by mechanical disruption with glass beads. The protein concentration of the lysates was determined by the Bradford assay (BioRad).

3.5.9 Bioorthogonal chemistries

DAz-2 modified Gpx3 was conjugated to biotin *via* Staudinger ligation with phosphine biotin (p-Biotin; 250 μM) for 2 h at 37 °C as previously described[35] or *via* click chemistry with alkyne-biotin (100 μM alkyne-biotin, 1 mM TCEP, 100 μM TBTA, 1 mM $CuSO_4$) for 1 h at rt. Lysates (20 – 50 μg) generated from DAz-2 treated cells were conjugated to biotin or TAMRA *via* click chemistry (100 μM alkyne-biotin or alkyne-TAMRA, 1 mM TCEP, 100 μM TBTA, 1 mM $CuSO_4$) for 1 h at rt. Reactions with alkyne-TAMRA were performed in the dark. Afterwards, the reactions were quenched by methanol precipitation and the resulting protein pellets were resuspended in SDS sample loading dye.

3.5.10 Western blot and in-gel fluorescence analyses

Protein samples were subjected to SDS-PAGE and Western blot analyses as previously described [32,35]. Briefly, biotinylated proteins were detected by blocking the PVDF membrane with 3% BSA in Tris-buffered saline Tween-20 (TBST) for 1 h at rt, washing with TBST (3 x 5 min) and incubating with 1:25,000 – 1:30,00 streptavidin-HRP (GE Healthcare) in TBST for 1 h at rt. Western blots were developed with chemiluminescence (GE Healthcare ECL Plus Western Blot Detection System) and imaged on a Typhoon 9410. In-gel fluorescence of SDS-PAGE gels was imaged using the TAMRA settings on a Typhoon 9410.

3.6 References

1 D'Autreaux, B. & Toledano, M. B. ROS as signalling molecules: mechanisms that generate specificity in ROS homeostasis. *Nat Rev Mol Cell Biol* **8**, 813-824 (2007).

2 Paulsen, C. E. & Carroll, K. S. Orchestrating redox signaling networks through regulatory cysteine switches. *ACS Chem Biol* **5**, 47-62 (2010).

3 Rhee, S. G. Cell signaling. H2O2, a necessary evil for cell signaling. *Science* **312**, 1882-1883 (2006).

4 Stone, J. R. & Yang, S. Hydrogen peroxide: a signaling messenger. *Antioxid Redox Signal* **8**, 243-270 (2006).

5 Andersen, J. K. Oxidative stress in neurodegeneration: cause or consequence? *Nat Med* **10 Suppl**, S18-25 (2004).

6 Klaunig, J. E. & Kamendulis, L. M. The role of oxidative stress in carcinogenesis. *Annu Rev Pharmacol Toxicol* **44**, 239-267 (2004).

7 Lowell, B. B. & Shulman, G. I. Mitochondrial dysfunction and type 2 diabetes. *Science* **307**, 384-387 (2005).

8 A novel gene containing a trinucleotide repeat that is expanded and unstable on Huntington's disease chromosomes. The Huntington's Disease Collaborative Research Group. *Cell* **72**, 971-983 (1993).

9 Landles, C. & Bates, G. P. Huntingtin and the molecular pathogenesis of Huntington's disease. Fourth in molecular medicine review series. *EMBO Rep* **5**, 958-963 (2004).

10 Oliveira, J. M. *et al.* Mitochondrial dysfunction in Huntington's disease: the bioenergetics of isolated and in situ mitochondria from transgenic mice. *J Neurochem* **101**, 241-249 (2007).

11 Solans, A., Zambrano, A., Rodriguez, M. & Barrientos, A. Cytotoxicity of a mutant huntingtin fragment in yeast involves early alterations in mitochondrial OXPHOS complexes II and III. *Hum Mol Genet* **15**, 3063-3081 (2006).

12 Gu, M. *et al.* Mitochondrial defect in Huntington's disease caudate nucleus. *Ann Neurol* **39**, 385-389 (1996).

13 Trushina, E. & McMurray, C. T. Oxidative stress and mitochondrial dysfunction in neurodegenerative diseases. *Neuroscience* **145**, 1233-1248 (2007).

14 Butterfield, D. A. & Kanski, J. Brain protein oxidation in age-related neurodegenerative disorders that are associated with aggregated proteins. *Mech Ageing Dev* **122**, 945-962 (2001).

15 Klepac, N. *et al.* Oxidative stress parameters in plasma of Huntington's disease patients, asymptomatic Huntington's disease gene carriers and healthy subjects : a cross-sectional study. *J Neurol* **254**, 1676-1683 (2007).

16 Emerit, J., Edeas, M. & Bricaire, F. Neurodegenerative diseases and oxidative stress. *Biomed Pharmacother* **58**, 39-46 (2004).

17 Duennwald, M. L., Jagadish, S., Muchowski, P. J. & Lindquist, S. Flanking sequences profoundly alter polyglutamine toxicity in yeast. *Proc Natl Acad Sci U S A* **103**, 11045-11050 (2006).

18 Krobitsch, S. & Lindquist, S. Aggregation of huntingtin in yeast varies with the length of the polyglutamine expansion and the expression of chaperone proteins. *Proc Natl Acad Sci U S A* **97**, 1589-1594 (2000).

19 Milgrom, E., Diab, H., Middleton, F. & Kane, P. M. Loss of vacuolar proton-translocating ATPase activity in yeast results in chronic oxidative stress. *J Biol Chem* **282**, 7125-7136 (2007).

20 Fink, B. *et al.* Detection of intracellular superoxide formation in endothelial cells and intact tissues using dihydroethidium and an HPLC-based assay. *Am J Physiol Cell Physiol* **287**, C895-902 (2004).
21 Dansen, T. B. *et al.* Redox-sensitive cysteines bridge p300/CBP-mediated acetylation and FoxO4 activity. *Nat Chem Biol* **5**, 664-672 (2009).
22 Fomenko, D. E. *et al.* Thiol peroxidases mediate specific genome-wide regulation of gene expression in response to hydrogen peroxide. *Proc Natl Acad Sci U S A* **108**, 2729-2734 (2011).
23 Klomsiri, C., Karplus, P. A. & Poole, L. B. Cysteine-based redox switches in enzymes. *Antioxid Redox Signal* **14**, 1065-1077 (2011).
24 Weerapana, E. *et al.* Quantitative reactivity profiling predicts functional cysteines in proteomes. *Nature* **468**, 790-795 (2010).
25 Winterbourn, C. C. & Hampton, M. B. Thiol chemistry and specificity in redox signaling. *Free Radic Biol Med* **45**, 549-561 (2008).
26 Fox, J. H. *et al.* Cysteine oxidation within N-terminal mutant huntingtin promotes oligomerization and delays clearance of soluble protein. *J Biol Chem* **286**, 18320-18330 (2011).
27 Landles, C. *et al.* Proteolysis of mutant huntingtin produces an exon 1 fragment that accumulates as an aggregated protein in neuronal nuclei in Huntington disease. *J Biol Chem* **285**, 8808-8823 (2010).
28 Fox, J. H. *et al.* Mechanisms of copper ion mediated Huntington's disease progression. *PLoS One* **2**, e334 (2007).
29 Ramirez, D. C., Mejiba, S. E. & Mason, R. P. Copper-catalyzed protein oxidation and its modulation by carbon dioxide: enhancement of protein radicals in cells. *J Biol Chem* **280**, 27402-27411 (2005).
30 Charles, R. L. *et al.* Protein sulfenation as a redox sensor: proteomics studies using a novel biotinylated dimedone analogue. *Mol Cell Proteomics* **6**, 1473-1484 (2007).
31 Poole, L. B. *et al.* Fluorescent and affinity-based tools to detect cysteine sulfenic acid formation in proteins. *Bioconjug Chem* **18**, 2004-2017 (2007).
32 Reddie, K. G., Seo, Y. H., Muse III, W. B., Leonard, S. E. & Carroll, K. S. A chemical approach for detecting sulfenic acid-modified proteins in living cells. *Mol Biosyst* **4**, 521-531 (2008).
33 Seo, Y. H. & Carroll, K. S. Facile synthesis and biological evaluation of a cell-permeable probe to detect redox-regulated proteins. *Bioorg Med Chem Lett* **19**, 356-359 (2009).
34 Leonard, S. E., Reddie, K. G. & Carroll, K. S. Mining the thiol proteome for sulfenic acid modifications reveals new targets for oxidation in cells. *ACS Chem Biol* **4**, 783-799 (2009).
35 Paulsen, C. E. & Carroll, K. S. Chemical dissection of an essential redox switch in yeast. *Chem Biol* **16**, 217-225 (2009).
36 Sipos, G. & Kuchler, K. Fungal ATP-binding cassette (ABC) transporters in drug resistance & detoxification. *Curr Drug Targets* **7**, 471-481 (2006).
37 Lamping, E. *et al.* Characterization of three classes of membrane proteins involved in fungal azole resistance by functional hyperexpression in Saccharomyces cerevisiae. *Eukaryot Cell* **6**, 1150-1165 (2007).
38 Zhao, X. Z. *et al.* Biotinylated biphenyl ketone-containing 2,4-dioxobutanoic acids designed as HIV-1 integrase photoaffinity ligands. *Bioorg Med Chem* **14**, 7816-7825 (2006).

Chapter 4

Protein sulfenylation goes global: Probing intracellular targets of hydrogen peroxide produced for growth factor signaling

4.1 Abstract

Since its discovery, protein sulfenylation (–SOH) has been studied almost exclusively in the context of peroxide metabolism, oxidative stress and biomolecular damage. With the identification of new classes of sulfenylated proteins and associated enzyme reducing systems, the regulatory power of this modification is now coming to the fore. However, investigating the biological role of sulfenylation still poses a major challenge, particularly within complex biological environments. Herein, we report the design and synthesis of DYn-2, a new alkyne-functionalized probe for detecting cellular sulfenic acids with improved sensitivity. After establishing the utility of DYn-2 in prototype systems we show, for the first time, that hydrogen peroxide (H_2O_2) produced by growth factor stimulation leads to dynamic and global changes in protein sulfenylation in cells. Furthermore, we identify the epidermal growth factor receptor (EGFR) as a new and sensitive target of endogenous H_2O_2 generation, and provide evidence for proximity-based thiol oxidation vis-à-vis growth factor-dependent association of the receptor and the NADPH oxidase, Nox2. The site of EGFR oxidation was directly mapped to active site Cys797 and functional studies show that H_2O_2 modulates intrinsic receptor tyrosine kinase activity, indicating that sulfenylation as well as phosphorylation regulate EGFR function. These results shed new light on the molecular mechanisms that underlie redox

signaling pathways and also have implications for irreversible inhibitors that target oxidant-sensitive cysteine residues in kinases and other therapeutically important proteins.

4.2 Introduction

H_2O_2 is a source of oxidative stress, but also acts as an essential second messenger in signal transduction networks of normal healthy cells, wherein growth factors, cytokines and a variety of other ligands trigger production of hydrogen peroxide (H_2O_2) through activation of their corresponding receptors[1-3]. Indeed, H_2O_2 has been demonstrated to regulate many basic cellular processes including proliferation, differentiation, growth, migration, and survival. For instance, binding of epidermal growth factor (EGF) to the extracellular domain of the EGF receptor (EGFR) results in the assembly and activation of NADPH oxidase (Nox) complexes, which generate H_2O_2[4,5]. Once formed, peroxide modulates signaling cascades by reaction with specific biomolecular targets (**Figure 4.1a**).

There is now a wealth of evidence indicating that protein cysteine residues are sensitive and critical targets of H_2O_2, both by direct oxidation and vis-à-vis thiol peroxidases[6-11]. The product of the direct reaction between H_2O_2 and a protein thiolate ($–S^-$) is sulfenic acid (–SOH). Sulfenylation is reversible (either directly or indirectly by disulfide formation) and affords a mechanism in which changes in cellular redox state can be exploited to regulate protein function, analogous to phosphorylation[12-14]. Recent studies shed new light on the role of sulfenic acid and also expanded the repertoire of proteins that can undergo sulfenylation[15-21], hinting at the regulatory potential and significance of these modifications. However, the scope of protein sulfenylation in complex biological processes, particularly in mammalian signal transduction, remains virtually unknown.

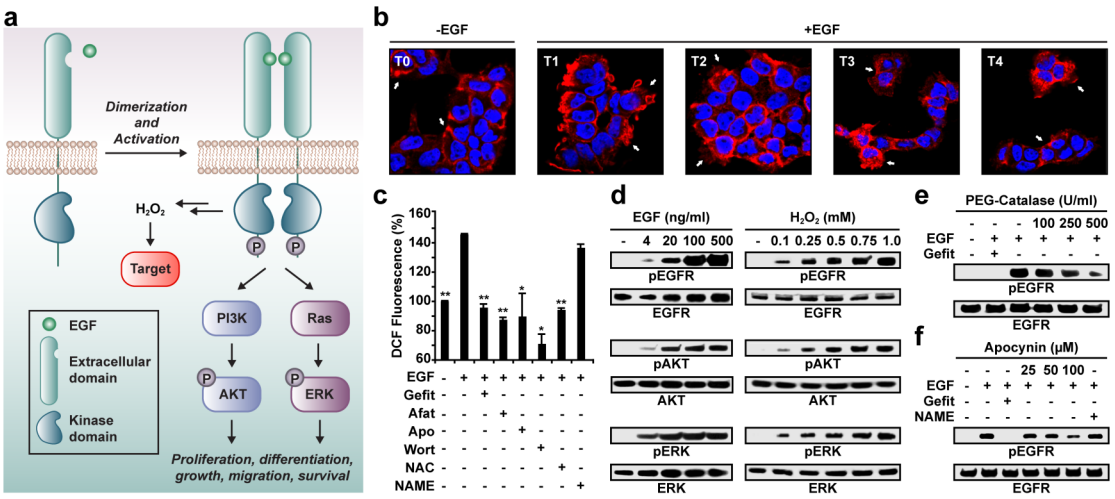

Figure 4.1. Cellular redox status affects epidermal growth factor (EGF)-mediated signaling. (**a**) Ligand binding to epidermal growth factor receptors (EGFRs) and their subsequent dimerization induces receptor auto-phosphorylation by the intrinsic tyrosine kinase activity on specific residues in the cytoplasmic domain. The phosphorylated sites serve as docking sites for various proteins involved in the activation and regulation of key prosurvival pathways, such as PI3K/AKT and RAS/ERK. Receptor-ligand interaction also results in activation of the Nox family of NADPH oxidases (not shown), which in turn stimulates the production of ROS and oxidation of intracellular biomolecules, leading to modulation of the signaling cascade. Protein targets of growth factor-induced ROS are generally implied from studies in complex lysates or recombinant proteins and, to date, have not been detected directly in cells. (**b**) Confocal fluorescence image of A431 cells before (T0) and after 100 ng/ml EGF stimulation for 2, 15, 30, and 60 min (labeled as T1, T2, T3, and T4, respectively). Cells were fixed and stained as described in Methods with rabbit anti-EGFR antibody (2 μg/ml) followed by Alexa594-conjugated (red) goat anti-rabbit secondary antibody (1:1000). White arrows highlight changes in receptor localization (T0, plasma membrane; T1, membrane ruffles; T2, regions of cell stretching and migration; T3, perinuclear and endosomal membranes; T4, plasma membrane and ruffles). Nuclei were counterstained with DAPI (blue). (**c**) EGF-induced ROS generation in A431 cells as revealed by DCF fluorescence. A431 cells were stimulated with 500 ng/ml EGF or vehicle for 5 min, after which the generation of intracellular ROS was measured by DCF fluorescence as described in Methods. Where indicated, A431 cells were treated with 10 μM gefitinib, 1 μM afatinib, 100 μM apocynin, 100 μM wortmannin or 100 μM L-NAME for 25 min or 20 mM NAC for 10 min before EGF stimulation. Data were normalized to the vehicle control and error bars show ± s.e.m. Statistical analysis was by a two-tailed Student's t test; ** indicates that $P < 0.001$, * indicates that $P < 0.05$ when compared against EGF-only treated cells. (**d**-**f**) Western blots showing phosphorylated (p) and total EGFR, AKT, and/or ERK. Phospho-antibodies recognize EGFR pY1068, AKT pS473, or ERK pT185/pY187. Note that the ERK1 and ERK2 isoforms (44 and 42 kDa, respectively) appear as a single band on the SDS-PAGE gradient gels. A431 cells were stimulated with the indicated concentrations of EGF or H_2O_2 or vehicle for 5 min (**d**), or stimulated with 100 ng/ml EGF or vehicle for 5 min (**e**,**f**). Where specified, cells were treated with the indicated concentrations of PEG-catalase for 30 min (**e**), or apocynin for 25 min (**f**) prior to EGF stimulation. Gefitinib treatment was performed as in **c**. pEGFR, pAKT, and/or pERK were analyzed from whole-cell lysates, and blots were stripped and reprobed for total protein as loading controls.

Investigating the functional role of protein sulfenylation still poses a major challenge, particularly within complex biological environments. To this end, we have developed DYn-2, a new alkyne-functionalized probe for detecting cellular sulfenic acids with improved sensitivity. After establishing its utility in prototype systems, we used this new

probe to show that EGFR-mediated generation of H_2O_2 is accompanied by dynamic and global changes in protein sulfenylation. We then demonstrate that protein tyrosine phosphatases (PTPs), which are important regulators of mitogenic signaling, undergo differential, EGF-dependent sulfenylation in cells. Furthermore, we identify EGFR as a new and sensitive target of endogenous H_2O_2 production, mediated by EGF-dependent association with Nox2. The site of EGFR oxidation was directly mapped to active site Cys797 and biochemical studies show that low levels of H_2O_2 can modulate intrinsic kinase activity, affording the first evidence that sulfenylation as well as phosphorylation can directly regulate receptor tyrosine kinase (RTK) function.

4.3 Results

4.3.1 EGF stimulation modulates cell morphology and EGFR trafficking

To investigate events after the interaction of EGF with its cell surface receptor we used the human epidermoid carcinoma A431 cell line, which naturally expresses high levels of EGFR. As shown by phase contrast microscopy, EGF stimulation induced rapid changes in cell shape and architecture (**Appendix 4.6.1**). Membrane ruffling was observed within 2 minutes; however, this activity subsided within 15 minutes, followed by retraction and regrowth. Next, we used immunofluorescence to determine whether EGF-dependent changes in cell morphology coincided with EGFR mobilization (red, **Figure 4.1b**). EGFR localized to the plasma membrane without EGF stimulation and concentrated at sites of membrane ruffling within two minutes of mitogen treatment. Fifteen minutes after EGF exposure, peripheral staining of EGFR had decreased and, by thirty minutes, the majority had accumulated in punctate foci throughout the peripheral cytoplasm. After one hour, some internalized receptors had recycled back to the plasma membrane. These data show that EGF stimulation leads to dramatic changes in A431

cell morphology and EGFR subcellular localization, consistent with immunohistochemistry and cryo-electron microscopy analysis[22,23], setting the stage to probe ROS-mediated signal transduction, as detailed below.

4.3.2 Cellular redox status affects EGF-mediated signaling in A431 cells

Although aspects of redox signaling have been studied in A431 cells, there is surprisingly limited data regarding the relationship between ROS and phosphorylation of major downstream receptor targets or EGFR inhibitors and thus, we first characterized these fundamental properties. Intracellular generation of ROS was measured using the conversion of the oxidant-sensitive probe 2',7'-dihydro-dichlorofluorescin diacetate (H_2DCF-DA) to fluorescent product DCF. Coincident with membrane ruffling, EGF-stimulated A431 cells exhibited an increase in DCF fluorescence intensity (**Figure 4.1c**). Moreover, reversible and irreversible inhibitors of EGFR (gefitinib and afatinib, respectively), Nox (apocynin), PI3K (wortmannin), and the antioxidant NAC (**Appendix 4.6.2**) attenuated EGF-dependent ROS generation. Control experiments with the NO synthase inhibitor, L-NAME, showed no significant impact on ROS levels (**Figure 4.1c**). These experiments support and extend seminal studies reported by Rhee and Chang[4,24] indicating that EGF-dependent ROS production requires EGFR and Nox activation.

We then investigated the effect of exogenously added H_2O_2 on the phosphorylation of EGFR and downstream signaling targets, AKT and ERK. ROS differentially modulates the activity of these downstream pathways in several cell types, including endothelial cells and neural progenitor cells[25-28]; however, this phenomenon has not been well characterized in A431 cells. **Figure 4.1d** (right panel) shows that treatment with H_2O_2 in the absence of EGF was sufficient to trigger a dose-dependent increase in phosphorylation of EGFR, consistent with prior studies[29,30]. Additionally, we found that

exogenous H_2O_2 increased AKT and ERK phosphorylation. Control experiments showed that all three signaling proteins were phosphorylated in response to EGF and that EGFR or PI3K inhibitors attenuated this effect (left panel, **Figure 4.1d** and **Appendix 4.6.3a**). Having established that exogenous H_2O_2 mimics EGF by inducing phosphorylation of EGFR and downstream signaling factors, we next examined the role of endogenous H_2O_2. Scavenging EGF-induced generation of H_2O_2 with PEG-catalase suppressed EGFR autophosphorylation (**Figure 4.1e**), global protein tyrosine phosphorylation, and AKT/ERK activation (**Appendix 4.6.3b** and **c**); similar modulatory effects were observed with NAC supplementation (**Appendix 4.6.3d** and **e**). Apocynin and DPI treatment inhibited EGFR, AKT, and ERK phosphorylation, whereas L-NAME had no apparent effect on these signaling pathways (**Figure 4.1f** and **Appendix 4.6.3f** and **g**). Collectively, these data underscore the importance of endogenous H_2O_2 production for EGFR signaling as a result of Nox activation in A431 cells.

Protein sulfenic acids are detected with high selectivity by reaction with the cyclic β-diketone, known as dimedone[31-33] (**Figure 4.2a**). The requirement for sulfenic acid formation in yeast H_2O_2 sensing[18] and T-cell activation[17] has been demonstrated by inhibition with dimedone, which blocks oxidation or reduction of sulfenic acid-modified proteins through covalent modification. To investigate this issue in growth factor signaling, A431 cells were incubated with EGF in the presence of increasing concentrations of dimedone. In the absence of dimedone, addition of EGF triggered phosphorylation of EGFR and effectors, while preincubation with dimedone resulted in dose-dependent inhibition (**Appendix 4.6.3h**). Treatment of cells with dimedone did not decrease H_2DCF-DA oxidation following activation (data not shown). Therefore, treatment of cells with dimedone, a small-molecule that reacts irreversibly with protein

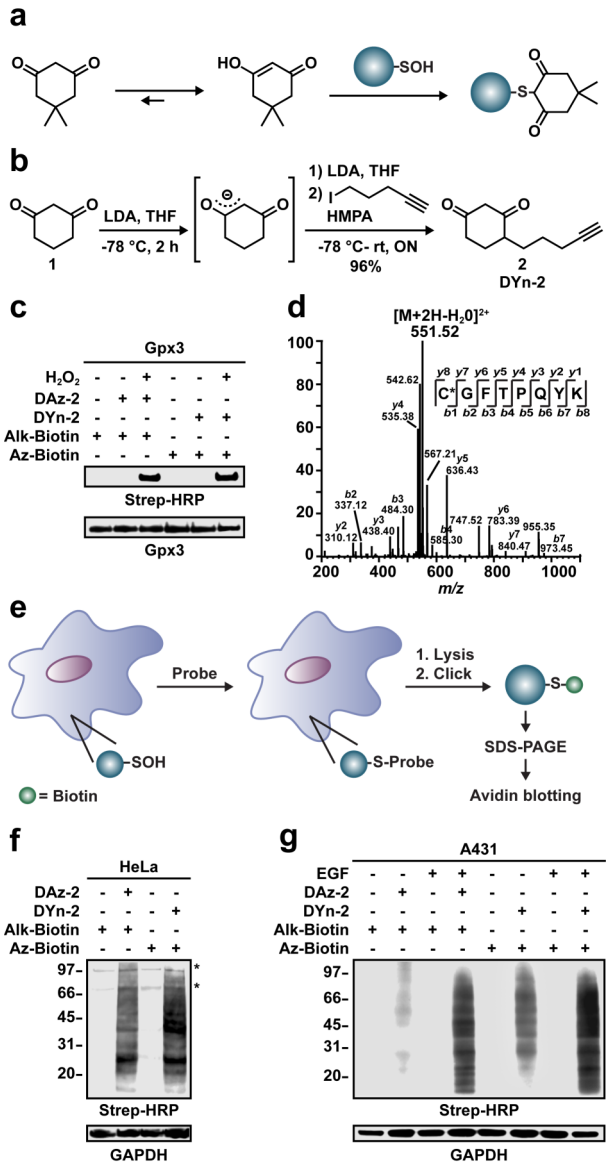

Figure 4.2. Development and validation of DYn-2 probe for detecting sulfenic acid. (**a**) Chemoselective reaction between sulfenic acid and the cyclic β-diketone, known as dimedone. (**b**) Design and synthesis of DYn-2 (**2**). LDA, lithium diisopropylamide; HMPA, hexamethyl phosphoramide; 5-iodopent-1-yne. (**c**) Comparison of DAz-2 and DYn-2 detection of sulfenic acid in recombinant Gpx3. 50 μM protein was untreated or exposed to 100 μM H_2O_2 and incubated in presence or absence of 1 mM probe for 15 min at 37 °C. Labeled proteins were then conjugated to azide-biotin (Az-Biotin) or alkyne-biotin (Alk-biotin) *via* copper(I)-catalyzed azide-alkyne [3+2] cycloaddition (click chemistry), separated by SDS-PAGE, and detected by streptavidin-HRP western blot, as described in Methods. Comparable protein loading was confirmed by reprobing the Western blot with anti-His tag antibody. (**d**) MS/MS analysis using collision-induced dissociation (CID) of the precursor ion *m/z* 551.52 $[M + 2H – H_2O]^{+2}$ corresponding to DYn-2-tagged peptide (C*GFTPQYK) derived from trypsin digest of Gpx3. (**e**) Bioorthogonal chemical reporter strategy to label sulfenylated proteins in cells and their subsequent detection using click chemistry and streptavidin-HRP Western blot. (**f**,**g**) Western blots showing DAz-2 and DYn-2 detection of protein sulfenic acids in cultured mammalian cells and total GAPDH. In (**f**), HeLa cells were incubated with 5 mM probe or vehicle for 2 h at 37 °C. In (**g**), A431 cells were stimulated with 100 ng/ml EGF or vehicle for 5 min, washed, collected as described in Methods, and then incubated with 5 mM probe or vehicle for 1 h at 37 °C. (**f**,**g**) Following probe treatment, cells were washed and harvested in modified RIPA buffer (50 mM triethanolamine, pH 7.4, 150 mM NaCl, 1% NP-40, 1% sodium deoxycholate, 0.1% SDS) supplemented with protease inhibitors and 200 U/ml catalase as described in Methods. Azide- or alkyne-tagged proteins in whole-cell lysate were biotinylated *via* click chemistry, and detected as in **c**. Astericks denote endogenously biotinylated proteins.

sulfenic acids, decreased EGFR tyrosine phosphorylation and subsequent activation of signaling pathways, suggesting that cysteine oxidation is critical for this process.

4.3.3 Synthesis and evaluation of alkyne chemical reporters for protein sulfenic acid

Although H_2O_2 is an essential second messenger that modulates signaling pathways, the scope and identity of cellular protein targets of peroxide remains largely unknown. Selective reaction with dimedone has been used to detect sulfenic acids in cell lysates through direct conjugation of the β-diketone warhead to biotin or fluorophores[15,34]. Recently, we have shown that functionalizing dimedone with a small azide chemical handle enables trapping of sulfenic acid-modified proteins directly in cells[16,35,36]. A key feature of this approach is that it preserves structural integrity and redox potentials between different subcellular compartments[37]. Our first probe, DAz-1, combined the 1,3-cyclohexadione nucleophile and an azide group installed at position 5 *via* an amide linkage[35,36]. Studies with this azide derivative, in conjunction with Staudinger ligation or click chemistry for bioconjugation to affinity and detection reagents, showed utility for visualizing cellular sulfenylation. In our next probe, DAz-2, we replaced the amide bond by a short alkyl azide linker at the 4-position[16]. This reagent exhibited enhanced potency compared to DAz-1, enabling identification of sulfenylated proteins in resting HeLa cells[16] and elucidation of a protein system in the bacterial periplasm that protects single cysteines from hyperoxidation[38].

Previous studies demonstrate that alkynyl-chemical reporters in combination with azide-bearing detection tags offer improved sensitivity compared to the reverse orientation, due to decreased background signal[39-42]. In view of these observations, we sought to determine whether the orientation of the azide and alkyne partners could be reversed.

Toward this end, we designed and synthesized the alkyne-modified 1,3-cyclohexadione analogs, DYn-1 (**4**) and DYn-2 (**2**) (**Figure 4.2b** and **Appendix 4.6.2**). The synthesis began with ethyl protection of the reactive diketone. Alkylation of 3-ethoxy-cyclohex-2-enone at position 4 with 3-bromopropyne proceeded smoothly, owing to the activated nature of the alpha carbon; however, poor yields were obtained for longer bifunctional haloalkyl linkers (~20%). This difficulty was also encountered, but not overcome, in the synthesis of DAz-2 and related analogs[16,34]. A variety of bases and additives were evaluated to increase the efficiency of alkylation (data not shown). After much experimentation, we found that the addition of anhydrous zinc chloride and the cyclic urea DMPU resulted in a moderate improvement in yield; however, this necessitated cumbersome protection and deprotection of the terminal alkyne. To overcome the issue of poor reactivity, we examined monoalkylation of the dianion generated from 1,3-cyclohexadione. Using this method, we were able to prepare DYn-2 without protecting groups in a single step from commercially available materials in 96% yield (**Figure 4.2b**).

With DYn-1 and DYn-2 in hand, we performed comparative studies to determine their utility for detecting protein sulfenic acid modifications alongside DAz-2. To this end, we used a recombinant thiol peroxidase from budding yeast, known as Gpx3, with an active site cysteine (Cys36) that is readily oxidized to sulfenic acid[18]. In these experiments, Gpx3 was exposed to H_2O_2 or untreated, and then reacted with DYn-1, DYn-2, DAz-2 or vehicle control. Following treatment, excess probe was removed by spin filtration, and reporter-tagged Gpx3 was coupled to azide- or alkyne-biotin (**Appendix 4.6.2**) *via* click chemistry. Analysis by streptavidin-HRP Western blot revealed robust, H_2O_2-dependent labeling of Gpx3 by DYn-2, with a slightly increased intensity relative to DAz-2 (**Figure 4.2c**). In contrast, DYn-1 displayed significantly reduced labeling, as compared to DYn-2 and DAz-2 (data not shown). Model chemical reactions indicated a decrease in click

reaction yield, likely due to steric hindrance around the reactive site. As a result, DYn-1 was not pursued further. Control reactions performed in the absence of probe showed no detectable signal by Western blot (**Figure 4.2c**). Next, we verified the nature of the covalent adduct formed between oxidized Gpx3 and DYn-2 by electrospray ionization mass spectrometry (ESI-MS). ESI-LC/MS analysis of intact protein afforded a single major species with a molecular weight of 22916.39 Da, consistent with a single DYn-2 adduct (**Appendix 4.6.4a**). Detailed analysis of trypsin cleavage products from this reaction by ESI-LC/MS/MS definitively confirmed Gpx3 Cys36 as the site of DYn-2 modification from the doubly-charged peptide ion at *m/z* 551.52 corresponding to H_2N-C-(**2**)GFTPQYK-OH (**Figure 4.2d**). Upon inspection, the expected series of b and y-ions of this sequence matched nicely to the major fragment ions in the spectrum. Overall, Western blot analysis as well as intact protein measurement and proteolytic fragmentation characterization MS approaches confirm that DYn-2 selectively targets protein sulfenic acid modifications.

4.3.4 Validation of DYn-2 for detecting protein sulfenylation in cell culture

Having confirmed the reactivity of DYn-2 with a prototype protein *in vitro*, we next evaluated the ability of this reagent to detect protein sulfenylation in cultured cells using the approach outlined in **Figure 4.2e**. Briefly, HeLa or A431 cells were incubated with DYn-2, DAz-2, or vehicle control. After treatment, cells were washed thoroughly to remove excess probe, lysed and tagged proteins were conjugated to azide- or alkyne-biotin under click chemistry conditions. Streptavidin-HRP Western blot analysis showed the existence of sulfenylated proteins in HeLa and A431 cells (**Figure 4.2f** and **g**). The qualitative profile of DYn-2 labeling was similar to DAz-2, suggesting that the probes reacted with the same protein targets. Notably, the total signal from DYn-2 cell labeling was greater than the signal from DAz-2 under identical conditions (**Appendix 4.6.5a**),

and the signal ratio between EGF-stimulated and unstimulated A431 cells was almost 40% greater for DYn-2 (**Appendix 4.6.5a**, **right panel**), which may facilitate detection of sulfenic acid modifications in low-abundance signaling proteins.

DYn-2 detection of sulfenylated proteins in A431 cells was EGF-responsive (**Figure 4.2g**), and dependent on probe dose and time of incubation (**Appendix 4.6.5b** and **c**). Controls performed with or without catalase in lysis buffer further confirmed that DYn-2 labeling did not occur post cell disruption (**Appendix 4.6.5d**). Furthermore, phosphorylation of EGFR and downstream targets was unaffected by DYn-2 addition to cells, before or after EGF treatment (**Appendix 4.6.3h**,**i**). The lack of inhibition by DYn-2 contrasts that observed for dimedone and may be rationalized in terms of decreased reactivity inherent to certain 4- and 5-functionalized analogs[16,34]. Lastly, probe-treated cells showed no loss of viability and maintained normal redox homeostasis relative to vehicle control (**Appendix 4.6.6**). Taken together, these results validate DYn-2 as a robust chemical reporter for protein sulfenylation in cells and provide further support for our general approach of tagging oxidized proteins *in situ*.

4.3.5 DYn-2 reveals that A431 cells exhibit dynamic protein sulfenylation in response to EGF stimulation

The preceding studies reveal growth factor-dependent changes in cellular protein sulfenylation (**Figure 4.2g**). This observation is the first of its kind and thus, we investigated this discovery in greater detail. Addition of EGF to A431 cells increased intracellular ROS (**Figure 4.3a**) and protein sulfenylation (**Figure 4.3b** and **c**) in a dose-dependent manner; the maximal increase in sulfenic acid modification was apparent at 100 ng/ml EGF, which fell to the basal level at 500 ng/ml. ROS generation (**Figure 4.3d**) and protein sulfenylation (**Figure 4.3e** and **f**) were also dynamic temporal events,

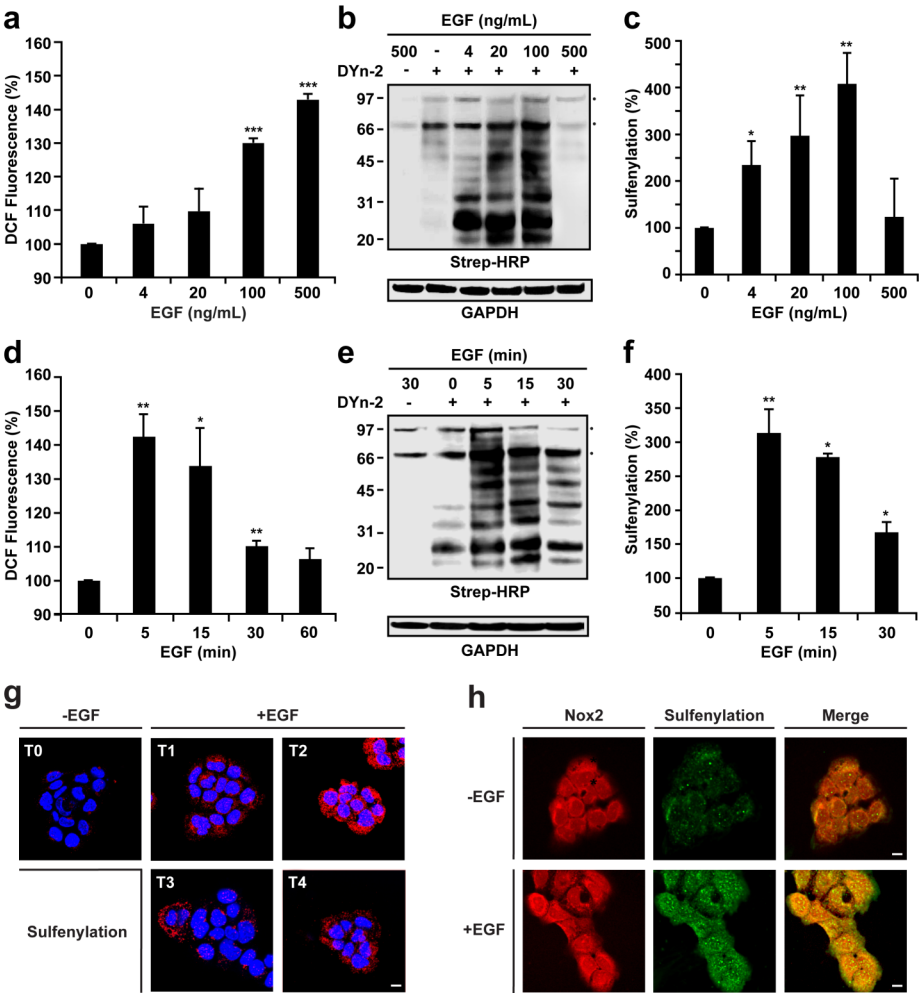

Figure 4.3. Profiling EGF-mediated ROS production and global protein sulfenylation in A431 cells. A431 cells were incubated with EGF at the indicated concentrations (**a, b**) or for the indicated times (**d**,**e**). In (**a**), A431 cells were stimulated with EGF or vehicle for 5 min, after which intracellular ROS was measured by DCF fluorescence. In (**b**), A431 cells were stimulated with EGF or vehicle for 2 min and sulfenic acids were detected by streptavidin-HRP Western blot as in Figure 4.2g. (**c**) Densitometric quantification of each electrophoretic lane in **b** to analyze the total amount of protein sulfenylation. In (**d**), A431 cells were stimulated with 500 ng/ml EGF or vehicle, after which the generation of ROS was measured by DCF fluorescence. In (**e**), A431 cells were stimulated with 100 ng/ml EGF or vehicle and sulfenic acids were detected as in **b**. (**f**) Densitometric quantification of each electrophoretic lane in **f** to analyze the total amount of protein sulfenylation. Western blots were reprobed for GAPDH as loading controls. (**b**,**e**) Filled circles denote endogenously biotinylated proteins. Error bars show ± s.e.m. Statistical analysis was by a two-tailed Student's t test; *** indicates that $P < 0.001$, ** indicates that $P < 0.01$, and * indicates that $P < 0.05$ as compared against vehicle control. (**g**) Confocal fluorescence images of sulfenylation in A431 cells before (T0) and after stimulation with 100 ng/mL EGF for 0.5, 1, 1.5, or 2 min, then treated with 5 mM dimedone for 5 min at 37 °C in EGF-containing media; the total time of exposure to EGF was 5.5, 6, 6.5 and 7 min (identified as T1, T2, T3, and T4, respectively). Cells were fixed and stained as described in Methods with rabbit anti-2-thiodimedone antibody (1:3000) followed by Alexa594-conjugated (red) goat anti-rabbit secondary antibody (1:1000). Nuclei were counterstained with DAPI (blue). In (**h**), A431 cells were stimulated with 100 ng/mL EGF or vehicle for 0.5 min, then treated with 5 mM dimedone for 5 min at 37 °C in EGF-containing media. Cells were fixed as in **g** and double stained with rabbit anti-2-thiodimedone antibody (1:3000) and PE-conjugated (red) mouse anti-Nox2 antibody followed by Alexa488-conjugated (green) goat anti-rabbit secondary antibody (1:1000). The merged image reveals partial co-localization (yellow).

peaking 5 min after EGF (100 ng/ml) stimulation and declining thereafter. EGF-dependent protein sulfenylation was then imaged by immunofluorescence microscopy using an antibody that recognizes the thio-dimedone adduct (**Figure 4.3g**)[20]. Unstimulated cells exhibited low intracellular fluorescence (T0, **Figure 4.3g**). Treatment with EGF markedly increased the signal intensity (T1, **Figure 4.3g**) with a peak at 6 min (T2, **Figure 4.3g**) that decayed over time (T3/T4, **Figure 4.3g**), whereas control samples omitting the primary antibody showed no specific signal (**Appendix 4.6.7a**), further highlighting the dynamic nature of growth factor-mediated protein sulfenylation. The apparent 1 min difference between the peak of sulfenylation levels observed by Western blot (and of ROS levels by DCF; **Figure 4.3d-f**) and immunofluorescence analyses (**Figure 4.3g**) is most likely related to minor variations in sample handling that are inherent to each assay procedure (see Methods and Supplementary Methods). We then investigated the effect of EGFR inhibitors and redox modulating agents on global protein sulfenylation levels. Treatment with reversible (gefitinib) and irreversible (afatinib, canertinib, and pelitinib) EGFR inhibitors, PEG-catalase, NAC, wortmannin, apocynin, but not L-NAME, attenuated protein sulfenylation (**Appendix 4.6.8a**-**d**). Taken together, these data show that EGF-stimulated generation of H_2O_2 leads to global changes in protein sulfenylation.

4.3.6 Nox is an important source of ROS in stimulated A431 cells

The foregoing experiments indicate that Nox activity is important for production of H_2O_2 and global protein sulfenylation during EGF signaling. There are seven known isoforms of Nox (Nox1-5 and Duox1 and 2) that exhibit unique activation mechanisms and tissue-specific expression[43]. To determine which Nox isoforms are present in A431 cells we used Western blotting and immunofluorescence, in combination with a panel of isoform-specific and selective antibodies. In aggregate, these studies show that Nox2 is the

most abundant isoform, in conjunction with very low levels of Nox1, Nox4, and Nox5 (see **Appendix 4.6.9a** and **b** for representative data). Because proteins in the vicinity of Nox are prime targets for oxidation, we wondered whether Nox2 might colocalize with sites of protein sulfenylation. To test this possibility, A431 cells were stimulated with EGF or vehicle, fixed and then costained with antibodies against Nox2 and the thio-dimedone adduct. Immunofluorescence of Nox2 (red, **Figure 4.3h**) indicates distribution at the plasma membrane and perinuclear area, similar to other cell types[44,45]. Immunofluorescence labeling of an extracellular Nox2 epitope under nonpermeabilized conditions also confirmed its plasma membrane association (**Appendix 4.6.7b**). Protein sulfenylation (green, **Figure 4.3h**) increased with EGF stimulation and, remarkably, the merged image reveals abundant colocalization with Nox2 (yellow, **Figure 4.3h**). These findings indicate that Nox2 is the major isoform in A431 cells and its distribution shows overlapping regions with EGF-dependent protein sulfenylation.

4.3.7 Differential sulfenylation of protein tyrosine phosphatases (PTPs) in A431 cells stimulated with EGF

Having established that EGF-induced H_2O_2 generation results in dynamic, global protein sulfenylation we next sought to identify potential targets of H_2O_2 within the EGFR pathway. Along these lines, we noted that growth factor-induced ROS generation has been attributed to oxidation and inactivation of an essential active site cysteine in protein tyrosine phosphatases (PTPs), which would promote signaling. This model is supported by seminal work from Rhee and others vis-à-vis alkylation and enzyme activity studies in cell lysates[17,46-49]. However, the reaction between H_2O_2 and PTP thiolate is ~10^5 times slower than the equivalent reaction with H_2O_2-metabolizing enzymes, such as peroxiredoxin (Prx), raising the question as to whether such oxidation occurs in a cellular context[2,14,50]. In view of the fact that no direct evidence is available as to whether PTP

oxidation occurs directly in cells we used DYn-2 to probe for possible sulfenylation of three phosphatases implicated in EGFR signaling: PTEN, PTP1B and SHP2. PTEN is a cytoplasmic dual-specificity phosphatase that functions as a negative regulator of phosphatidylinositol-3,4,5-triphosphate (PIP3) levels reciprocal to PI3K[51]. PTP1B is localized exclusively to the cytoplasmic face of the ER and dephosphorylates endocytosed RTKs, including EGFR, thereby modulating signal duration[52]. Lastly, SHP2 interacts directly with EGFR through its SH2 domains and regulates interaction with downstream signaling components[53].

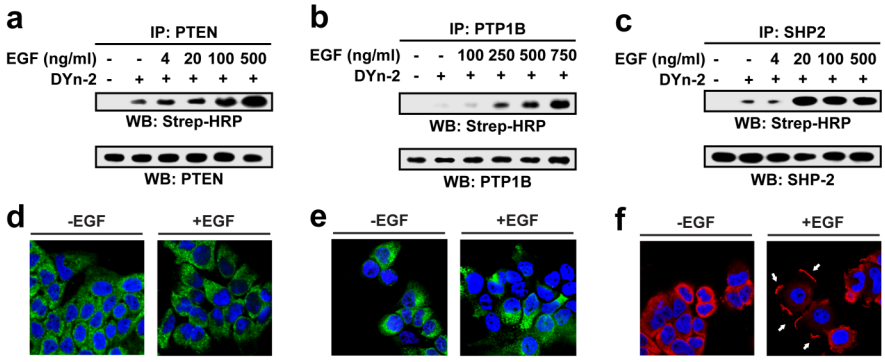

Figure 4.4. Differential sulfenylation of protein tyrosine phosphatases (PTPs) in EGF-stimulated A431 cells. (**a**-**c**) Western blots showing sulfenylated and total immunoprecipitated PTEN, PTP1B, and SHP2. A431 cells were stimulated with EGF or vehicle for 2 min at the indicated concentrations, washed, collected as described in Methods, and then incubated with 5 mM DYn-2 or vehicle for 1 h at 37 °C. Following treatment, lysates were prepared as in Figure 4.2g and immunoprecipitated with mouse anti-PTEN (**a**), mouse anti-PTP1B (**b**), or rabbit anti-SHP2 (**c**) antibodies and recovered with protein A or G coated beads as described in Methods. Sulfenylation of PTPs was detected by streptavidin-HRP Western blot as in Figure 4.2g. To verify equivalent recovery of immunoprecipitated protein, Western blots were reprobed for total PTP as indicated. (**d**-**f**) Confocal fluorescence images of A431 cells stimulated with vehicle or 100 ng/ml EGF for 5 min. Cells were fixed and stained with anti-PTEN (**d**), anti-PTP1B (**e**), or anti-SHP2 (**f**) antibodies at 2 μg/ml, followed by Alexa488-conjugated goat anti-mouse (green) (**d**,**e**) or Alexa594-conjugated goat anti-rabbit (red) (**f**) secondary antibodies (1:1000). Nuclei were counterstained with DAPI (blue). The white arrows in (**f**) highlight the change in subcellular localization of SHP2 after stimulation with EGF.

To overcome issues associated with detection of low abundance endogenous signaling proteins, for these experiments, we immunoprecipitated PTPs from A431 cells treated with DYn-2 or vehicle control in the absence or presence of increasing concentrations of EGF. Streptavidin-HRP Western blot analysis of these reactions showed that each PTP

underwent EGF-dependent sulfenylation in cells (**Figure 4.4a**-**c**). Moreover, individual PTPs displayed distinct oxidation profiles as a function of growth factor concentration (**Figure 4.4a**-**c** and **Figure 4.6a**): SHP2 sulfenylation peaked at a relatively low level of EGF (20 ng/ml), followed by PTEN (500 ng/ml), and finally PTP1B (750 ng/ml). Unfortunately, the SHP2 homologue, SHP1 was not abundant enough in A431 cells to permit detection (data not shown). As discussed below, the apparent decrease in the sulfenic acid state of SHP2 and PTEN at higher EGF concentrations may reflect the formation of intramolecular disulfide bonds (**Appendix 4.6.10d**). Next, we investigated PTP localization in A431 cells before and after EGF treatment. Immunofluorescence staining showed that SHP2 underwent a dramatic change in localization in response to EGF, concentrating at sites of plasma membrane ruffling, whereas the growth factor had no apparent effect on PTEN or PTP1B (**Figure 4.4d**-**f**). Overall, these data show that PTPs undergo EGF-mediated oxidation within cells and suggest that relative sensitivity to H_2O_2 may be related to subcellular protein location.

4.3.8 Identification of EGFR as a new target of H_2O_2 produced for EGF signaling in A431 cells

The foregoing data show that EGF-mediated H_2O_2 production is required for EGFR autophosphorylation (**Figure 4.1e** and **f**). In general, the degree of EGFR tyrosine phosphorylation reflects the balance between opposing kinase and PTP activities. H_2O_2-induced inhibition of PTPs would shift the balance toward phosphorylation; however, the increase in receptor phosphorylation could similarly be accounted for by H_2O_2-mediated activation of intrinsic EGFR kinase activity. To test this possibility, we examined whether EGFR was a target of H_2O_2 in cells using the immunoprecipitation approach outlined above. Strikingly, these experiments revealed that EGF treatment lead to robust sulfenic acid modification of EGFR (**Figure 4.5a**), a finding that was replicated by exogenous

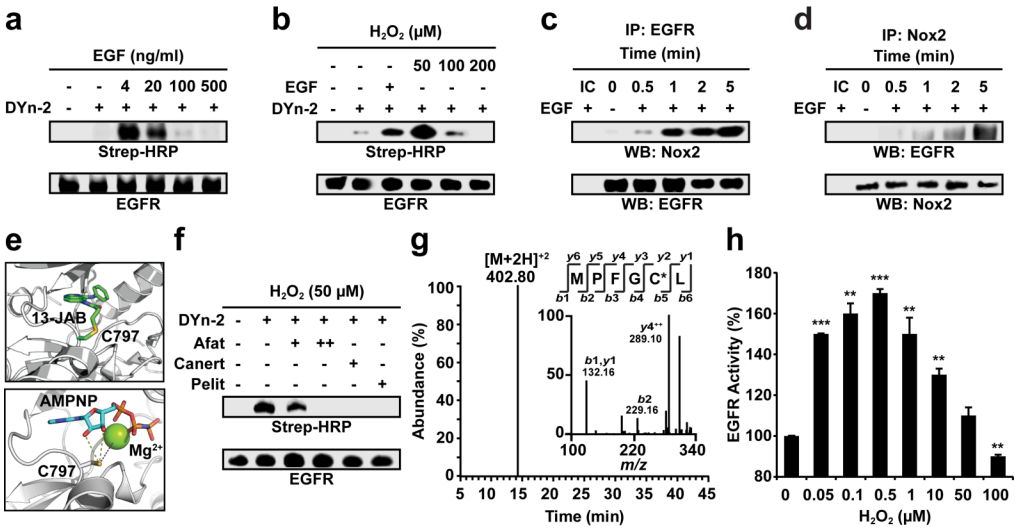

Figure 4.5. EGF-mediated sulfenylation of EGFR active site Cys797 in cells. (**a**,**b**) Western blots showing sulfenylated and total EGFR. A431 cells were stimulated with EGF at the indicated concentrations or vehicle for 2 min (**a**) or H_2O_2 for 10 min (**b**) and sulfenic acids were detected by streptavidin-HRP Western blot as in Figure 4.4a-c, except that rabbit anti-EGFR antibody was used for immunoprecipitation. (**c**,**d**) Western blots showing coimmunprecipitation of Nox2 and EGFR. A431 cells were stimulated with 100 ng/ml EGF or vehicle for the indicated times, harvested in native lysis buffer to preserve protein-protein interactions, and subjected to immunoprecipitation using goat anti-EGFR antibody (**c**) or rabbit anti-Nox2 antibody (**d**) as described in Methods. (**c**) The presence of Nox2 was evaluated using a goat anti-Nox2 antibody and comparable recovery of immunoprecipitated EGFR was confirmed by probing the Western blot with rabbit anti-EGFR antibody. IC, isotype control. (**d**) The presence of EGFR was evaluated using rabbit anti-EGFR antibody and comparable recovery of immunoprecipitated Nox2 was confirmed by probing the Western blot with goat anti-Nox2 antibody. (**e**) Crystal structure of EGFR kinase domain with irreversible inhibitor, 13-JAB bound covalently to Cys797 (top panel; PDB 2J5E) or non-covalently associated with the ATP analog, AMPNP and Mg^{2+} (bottom panel; PDB 3GT8). Molecular images were generated with Pymol (http://pymol.sourceforge.net). (**f**) Western blot showing sulfenylated and total EGFR. A431 cells were incubated with 1 or 5 μM afatinib (labeled as + and ++, respectively), 10 μM canertinib, 1 μM pelitinib or vehicle for 25 min before treatment with H_2O_2 for 10 min and EGFR sulfenylation was detected as in **b**. (**g**) Extracted ion (ion current at *m/z* 402.8) chromatogram (left) and MS/MS spectrum (right) of the precursor ion *m/z* of 402.80 $[M + 2H]^{+2}$ corresponding to dimedone-tagged peptide (MPFGC*L) from native EGFR. A431 cells were stimulated with 4 ng/ml EGF for 2 min, washed, incubated with 5 mM dimedone for 1 h at 37 °C, immunoprecipitated with anti-EGFR antibody as in **a**, and resolved by SDS-PAGE. The band corresponding to EGFR (~170 kDa) was excised, digested with pepsin, and analyzed by ESI-LC/MS/MS as described in Methods. (**h**) Measurement of EGFR tyrosine kinase activity *in vitro*. Recombinant EGFR kinase domain (amino acids 695-end) was untreated or exposed to H_2O_2 at the indicated concentrations and assayed for kinase activity at 25 °C for 60 min as described in Methods. Error bars show ± s.e.m. Statistical analysis was by a two-tailed Student's t test; *** indicates that $P < 0.001$, ** indicates that $P < 0.01$, and * indicates that $P < 0.05$ when compared against vehicle control.

H_2O_2 (**Figure 4.5b**). EGFR sulfenylation peaked at the lowest concentration of EGF employed in this study (4 ng/ml; **Figure 4.6a**) and at ~10 μM exogenous H_2O_2 (**Appendix 4.6.9c**). Given the marked increase in EGFR oxidation at lower EGF concentrations, we wondered whether the receptor might form a complex with Nox2.

This proposal was confirmed by co-immunoprecipitation, which demonstrated EGF- and time-dependent association of Nox2 with EGFR and visa versa (**Figure 4.5c** and **d**). In addition, we also found that SHP2 co-immunoprecipitates with the EGFR/Nox 2 complex in EGF-stimulated cells (**Appendix 4.6.9d**).

4.3.9 EGF-mediated sulfenylation of EGFR active site Cys797 in A431 cells

Having shown that EGFR undergoes growth factor-dependent oxidation in cells, we then sought to identify the specific site(s) of sulfenic acid modification. The intracellular portion of EGFR contains nine cysteine residues; in particular, the kinase domain is distinguished by Cys797, which is positioned at the edge of the active site cleft at the top of an α-helix formed by residues 798-804 (top, **Figure 4.5e**). This residue is selectively targeted by irreversible inhibitors, such as afatinib, which is extensively used in basic science research and clinical trials for breast and non-small cell lung cancers[54,55]. On this basis, we hypothesized that Cys797 may represent the site of EGF- and H_2O_2-mediated sulfenylation. To test this possibility, we pretreated A431 cells with afatinib, canertinib, or pelitinib and assessed the effect of these irreversible inhibitors on the ability of DYn-2 to detect EGFR oxidation by exogenous H_2O_2. Each compound prevented H_2O_2-mediated sulfenylation of EGFR, as evidenced by the loss of DYn-2 labeling (**Figure 4.5f**), suggesting that Cys797 may be susceptible to oxidation. To examine this possibility in further detail, we directly mapped the site of oxidation using mass spectrometry. In these experiments, A431 cells were stimulated with EGF, pulsed with dimedone, immunoprecipitated for EGFR, and resolved by SDS-PAGE. The EGFR band was excised and digested in situ with pepsin. ESI-LC/MS/MS analysis of the resulting cleavage products confirmed Cys797 as the site of covalent modification from the doubly-charged peptide ion at *m/z* 402.80 corresponding to H_2N-MPFGC*L-OH (**Figure 4.5g**, left) and the series of b- and y-type ions observed in the MS/MS spectrum

(**Figure 4.5g**, inset). Of note, the unmodified peptide was also detected in these experiments and the ratio of peak areas of the dimedone-modified peptide ion relative to the unmodified version was approximately 6:1 (**Appendix 4.6.4b**).

Given the proximity of Cys797 to the ligand and associated Mg^{2+} ion in the active site (bottom, **Figure 4.5e**), we wondered whether oxidation of this residue would affect intrinsic kinase activity. To test this possibility, we performed activity assays with the purified tyrosine kinase domain of EGFR. First, we verified that activity increased as a function of enzyme concentration and decreased with inhibitor treatment (**Appendix 4.6.9e**-**g**). Subsequent studies revealed a biphasic dose-dependent effect of H_2O_2. Kinase activity increased when EGFR was exposed to 0.05–0.5 μM of H_2O_2 followed by a decline at higher concentrations (1-50 μM) eventually leading to inhibition relative to untreated enzyme (100μM, **Figure 4.5h**). In this regard, we note that incubation with the reducing agent dithiothreitol (DTT) mitigated H_2O_2 inhibition (**Appendix 4.6.9h**), suggesting that the decline in EGFR activity at higher peroxide concentrations may involve reversible thiol oxidation. Control experiments showed that H_2O_2 had no significant effect on other components of the assay system (**Appendix 4.6.9i**). These results demonstrate that EGFR Cys797 is a direct target of H_2O_2 in A431 cells stimulated by EGF, ostensibly through growth factor-dependent association with Nox2. Furthermore, we show that low levels of H_2O_2 enhance EGFR kinase activity, and this stimulatory effect was lost at higher, likely cytotoxic levels of H_2O_2.

4.4 Discussion

In this work, we have investigated EGF-mediated redox signaling and cysteine oxidation in A431 cells using DYn-2, a new alkyne-functionalized chemical probe for detecting

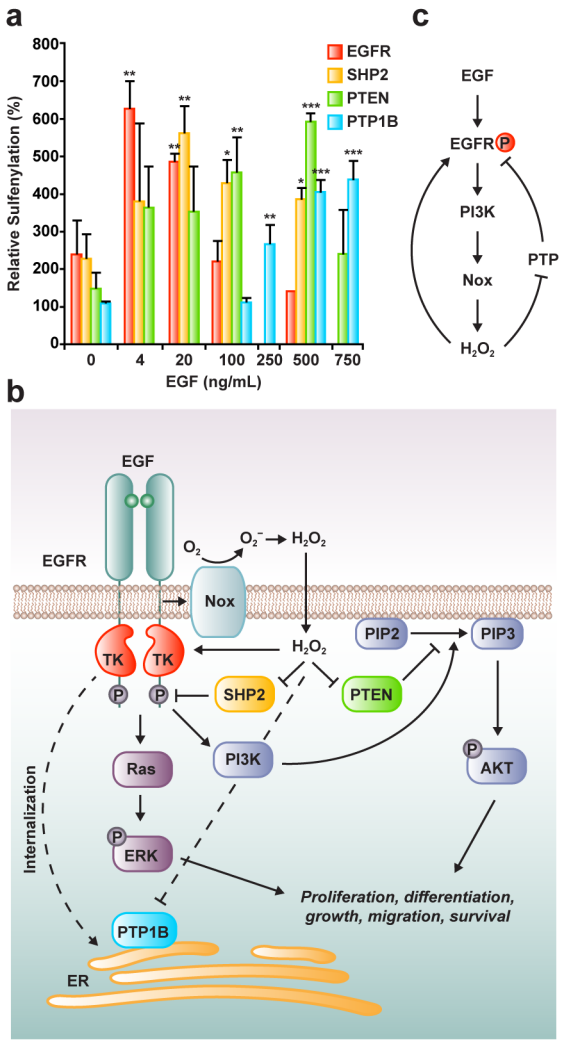

Figure 4.6. Model for redox regulation of EGFR signaling. (**a**) Densitometric quantification of EGFR and PTP sulfenylation from Western blots in Figure 4.4a-c and Figure 4.5a**.** Error bars show ± s.e.m. * indicates that $P < 0.05$, ** indicates that $P < 0.01$ and *** indicates that $P < 0.001$ when compared against vehicle control. (**b**) Receptor activation by EGF induces association with Nox2 and ROS production. The transient increase in ROS leads to oxidation of active site cysteine residues in EGFR, PTEN, PTP1B, SHP2 and other proteins that remain to be identified. EGF-mediated ROS stimulates intrinsic EGFR tyrosine kinase activity, whereas oxidation inhibits tyrosine phosphatase activity. Augmentation of EGFR activity and inhibition of PTEN potentiates signaling through the PI3K/AKT and RAS/ERK pathways. The cellular function of SHP2 is complex, however, oxidative inactivation of this protein leads to increased phosphorylation of EGFR and modulates the RAS/ERK cascade. Notably, EGFR and the aforementioned PTPs exhibit differential dose-dependent effects of EGF on sulfenylation. This finding may be related to the relative proximity of target proteins to the oxidant source, Nox2. EGFR signal duration is regulated by receptor internalization and de-phosphorylation by PTP1B, located on the cytoplasmic face of the ER membrane. Although PTP1B does not appear to be the most sensitive target of EGF-induced ROS, the present study shows that PTP1B undergoes oxidation in cells, which prolongs EGFR signaling, and could be particularly relevant in diseases associated with chronic oxidative stress. Dashed lines are relevant to receptor internalization. (**c**) Model for H_2O_2-dependent increase in EGFR autophosphorylation in A431 cells. EGF stimulation induces production of H_2O_2 in A431 cells, which can oxidize and activates the intrinsic tyrosine kinase activity of EGFR, and also serves to deactivate PTPs, which promotes signaling through downstream pathways. Collectively, our findings indicate that sulfenylation, as well as phosphorylation, modulates EGFR activity.

protein sulfenylation. We now turn to a more detailed discussion of the results of this paper.

EGF stimulation of A431 cells modulates cell morphology, receptor localization, and protein phosphorylation. We also found that EGF treatment increases intracellular ROS, consistent with prior studies[4,24,56]. Moreover, using small-molecule inhibitors, we show that EGFR tyrosine kinase activity is required for growth factor-induced ROS generation. These data complement and extend earlier observations in NIH-3T3 cells expressing a C-terminally truncated mutant of EGFR[24]. To facilitate a comparison between our results and those obtained in other studies[24,56] DCF fluorescence was used to monitor the generation of ROS. In this regard, we note that DCF does not provide information as to the exact nature of ROS being measured in cells[57]. A key advance in this area has been the development of fluorescent probes for selectively imaging H_2O_2 based on boronate deprotection[57,58]. Use of these probes in A431 cells[4,59] as well as another study employing SOD inhibitors[60] distinctly implicates H_2O_2 in EGF-mediated signal transduction.

Further indication that redox homeostasis is important for EGFR signaling comes from modulation of intracellular ROS levels. NAC, a precursor to glutathione and a general ROS scavenger, inhibits protein phosphorylation in PDGF[61] and FGF[27] signaling as well as in Ras-transformed cells[62]. In this study, NAC suppressed global changes in EGF-mediated protein phosphorylation, including EGFR and AKT. To investigate the role of H_2O_2 in growth factor signaling, catalase has been introduced into A431 cells by electroporation and transfection. Our study indicates that pretreating A431 cells with PEG-catalase achieves the same result without any genetic or mechanical manipulation to the cells, akin to other cell types[63]. Indeed, EGF-dependent protein phosphorylation,

particularly of EGFR, AKT, and ERK was attenuated in A431 cells loaded with PEG-catalase, providing additional support for the proposed role of endogenous H_2O_2 in EGF signaling. This link is further strengthened by the observation that exogenous H_2O_2 mimics EGF stimulation by inducing phosphorylation of EGFR, AKT and ERK in A431 cells. However, because treatment with exogenous H_2O_2 may not always recapitulate the effect of endogenous ROS due to differences in overall dose and localized concentration we have focused our analysis on growth factor-induced H_2O_2.

Growing evidence indicates that Nox is primarily responsible for receptor-dependent H_2O_2 generation[43,64,65]. Consistent with this proposed role, we show that Nox inhibitors apocynin and DPI diminished EGF-stimulated ROS production and phosphorylation of EGFR, AKT, and ERK in A431 cells. While apocynin is a potent inhibitor of Nox assembly in neutrophils[66] and epithelial cells[67] the effects of this methoxy-substituted catechol should be interpreted with care as this mode of action may not apply to all cell types[68]. Western blot and immunofluorescence analyses indicate that Nox2 is the most abundant isoform in A431 cells; however, very low levels of Nox1, Nox4 and Nox5 are also present. Despite repeated attempts, we failed to knock down Nox isoforms in A431 cells by siRNA-mediated gene targeting (data not shown). Among other issues, these experiments were thwarted by low transfection efficiency and toxicity associated with cationic liposome-mediated gene transfer. Because Nox3-5 and Duox1-2 do not seem to depend on PI3K/Rac1, the requirements for PI3K activation in EGF-induced H_2O_2 observed in the present study and earlier work[69-71] provide further support for Nox2 involvement. Even so, we cannot rule out contributions from Nox1 and other, less abundant isoforms regarding EGF-mediated ROS production in A431 cells; this general issue highlights the urgent need for isoform- and class-selective Nox inhibitors.

Given the importance of cysteine oxidation to human health and disease, indirect and direct chemical methods have been developed to investigate these modifications[32]. The majority of indirect methods to monitor changes in the redox state of cysteines rely on the loss of reactivity with thiol-modifying reagents or restoration of labeling by reducing agents (**Appendix 4.6.10a** and **b**). Such approaches require that free thiols are completely blocked by alkylating agents prior to the reduction step and, for this reason, are restricted to analysis of cell lysates or purified proteins. Alternatively, individual cysteine modifications, such as sulfenic acid or nitrosothiols, can be detected on the basis of their distinct chemical attributes using selective small-molecule probes (**Appendix 4.6.10c**). Provided that the probe is membrane permeable, direct chemical methods enable cysteine oxidation to be examined in cells. This is not a trivial consideration since redox potentials differ markedly among subcellular compartments[37]. When the finely tuned redox balance of the cell is disrupted by the lysis procedure, proteins can undergo artifactual oxidation, which increases the challenges associated with detecting low-abundance modifications and interpreting biological significance. Strategies to decrease oxidation artifacts in lysates have been reported[72,73]; however, limitations inherent to studies in lysates, such as protein denaturation with concomitant loss of labile modifications, are not addressed. On the other hand, cellular probes can perturb the underlying biological processes being examined. This can be addressed, at least in part, by fine-tuning chemical reactivity, addition of probe after triggering the process of interest, and by examining relevant biological markers in probed and unprobed cells, analogous to studies of nonredox phenomena.

With the development and application of DYn-2, we expand the chemical toolbox with which to probe protein sulfenic acid formation in cells. Like its prototypes, DYn-2 is equipped with a 1,3-cyclohexadione moiety to permit selective reaction with protein

sulfenic acids, but is uniquely functionalized with an alkyne chemical handle. Compared to the reverse orientation, DYn-2 showed a modest increase in sensitivity that might facilitate detection of sulfenic acid modifications in low-abundance proteins. No extrinsic probe can ever be a truly inert spectator, but DYn-2 is non-toxic and did not significantly perturb cellular redox balance or EGF-signaling in A431 cells, consistent with this goal. The synthetic route presented for DYn-2 eliminates several steps and tedious intermediate purifications, and can be conducted on a gram scale. Key to the success of our synthetic strategy is the solubility of the dianion generated from 1,3-cyclohexadione in THF and enhanced reactivity compared to the monoanion.

Application of DYn-2 in A431 cells shows that protein sulfenylation is a dynamic process during growth factor signaling and likely has broader implications for other receptor-mediated processes. Consistent with this proposal, alterations in sulfenic acid modifications have been observed in lysates generated from HEK293 cells treated with the cytokine TNFα[33] and CD8+ T cells stimulated with CD3/CD28 antibodies[17]. The relative changes in cysteine oxidation that we observe depend on EGF dosage and time of stimulation, and show a strong positive correlation with ROS levels. One interesting exception is the case of 500 ng/ml EGF, wherein we routinely observe a decrease in sulfenylation. Our findings are consistent with the absence of global disulfide bond formation at this EGF concentration in A431 cells, as reported by Winterbourne and colleagues[56]. The apparent lack of sulfenylation at the highest level of growth factor tested may result from oxidation of sulfenic to sulfinic acid, upregulation of drug efflux transporters, dissociation of EGFR clusters from lipid rafts, and/or activation of alternate pathways that function independent of cysteine oxidation. While additional studies will be required to distinguish among these possibilities, it is important to note that 500 ng/ml EGF well exceeds physiological levels and has been associated with apoptosis[74].

Attenuation of EGF-dependent protein sulfenylation with inhibitors of EGFR, Nox and PI3K underscores the importance of receptor and Nox activation for intracellular H_2O_2 generation and concomitant cysteine oxidation. Curiously, DPI-treated A431 cells reveal a complex effect of this reagent on protein sulfenylation (**Appendix 4.6.8e**). When applied at 25 μM, DPI decreased sulfenic acid modification of proteins; however, higher doses were associated with an increase in sulfenylation relative to control samples. DPI is a general inhibitor of flavin-containing enzymes, including the thioredoxin-thioredoxin reductase system that returns oxidized protein thiols to their reduced state. This may explain the apparent paradox of elevated protein sulfenic acid formation at higher concentrations of DPI. Cellular sulfenylation and Nox2 exhibit a high, but not complete, degree of colocalization. Areas of protein oxidation that do not overlap with Nox2 may indicate diffusion of H_2O_2 and/or EGF-mediated activation of other oxidases. The ability of NAC and PEG-catalase to mitigate sulfenic acid formation in cells, as detected by DYn-2, further highlights the selectivity and sensitivity of this new probe.

In this study, we use sulfenic acid as a marker of cysteine oxidation in cells. As first pointed out by Poole[12], an early pioneer in this field, detection of sulfenic acid in proteins has the advantage of targeting the direct product of cysteine modification by H_2O_2. Detection of sulfenic acid also enables identification of the reactive site where oxidation chemistry was originated, while detection of downstream products, such as disulfides, may be more difficult to dissect. Moreover, not all sulfenic acids are converted to other oxidation states[16]. On the other hand, some sulfenic acids in proteins may be short-lived and therefore, more difficult to detect. For clarity, we note that the sulfenic acid detected by our experiments is a function of the rate of thiolate oxidation by H_2O_2, probe trapping, and competing reduction or condensation reactions (**Appendix 4.6.10d**).

To gauge the propensity of PTPs toward oxidation in cells we monitored sulfenylation as a function of H_2O_2 produced endogenously by EGF stimulation. PTPs analyzed in our study exhibit varying basal levels of oxidation and sensitivity to EGF-mediated oxidation in cells (**Figure 4.6a**). Because the rate of PTP oxidation is quite similar in biochemical studies[75,76] their disparate susceptibility to oxidation in cells is notable. One likely explanation is that PTPs do not encounter equivalent amounts of intracellular H_2O_2. As first proposed by Tonks[48], the proximity of proteins to the oxidant source may play a major role in determining which cysteine residues become oxidized (**Figure 4.6b**). Consistent with this model, we observe that SHP2, which preferentially localizes to membrane ruffles and associates with the EGFR/Nox2 complex, undergoes a robust increase in oxidation at low growth factor concentrations. At the other extreme, PTP1B is localized to the cytoplasmic face of the ER membrane and oxidation is not observed until higher EGF concentrations. In further support of our findings, Keaney and colleagues have shown that oxidation of PTP1B by Nox4 in aortic endothelial cells requires ER localization of both proteins[26]. The absence of PTP1B oxidation at lower EGF concentrations could also stem from sulfenyl-amide formation outcompeting the DYn-2 trap (**Appendix 4.6.10d**). However, this scenario seems unlikely as the sulfenyl-amide condensation in PTP1B is expected to be at least 100-fold slower than intramolecular disulfide formation[77,78] in PTEN and SHP2. Finally, we point out that PTP oxidation is detected at 500 ng/ml EGF, despite the overall decrease in global sulfenylation and may indicate that endogenous low-abundance targets are not effectively observed without immunoprecipitation using a protein-specific antibody.

Our results, in conjunction with other studies[24,29,61], demonstrate that exogenous and endogenous H_2O_2 leads to an increase in EGFR autophosphorylation. In addition to inactivation of PTP activity through oxidation, it is also conceivable that intrinsic RTK

activity is stimulated by H_2O_2 (**Figure 4.6b**,**c**). Consistent with this proposal, our data show that EGF- and H_2O_2-stimulation of A431 cells leads to sulfenylation of EGFR; moreover, a robust increase in receptor oxidation was evident at the lowest concentration of EGF tested (4 ng/ml). The relative sensitivity of EGFR to oxidation may be rationalized on the basis of association with Nox2, an important source of H_2O_2. To the best of our knowledge, this is the first documented example of Nox interaction with a growth factor receptor and, since redox regulation appears to be widespread in mitogenic signaling, this finding may apply to other RTKs. To date, the only other documented case of Nox-receptor interaction is with a member of the tumor necrosis receptor subfamily, TNFR1, and is mediated by riboflavin kinase that binds both to the receptor and to p22phox, the common subunit of NADPH oxidase isoforms[79]. At present, it is not known whether the association between EGFR and Nox2 is direct or mediated by another protein and additional experiments will be required to define this interaction.

Competitive labeling experiments and LC-MS/MS analysis establish Cys797 as the site of EGFR sulfenylation in cells. When cells were stimulated with 4 ng/ml EGF, the ion intensity for the dimedone-modified peptide, relative to the unmodified form, was nearly 6:1. Because the effect of dimedone on the ionization efficiency of this peptide is not known, this analysis may not reflect absolute quantification, but is useful for qualitative comparison. Although exact rates have not been reported, Haber and colleagues report that Cys797 is not essential for catalytic activity[80]. Nonetheless, its location in the active site suggests that oxidation could modulate kinase function, by analogy to redox regulation of GTPases, such as Ras. To isolate the effect of H_2O_2 on EGFR activity from oxidative PTP inhibition, we performed a direct kinase assay using purified, recombinant EGFR. These biochemical studies show that low H_2O_2 concentrations stimulate intrinsic

EGFR kinase activity and this finding is supported by studies in crude membrane fractions isolated from NA cells, which show that H_2O_2 treatment stimulates EGFR autophosphorylation[29]. The following decline in kinase activity that we observe at higher peroxide concentrations may reflect formation of a disulfide bond with another cysteine in this domain, and future studies are required to address this possibility. The biphasic response of EGFR activity with exogenous H_2O_2 parallels that of receptor sulfenic acid modification in cells; however, the peroxide concentration required for maximal rate enhancement is approximately 20-fold lower than for cellular sulfenylation. The most likely explanation for this difference is that antioxidant enzymes and other biomolecular targets consume the H_2O_2 applied to cells. Another noteworthy aspect of this behavior is that both cellular sulfenylation and kinase activity decrease above ~50 μM H_2O_2, whereas EGFR autophosphorylation increases at peroxide levels above 500 μM. These findings suggest a complex interplay between EGFR kinase activity and PTP inhibition at different concentrations of H_2O_2, wherein low levels stimulate catalysis, an effect that is lost at higher doses, but is compensated for by PTP inactivation. Additionally, oxidation of Cys797 could positively regulate other aspects of EGFR function, including protein-protein interactions.

It is intriguing to consider the possibility that cysteine oxidation may serve as a general mechanism to regulate RTK activity. Of the ~95 receptor and non-receptor protein tyrosine kinases (PTKs) in the human genome, nine additional members harbor a cysteine residue at the position that corresponds to Cys797, including two additional EGFR family members, Her2 and Her4. Another subfamily of PTKs, which includes cytoplasmic Src as well as FGFR1, have a cysteine residue within a conserved glycine rich loop that interacts with the γ-phosphate of ATP. Interestingly, cellular studies implicate cysteine oxidation in Src regulation[81-83], albeit with apparently contradictory

results. Furthermore, biochemical analysis of Src shows that the glycine loop cysteine is reactive and that addition of DTT to recombinant FGFR1 stimulates kinase activity[84]. To date, however, it has not been ascertained whether Src is a direct target of signaling-mediated H_2O_2 in cells; nor has the reaction of peroxide with FGFR1 been reported.

EGFR is mutated or amplified in a number of human carcinomas including breast and lung cancers, which has motivated the development of selective kinase inhibitors, including analogs that covalently modify Cys797[55]. Indeed, several irreversible inhibitors of EGFR, including Afatinib, are now under preclinical or clinical trials[54]. We have recently reported that overexpression of EGFR and Her2 in breast cancer cell lines correlates with elevated H_2O_2 and global protein sulfenylation[20]. Coupled to the discovery that EGFR Cys797 undergoes sulfenic acid modification, these findings raise several fundamental questions vis-à-vis cysteine oxidation and thiol-targeted irreversible inhibitors. For example, the acrylamide moiety of the aforementioned EGFR inhibitors undergoes Michael addition with Cys797 in its thiol form, but these inhibitors would not react with the sulfenic acid or disulfide states, which could influence the potency of these drugs. In addition, can the propensity for a particular cysteine residue to undergo oxidation be exploited in the design of irreversible inhibitors with a nucleophilic warhead targeting the sulfenylated protein? Taking this one step further, could this strategy be exploited to selectively target proteins in cells under oxidative stress, a condition that is associated with cancer, diabetes, and neurodegeneration? These topics represent new and exciting avenues for future research.

In closing, we have developed a new sulfenic acid-specific probe, DYn-2 and applied this reagent to reveal dynamic sulfenylation associated with growth factor signaling. During the course of these studies, we have profiled PTP oxidation directly in cells and

discovered EGFR as a previously unknown target of signal-mediated H_2O_2, ostensibly through its association with Nox2. From a broader perspective, our findings shed new light on mechanisms of redox signaling, allude to new redox-based strategies for targeted therapy development, and presage the establishment of comprehensive sulfenomes that will continue to expand the scope and biological role of sulfenylation, wherein rich research frontiers lie ahead.

4.5 Experimental procedures

4.5.1 Synthetic materials and methods

All reactions were performed under a nitrogen atmosphere in oven-dried glassware. Tetrahydrofuran was distilled over sodium hydride prior to use. All other reagents and solvents were purchased from Sigma and were used without further purification. Analytical thin layer chromatography (TLC) was carried out using Analtech Uniplate silica gel plates and visualized using a combination of UV and potassium permanganate staining. Flash chromatography was performed using silica gel (32-63 μM, 60 Å pore size) from Sorbent Technologies Incorporated. NMR spectra were obtained on a Bruker Avance 400 (400 MHz for ^{1}H; 100 MHz for ^{13}C) in $CDCl_3$ (Cambridge Isotope Laboratories). ^{1}H and ^{13}C NMR chemical shifts are reported in parts per million (ppm) referenced to the residual $CHCl_3$. Low-resolution electrospray ionization (ESI) mass spectra were obtained with an Agilent 6120 Single Quadrupole LC/MS.

4.5.2 3-ethoxy-6-(prop-2-yn-1-yl)cyclohex-2-enone (3)

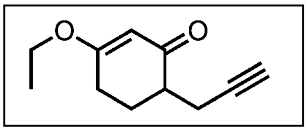

To a lithium diisopropylamide (LDA) solution, prepared from diisopropylamine (1.66 mL, 12 mmol) and *n*-BuLi (4.8 mL of a 2.5 M solution in hexanes, 12 mmol) in anhydrous THF (45 mL) at -78 °C under argon, was added 3-ethoxycyclohex-2-enone (1.4 g, 10 mmol) in THF (20 mL), dropwise over 0.5 h. The reaction was stirred for an additional 2 h at -78 °C. Stirring was followed by the dropwise addition of propargyl bromide (1.3 mL, 12 mmol). The reaction was allowed to warm to rt and stirred for 8 h. The reaction was quenched with water (20 mL) and sat. NH_4Cl (20 mL). The aqueous phase was extracted with DCM (3x50 mL), and the organic phases were combined, washed with brine (20 mL), dried over Na_2SO_4, and concentrated. The resulting syrup was purified with silica gel column chromatography using 6:4 Hexanes: ethyl acetate resulting in a yellow oil **3** (1.6 g, 8.99 mmol) in 89% yield. R_f: 0.6 (1:1 hexanes: ethyl acetate). ^1H NMR (400 MHz, $CDCl_3$) 5.31 (s, 1H), 3.98 – 3.78 (m, 2H), 2.76 (dt, *J* = 16.6, 3.2 Hz, 1H), 2.59 – 2.41 (m, 2H), 2.41 – 2.20 (m, 4H), 1.95 (q, *J* = 2.3 Hz, 1H), 1.82 (dtd, *J* = 16.8, 11.5, 5.1 Hz, 1H), 1.45 – 1.27 (m, 3H). ESI-LRMS: *m/z* for $C_{11}H_{14}O_2$ calculated 178.10; observed 179.1 $[M+H]^+$.

4.5.3 4-(prop-2-yn-1-yl)cyclohexane-1,3-dione (4)

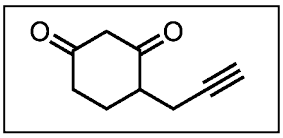

To a solution of **3** (0.05 g, 0.29 mmol) in acetonitrile (2 mL) and water (2 mL) was added CAN (0.015 g, 0.028 mmol). The solution was heated to reflux for 2 hr. The reaction mixture was then diluted with brine (20 mL), and extracted with EtOAc (3x20 mL). The organic phases were combined, washed with brine (30 mL), dried over Na_2SO_4, and

concentrated *in vacuo*. The resulting orange solid was purified by silica gel column chromatography using 1:1 Hexanes:EtOAc to give compound **4** as a pale yellow solid (0.042 g, 0.28 mmol) in 96% yield. R_f: 0.3 (1:1 Hexanes:EtOAc). ^{1}H NMR (400 MHz, dmso-d_6) δ 11.05 (s, 1H), 5.25 (s, 1H), 3.43 – 3.14 (m, 1H), 2.76 (d, *J* = 24.8 Hz, 1H), 2.37 – 2.16 (m, 4H), 2.04 (dt, *J* = 28.7, 11.9 Hz, 1H), 1.81 – 1.57 (m, 1H). ESI-LRMS: *m/z* for $C_9H_{10}O_2$ calculated: 150.07; observed: 151.1 $[M+H]^+$.

4.5.4 DYn-2 (2)

Lithium diisopropylamide (LDA) was prepared by the dropwise addition of 2.5 M solution of *n*-BuLi (15.7 ml, 39.2 mmol) to a solution of diisopropylamine (3.97 g, 39.2 mmol) in THF (40 ml) and the resulting pale yellow mixture was stirred at -78 °C for 30 min in a 250 ml flask equipped with a magnetic stir bar under N_2 pressure. A solution of 1,3-cyclohexadione (**1**, 2.0 g, 17.8 mmol) in THF (20 ml) and HMPA (10 ml) was added dropwise to the LDA solution at -78 °C. The resulting mixture was allowed to stir at -78 °C for 1.5 h. The temperature was increased to 0 °C briefly to facilitate the stirring, and then cooled again to -78 °C. To this dianion slurry, a solution of 5-iodopent-1-yne (3.81 g, 19.6 mmol) in THF (20 ml) was added dropwise at -78 °C. The reaction was stirred and allowed to warm to rt over 2 h. The mixture was then neutralized with 1.0 M HCl (22 ml) and concentrated under reduced pressure. The residue was diluted with H_2O extracted with ethyl acetate (3 x 50 ml). The organic phase was then washed with brine, dried over anhydrous $MgSO_4$, and concentrated. Purification by column chromatography (gradient: dichloromethane/methanol from 100:0 to 98:2) afforded compound **2** as a mixture of the keto and enol forms (3.0 g, 96% yield). The product was further purified by reversed-phase preparative HPLC (Varian Polaris 5 C18-A 150 x 21.2 mm column) using a gradient of water/acetonitrile from 95:5 to 5:95 over 30 min. ^{1}H-NMR (400 MHz, $CDCl_3$): δ 5.42 (s, 1H), 3.41 (d, *J* = 4.0 Hz, 2H), 2.75 – 1.72 (m, 16H), 1.68 – 1.45 (m,

6H). ^{13}C-NMR (100 MHz, $CDCl_3$): δ 204.9, 204.4, 197.0, 189.2, 104.2, 84.4, 84.1, 69.1, 68.9, 58.5, 49.1, 41.8, 39.9, 30.1, 29.6, 28.5, 26.4, 26.2, 26.1, 24.7, 18.8, 18.7. ESI-LRMS: *m/z* for $C_{11}H_{14}O_2$ calculated: 178.23; observed: 179.1 $[M+H]^+$.

4.5.5 Synthesis of 5-iodo-pent-1-yne, alkyne-biotin and azide-biotin

5-iodopent-1-yne was synthesized according established literature procedures[85]. Alkyne-biotin was synthesized according to established literature procedures[86]. Azide-biotin was synthesized according to established literature procedures[87]. In all cases, ESI-MS, ^{1}H and ^{13}C NMR NMR spectra matched literature values[85-87].

4.5.6 Stocks

All stocks were stored at -20 ^{o}C, unless otherwise indicated. The stock EGF (BD Biosciences) solution was prepared at 30 µg/ml in ddH_2O. H_2O_2 was purchased from Sigma and lower concentrations were made by dilution of the stock solution with ddH_2O. Gefitinib (1 mM, Santa Cruz Biotechnology), Afatinib (100 µM and 500 µM, Chemietek), Canertinib (1 mM, Chemietek), Pelitinib (100 µM, Santa Cruz Biotechnology), Apocynin (10 mM, Calbiochem), Wortmannin (10 mM, Cayman Chemicals), and DPI (100x, Sigma) stocks were prepared in DMSO at the indicated concentrations. DAz-2 was synthesized and purified as previously described[88]. DAz-2 and DYn-2 were prepared in DMSO at 250 mM. Dimedone was prepared as a 50:50 mixture of DMSO and 0.5 M Bis-Tris HCl (pH 7.0) at 250 mM. Catalase (20,000 U/ml, Sigma) included in lysis buffers and PEG-catalase (100,000 U/ml, Sigma) were prepared in 50 mM Tris-HCl (pH 7.4) and stored at -80 °C or made up fresh, respectively. L-NAME (10 mM, Calbiochem) and NAC (1 M, Research Products International) were freshly prepared in serum-free DMEM at the indicated concentrations. Azide- or alkyne-biotin were prepared at 5 mM

in DMSO, TBTA ligand was prepared at 2 mM stock in 4:1 DMSO:tBuOH, and TCEP-HCl (Sigma) and $CuSO_4$ (Sigma) were freshly prepared at 50 mM in ddH_2O.

4.5.7 Expression, purification, and labeling of sulfenylated Gpx3

Recombinant Cys82Ser Gpx3 and Cys64Ser Cys82Ser Gpx3 were expressed and purified as previously described[89]. Cys82Ser Gpx3 and Cys64Ser Cys82Ser Gpx3 were previously stored in 50 mM Tris HCl pH 7.4, 300 mM NaCl, 10% glycerol, and 5 mM DTT. DTT was removed from Gpx3 mutants *via* spin filtration using P-30 micro BioSpin columns (BioRad) pre-equilibrated with Gpx3 buffer (50 mM Tris HCl pH 7.4, 300 mM NaCl). 50 µM Cys82Ser Gpx3 was treated with 1 mM DAz-2, 1 mM DYn-2 or vehicle in the presence or absence of 100 µM H_2O_2 for 15 min at 37 °C. Excess probe was removed by spin filtration, and azide- or alkyne-modified Cys82Ser Gpx3 was biotinylated and analyzed as described in Methods. After click chemistry, the reactions were quenched by addition of an equal volume of Laemmli sample buffer. To verify the DYn-2 adduct by mass spectrometry, Cys64Ser Cys82Ser Gpx3 was incubated with H_2O_2 and 10 mM DYn-2 for 1 h at 37 °C with gentle rocking. The concentrations of Cys64Ser Cys82Ser Gpx3 and H_2O_2 used are indicated in the figure legends. Excess reagent was removed by spin filtration as described above.

4.5.8 Cell culture

HeLa cells were cultured as previously described[16]. A431 cells (American Type Culture Collection) were maintained at 37 °C in a 5% CO_2 humidified atmosphere. Unless indicated otherwise, cells were cultured in high-glucose DMEM medium (Invitrogen) containing 10% FBS (Invitrogen), 1% GlutaMax (Invitrogen), 1% MEM nonessential amino acids (Invitrogen), and 1% penicillin-streptomycin (Invitrogen), hereafter referred to as DMEM complete culture medium (DMEM-CCM). For EGF treatment, cells were

cultured until 80-90% confluent, rinsed with PBS, and placed in high-glucose DMEM medium without serum for 16-18 h. Following serum-deprivation, cells were treated with the indicated concentration of EGF for the indicated time period. EGF treatment was stopped by the removal of the medium and washing with PBS.

4.5.9 Sulfenic acid labeling in cell culture

HeLa cells were labeled as previously described[16]. A431 cells were lifted with 0.25% trypsin-EDTA, harvested by centrifugation at 1500*g* for 2 min, washed, and resuspended in serum-free DMEM at a density of 3-4 x 10^6 cells/ml. Intact cells in suspension were incubated with DMSO vehicle (2% v/v) or the indicated concentration of sulfenic acid probe (DYn-2, DAz-2, or dimedone) at 37 °C in a 5% CO_2 humidified atmosphere with periodic gentle agitation. Following treatment for the indicated time, cells were collected, and washed with PBS. The resulting cells were routinely counted using a hemocytometer and uniformly displayed greater than 90% viability by trypan blue exclusion. Lysates were prepared by resuspending washed cell pellets in lysis buffer as described in Methods. Western blot analysis confirmed EGF-dependent tyrosine phosphorylation of EGFR and downstream targets under these conditions (**Appendix 4.6.2h** and **i**).

4.5.10 Lysate preparation

Cells were harvested in modified RIPA lysis buffer [50 mM triethanolamine, pH 7.4, 150 mM NaCl, 1% NP-40, 1% sodium deoxycholate, 0.1% SDS, 1x EDTA-free complete mini protease inhibitors (Roche), 200 U/ml catalase (Sigma)]. After 20 min incubation on ice with frequent mixing, unlysed cell fragments were removed by centrifugation at 14000*g* for 15 min at 4 °C, and protein concentration was determined by BCA assay (Pierce). For analysis of protein phosphorylation, cells were harvested in phosphorylation lysis

buffer [50 mM triethanolamine, pH 7.4, 150 mM NaCl, 1% NP-40, 1% sodium deoxycholate, 0.1% SDS, 5 mM sodium pyrophosphate, 50 mM sodium fluoride, 10 µM β-glycerophosphate, 1 mM sodium orthovanadate, 0.5 mM DTT, and 1x complete mini protease inhibitors (Roche)]. For co-immunoprecipitation of Nox2 with EGFR, cells were harvested by gentle scraping with a rubber policeman in native lysis buffer A (50 mM Tris-HCl, pH 7.4, 150 mM NaCl, 0.1% Triton X-100, 0.1% NP-40, 4 mM EDTA, 1 mM sodium orthovanadate, 2.5 mM sodium pyrophosphate, 1 mM β-glycerophosphate and 1x complete mini protease inhibitors) and lysed with gentle rotation at 4 °C for 1 h. Coimmunoprecipitation of EGFR with Nox2 was performed as described above, except in native lysis buffer B (50 mM Tris-HCl, pH 7.4, 150 mM NaCl, 3 mM EDTA, 0.5% NP-40, 20 mM β-glycerophosphate, 1 mM sodium orthovanadate, 1x complete mini protease inhibitors).

4.5.11 Click chemistry

Cell lysate (200 µg, 1 mg/ml) was pretreated with 75 µl NeutrAvidin-agarose (Pierce) to remove endogenously biotinylated proteins. The precleared lysate was incubated with 100 µM azide- or alkyne-biotin, 1 mM TCEP-HCl, 100 µM TBTA ligand, and 1 mM $CuSO_4$ for 1 h at 25 °C with gentle rocking (final reaction volume of 200 µl). The reaction was quenched by 40 mM EDTA, followed by methanol precipitation of the proteins. The resulting protein precipitate was then resolubilized in Laemmli sample buffer containing 5% of SDS in PBS. To analyze immunoprecipitated proteins, the resin was treated with 20 µl click chemistry mix (100 µM azide-biotin, 1 mM TCEP, 100 µM TBTA, 1 mM $CuSO_4$ in PBS) as above; reactions were quenched by boiling with 20 µl Laemmli sample buffer for 10 min.

4.5.12 Immunostaining and fluorescence imaging

A431 cells were seeded on collagen-coated coverslips (BD Biosciences) and cultured as described above. The cells were then fixed with 4% paraformaldehyde in PBS for 15 min, washed three times with PBS, followed by blocking in 5% horse serum, 0.1% Triton X-100 in PBS for 30 min at 25 °C (blocking solution). The cells were then treated with rabbit anti-EGFR (1005, Santa Cruz Biotechnology), mouse anti-PTEN (A2B1, Santa Cruz Biotechnology), mouse anti-PTP1B (FG6, Calbiochem), or rabbit anti-SHP2 (Santa Cruz Biotechnology), at 2 μg/ml in blocking solution for 1 h at 25 °C. Control cells were treated with PBS only. The cells were washed three times in PBS and incubated with Alexa594-conjugated goat anti-rabbit (Invitrogen), Alexa488-conjugated goat anti-rabbit (Invitrogen), or Alexa488-conjugated goat anti-mouse (Invitrogen) secondary antibodies diluted to 1:1000 in blocking solution for 1 h at 25 °C in the dark. For experiments involving dimedone, cells were fixed in cold methanol:acetone (1:1), blocked, and treated with rabbit anti-2-thiodimedone (1:3000) as previously described[20]. The cells were then washed three times with PBS and stained by Alexa594-conjugated goat anti-rabbit secondary antibody (1:1000) for 1 h at 25 °C in the dark. To visualize Nox2, cells were double stained with rabbit anti-2-thiodimedone antibody (1:3000) and PE-conjugated mouse anti-Nox2 antibody (7D5, MBL International, 1:1000), followed by Alexa488-conjugated goat anti-rabbit secondary antibody (1:1000). Cells were then washed three times with blocking solution, counterstained with 0.1 mg/ml DAPI, washed with PBS, and mounted with Fluoromount G (Southern Biotech). Confocal fluorescence imaging studies on A431 cells were performed with an Olympus FV1000 microscope and an x100 oil-immersion objective lens. Excitation of Alexa488-conjugate was carried out with an argon laser and emission was collected using a 488- to 515-nm filter set. Excitation of Alexa594- or PE-conjugate was carried out with a HeNe laser, and emission was collected using a 548- to 644-nm filter set.

4.5.13 Western blot

Protein samples were separated by SDS-PAGE using Mini-Protean TGX 4-15% Tris-Glycine gels (BioRad) and transferred to a polyvinylidene difluoride (PVDF) membrane (BioRad). After transfer, the membrane was blocked with 3% BSA or 5% milk (pAKT/AKT blotting) in TBST for 1 h at 25 °C. The membrane was washed with TBST and immunoblotting was performed with the following primary and secondary antibodies at the indicated dilutions in TBST, unless otherwise noted: phospho-EGFR (pY1068, Abcam, 1:1000), EGFR (1005, Santa Cruz Biotechnology, 1:200), phospho-AKT (pS473 XP, Cell Signaling Technology, 1:2000 or pT308, Cell Signaling Technology, 1:1000), AKT (Cell Signaling Technology, 1:2000), phospho-ERK (pT185/pY187, Invitrogen, 1:1000), ERK (Invitrogen, 1:1000), Streptavidin-HRP (GE Healthcare, 1:8000 – 1:80000), His-HRP (Pierce, 1:50000), GAPDH (Santa Cruz Biotechnology, 1:200), PTEN (A2B1, Santa Cruz Biotechnology, 1:200), PTP1B (Calbiochem, 1:1000), SHP2 (Santa Cruz Biotechnology, 1:200), Nox2 (ab31092, Abcam, or Santa Cruz Biotechnology, 1:500 – 1:1000 in PBST), Nox1 (ab55831, Abcam, 1:500 in PBST), phospho-Tyrosine (Millipore, 1:1000), goat anti-rabbit IgG-HRP (Calbiochem, 1:2000 – 1:50000), rabbit anti-mouse IgG-HRP (Invitrogen, 1:30000), and donkey anti-goat IgG-HRP (Santa Cruz Biotechnology, 1:30000 in PBST). PVDF membrane was developed with chemiluminescence (GE Healthcare ECL Plus Western Blot Detection System) and imaged by film. Data was quantified by densitometry with ImageJ (Wayne Rasband, US National Institutes of Health, http://rsbweb.nih.gov/ij/). PVDF membranes were stripped using mild stripping buffer (200 mM glycine pH 2.2, 0.1% SDS, 1% Tween-20) according to established protocol (www.abcam.com) before reprobing.

4.5.14 Immunoprecipitation

EGFR was immunoprecipitated from 500 µg cell lysate (1 mg/ml) with 1 µg of anti-EGFR antibody. PTPs were immunoprecipitated from 1 mg lysate prepared from A431 cells cultured in low-glucose DMEM with 1 µg anti-PTEN antibody, anti-PTP1B antibody (BD Transduction Laboratories), or anti-SHP2 antibody overnight at 4 °C with gentle rocking. The immunocomplexes were isolated by incubating 20 µl protein A sepharose (EGFR and SHP2; GE Healthcare) or protein G agarose (PTEN and PTP1B; Roche) for an additional 2 h at 4 °C with rocking. The resin was collected by centrifugation at 100*g* for 2 min at 25 °C, washed three times with cold RIPA buffer (Boston BioProducts), subjected to click chemistry as described in Methods, and proteins were eluted by boiling with Laemmli sample buffer for 10 min. Nox2 was co-immunoprecipitated with EGFR from 500 µg of lysate with 20 µl goat anti-EGFR antibody-conjugated agarose (Santa Cruz Biotechnology) or isotype control (normal goat IgG) in a total volume of 500 µl for 4 h at 4 °C with gentle rocking. The resin was collected as above and washed three times with cold native lysis buffer, and eluted as above. EGFR was coimmunoprecipated with Nox2 as above, except using 20 µl rabbit anti-Nox2 antibody-conjugated agarose (Santa Cruz Biotechnology) or normal rabbit IgG as an isotype control. For ESI-MS analysis in **Figure 4.5g**, A431 cells were stimulated with 4 ng/ml EGF for 2 min, harvested by trypsinization, and treated with dimedone as in Methods. Following treatment, EGFR was immunoprecipitated from 6 mg cell lysate as described above. The EGFR was eluted by boiling for 10 min in 10% SDS in ddH_2O and then precipitated by acetone. The resulting protein precipitate was resuspended in Laemmli sample buffer, and resolved by SDS-PAGE.

4.5.15 Intracellular ROS detection

Intracellular ROS were measured in a 96-well plate using the fluorescent probe DCF (the intracellular product of H_2-DCF diacetate that fluoresces in the presence of ROS, including H_2O_2). A431 cells were seeded at $1.5x10^4$ per well, grown and stimulated with EGF as described in Methods. Inhibitors/scavengers were added to culture medium prior to treatment for the period of time indicated in figure legends. Following stimulation, cells were washed twice with PBS, and incubated in the dark for 30 min at 25 °C with 10 μM 2',7'-dichlorodihydrofluorescein diacetate (H_2DCF-DA, Sigma) in PBS. H_2DCF-DA is a cell permeable indicator for ROS that is a nonfluorescent compound that can enter cells and is trapped by intracellular esterase cleavage of the diacetate group. DCF is converted into a fluorescent product upon interaction with intracellular ROS. After incubation, the intensity of fluorescence was measured at 488 nm (excitation) and 525 nm (emission) using a SpectraMax M5 microplate reader (Molecular Devices). To examine the effect of DYn-2 on intracellular ROS, serum-deprived A431 cells were washed three times with PBS and then harvested by 0.25 % trypsin/EDTA. The trypsin was neutralized with DMEM and cells were collected by centrifugation at 1500*g* for 2 min. Cells were aliquoted at 6×10^5 cells per microcentrifuge tube and treated with 5 mM DYn-2 or DMSO vehicle (2% v/v) for 1 h at 37 °C. Following treatment, the cells were washed three times with PBS, seeded into 96-well plates at 1×10^5 cells/well in triplicate, and analyzed for DCF fluorescence as described above.

4.5.16 Cell viability

Serum-deprived A431 cells were labeled with 5 mM DYn-2 or DMSO vehicle (2% v/v) as described in Methods. After labeling, the cells were washed three times with PBS and resuspended in 500 μl PBS with an equal volume of trypan blue solution (0.4 % w/v).

The mixture was incubated at 25 °C for 3 min, and 10 µl of the cell suspension was loaded onto a hemocytometer and counted under a microscope.

4.5.17 Quatification of glutathione in A431 cells

Serum-deprived A431 cells were treated with 5 mM DYn-2 or DMSO vehicle (2% v/v) as described in Methods. After labeling, the cells were washed three times with PBS and lysed in 1x GSH MES buffer (Cayman Chemicals). Levels of total, reduced, and oxidized glutathione were measured using the Glutathione Assay kit (Cayman Chemicals) according to the manufacturer's instructions.

4.5.18 Quantification of peroxiredoxin SO_3 in A431 cells

Serum-deprived A431 cells were treated with 5 mM DYn-2 or 2% (v/v) DMSO as described in Methods. After labeling, cells were lysed in modified RIPA lysis buffer, resolved by SDS-PAGE, and analyzed by anti-Peroxiredoxin-SO_3 (Abcam, 1:1000) Western blot.

4.5.19 In-gel trypsin digestion of Gpx3

DYn-2 labeled Gpx3 was resolved by SDS-PAGE and stained with SimplyBlue SafeStain (Invitrogen). After staining, the gels were washed with H_2O and bands of interest were excised. The excised bands were dehydrated in 2:1 ACN: 25 mM ammonium bicarbonate (Ambic), pH 8.0 and subsequently rehydrated with 25 mM Ambic pH 8.0 twice prior to reducing with 10 mM DTT for 1 h at 56 °C. DTT was removed and the samples were alkylated with 55 mM iodoacetamide for 45 minutes at 25 °C in the dark. Iodoacetamide was removed by and the excised bands were washed with 25 mM Ambic pH 8.0 then dehydrated and rehydrated two additional times. Sequencing grade modified trypsin (Promega) was added to the excised bands at a ratio

of 1:25 (w/w), and the samples were incubated overnight at 37 °C. Peptides were extracted from the gel by collecting the supernatant and by dehydrating and rehydrating the excised bands. Peptide samples were concentrated *via* vacuum centrifugation and analyzed by ESI-LC-MS/MS.

4.5.20 In-gel pepsin digestion of immunoprecipitated EGFR

The band corresponding to EGFR was excised and the gel slice was processed as above with the following modifications. After iodoacetamide removal, the excised bands were washed with 75 mM K_2HPO_4/75 mM KH_2PO_4 pH 2.5 then dehydrated and rehydrated two additional times with 2:1 ACN: 75 mM K_2HPO_4/75 mM KH_2PO_4 pH 2.5 and 75 mM K_2HPO_4/75 mM KH_2PO_4 pH 2.5, respectively. Sequencing grade pepsin (Princeton Separations) was added to excised bands at 20 ng/µL and incubated overnight at 37 °C.

4.5.21 ESI-LC/MS/MS analysis

Gpx3 peptides were analyzed on an electrospray linear ion trap mass spectrometer (LTQ-XL, Thermo Scientific) after separation on an Agilent Eclipse XDB-C8 2.1 mm x 15 mm trap with mobile phases A (0.1% formic acid in water) and B (0.1% formic acid in acetonitrile) which was used to trap, desalt, and elute peptides onto a Vydac Everest reverse-phase C18 monomeric column (2.1 mm x 150 mm, 300 Å, 5 µm) with a gradient of 5% to 60% B in 60 min at a flow rate of 200 µL/min.

4.5.22 *In vitro* EGFR kinase assay

The tyrosine kinase activity of recombinant human EGFR kinase domain (Promega) was assayed using the ADP-Glo™ Kinase Assay (Promega) according to the manufacturer's protocol (www.promega.com), except that DTT was not included in the reaction buffer.

In brief, the ADP-Glo™ Kinase Assay is a luminescent assay that measures ADP formed from the EGFR kinase reaction; ADP is converted into ATP, which is a substrate in a reaction catalyzed by Ultra-Glo™ Luciferase that produces light. The luminescent signal positively correlates with ADP amount and kinase activity. Poly (4:1 Glu, Tyr) (Promega) was used as a peptide substrate. When present, EGFR inhibitors, H_2O_2 or DTT were added to the reaction mixture for the period of time indicated in figure legends.

4.6 Appendices

4.6.1 EGF-dependent morphological changes in A431 cells. Top images: Bright-field images of A431 cells before (T0) and after 100 ng/ml EGF stimulation for 2, 15, 30, and 60 min (labeled as T1, T2, T3, and T4, respectively). Bottom images: Combined bright-field and confocal fluorescence image of A431 cells (**Figure 4.1b** depicts the confocal fluorescence image alone). Cells were fixed and stained as described in Methods with rabbit anti-EGFR antibody (2 µg/ml) followed by Alexa594-conjugated (red) goat anti-rabbit secondary antibody (1:1000). Nuclei were counterstained with DAPI (blue). White arrows highlight changes in receptor localization (T0, plasma membrane; T1, membrane ruffles; T2, regions of cell stretching and migration; T3, perinuclear and endosomal membranes; T4, plasma membrane and ruffles).

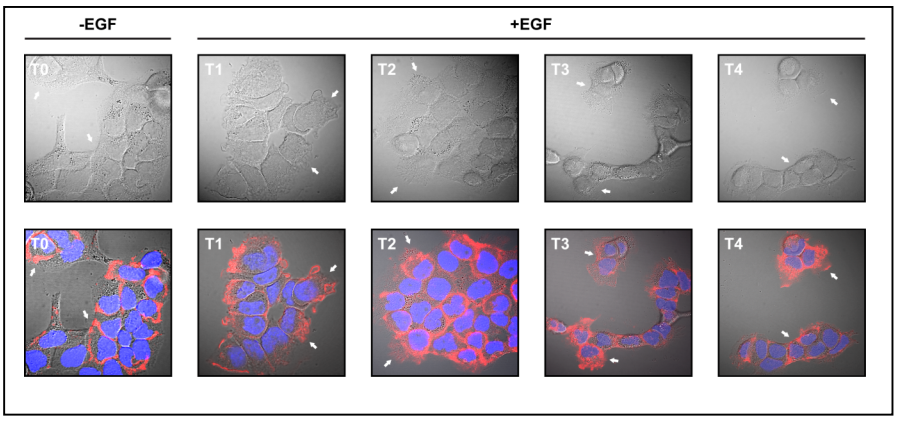

4.6.2 Structures of compounds used in this study. DAz-2 and DYn-2, sulfenic acid probes; alkyne-biotin and azide-biotin, biotinylation reagents; gefitinib, reversible EGFR kinase inhibitor; afatinib, canertinib and pelitinib, irreversible EGFR kinase inhibitors; *N*-acetyl cysteine (NAC), antioxidant; apocynin and DPI, reversible NOX inhibitors; wortmannin, reversible PI3K inhibitor.

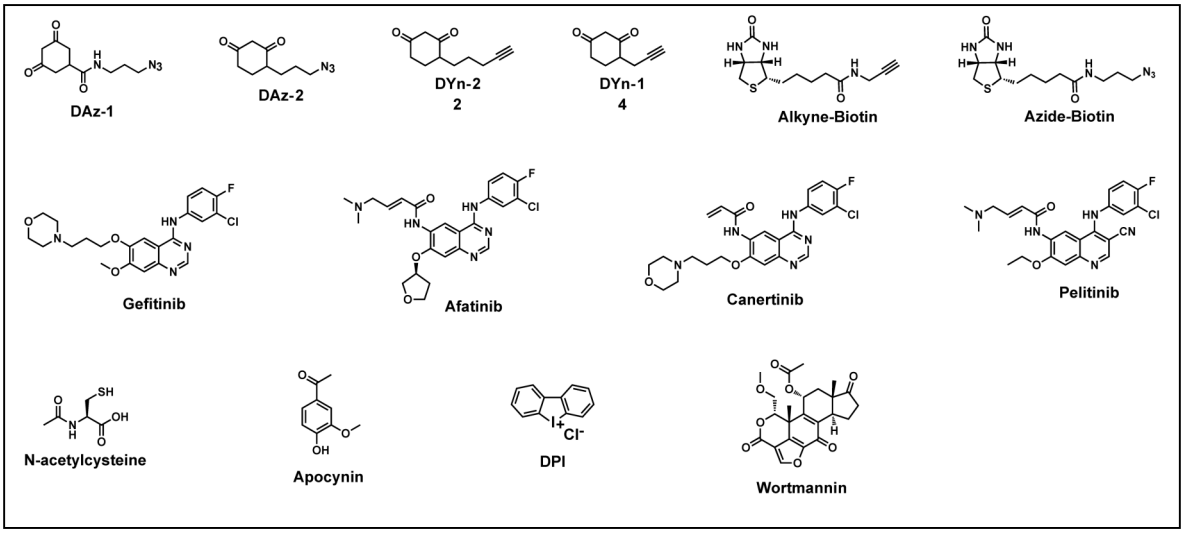

4.6.3 Effect of inhibitors, antioxidants, and sulfenic acid probes on EGF-mediated signaling. (**a**-**h**) Western blots showing global tyrosine phosphorylation (pTyr) or phosphorylated (p) EGFR, AKT and/or ERK and total EGFR, AKT, and/or ERK as loading controls. (**a**) A431 cells were stimulated with 100 ng/ml EGF or vehicle for 5 min. Where indicated, A431 cells were pretreated with 10 μM gefitinib, 100 μM afatinib or 100 μM wortmannin for 25 min. (**b**,**c**) A431 cells were treated with the indicated concentrations of PEG-catalase for 5 min (**b**) or 30 min (**c**) and then stimulated with 100 ng/ml EGF or vehicle for 5 min. Gefitinib treatment was as in **a**. (**d**,**e**) A431 cells were stimulated with 100 ng/ml EGF or vehicle for 5 min in the presence of the indicated concentrations of NAC. Gefitinib treatment was as in **a**. (**f**) A431 cells were stimulated with 100 ng/ml EGF or vehicle for 5 min. Where indicated, A431 cells were pretreated with the indicated concentrations of apocynin for 25 min before stimulation. (**g**) A431

cells were stimulated with 100 ng/ml EGF or vehicle for 5 min. Where indicated, A431 cells were pretreated with the indicated concentrations of DPI for 5 min before stimulation. (**h**) A431 cells were stimulated with 100 ng/ml EGF or vehicle for 5 min. Where indicated, A431 cells were pretreated with the indicated concentrations of DYn-2 or dimedone for 25 min before stimulation. (**i**) A431 cells were stimulated with 100 ng/ml EGF or vehicle for the indicated times, washed, harvested, resuspended in serum-free DMEM, and incubated with 5 mM DYn-2 or DMSO vehicle (2% v/v) for 15 min at 37 °C as described in Methods.

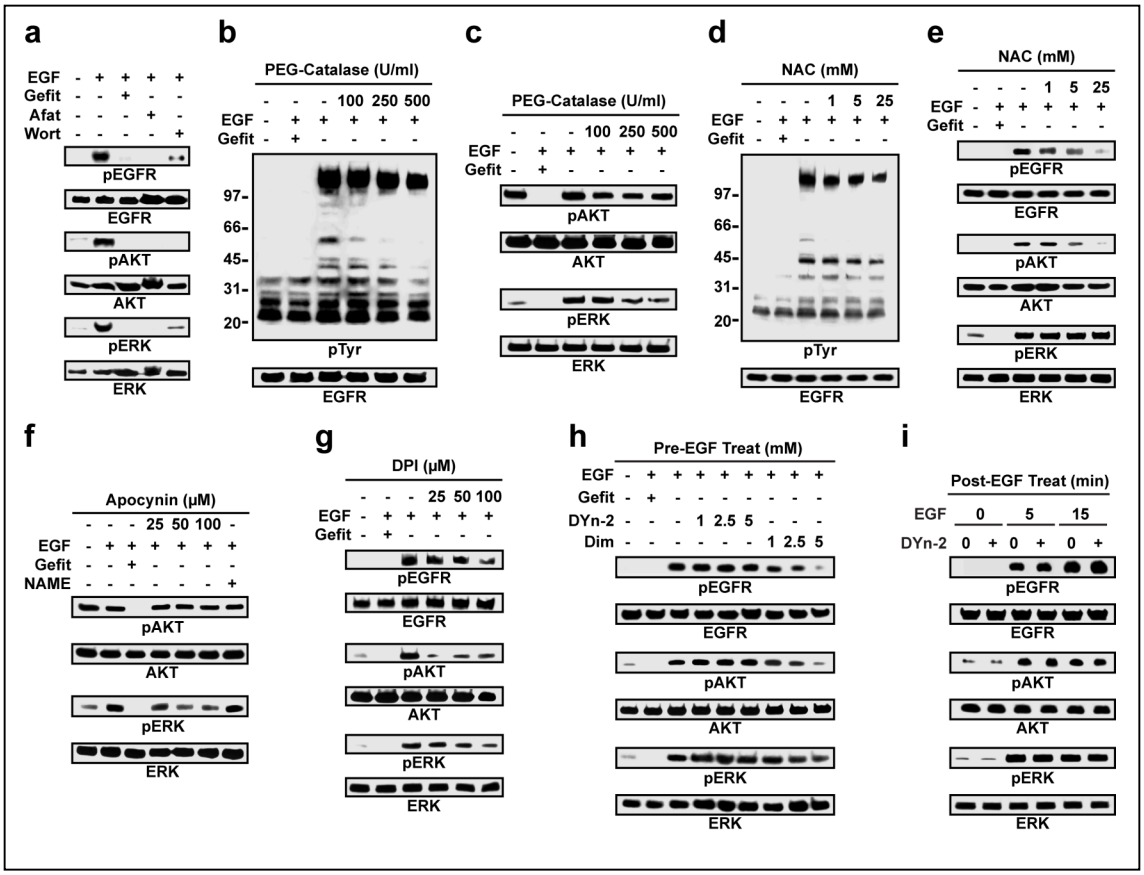

4.6.4 Detection of sulfenic acid modification with DYn-2. (**a**) LC/MS intact mass analysis shows the covalent attachment of a single DYn-2 molecule to Gpx3 (♦, 22916.39 Da). The inset shows the deconvoluted mass spectrum. The observed mass shift is 177.48 Da, whereas the expected mass shift for a single DYn-2 adduct is 176.08

Da. The slight discrepancy is well within range of the mass accuracy for the LTQ-XL instrument (100 ppm or ± 2.29 Da at 22916.39). Over-oxidation of the catalytic cysteine to sulfinic acid ($–SO_2H$) is also observed (★, 22776.36 Da). 25 μM Gpx3 was treated with 37.5 μM H_2O_2 and labeled with 10 mM DAz-2 for 1 h at 37 °C. (**b**) Top spectrum: Extracted ion (ion current at *m/z* 333.48 $[M+2H]^{+2}$) chromatogram corresponding to the unmodified peptide (MPFGCL) from native EGFR. Bottom spectrum: The extracted ion (ion current at *m/z* 402.80 $[M+2H]^{+2}$) chromatogram corresponding to the dimedone-tagged peptide (MPFGC*L) from native EGFR. The ratio of dimedone-modified to unmodified peptide was determined by taking the areas under the curves and was determined to be approximately 6:1. A431 cells were stimulated with 4 ng/ml EGF for 2 min, washed, incubated with 5 mM dimedone for 1 h at 37 °C, immunoprecipitated with anti-EGFR antibody, and resolved by SDS-PAGE. The band corresponding to EGFR (~170 kDa) was excised, digested with pepsin, and analyzed by ESI-LC-MS/MS as described in Methods.

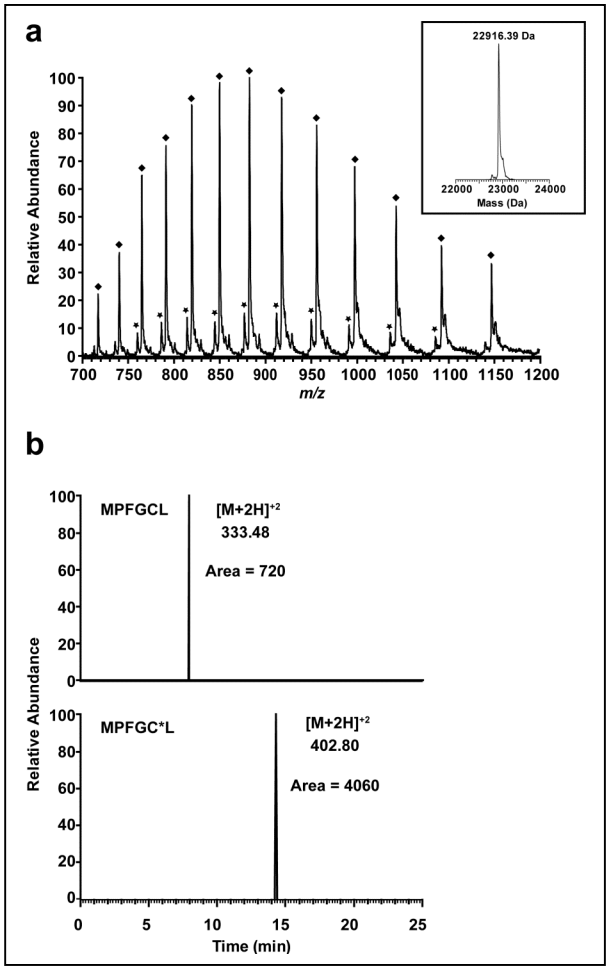

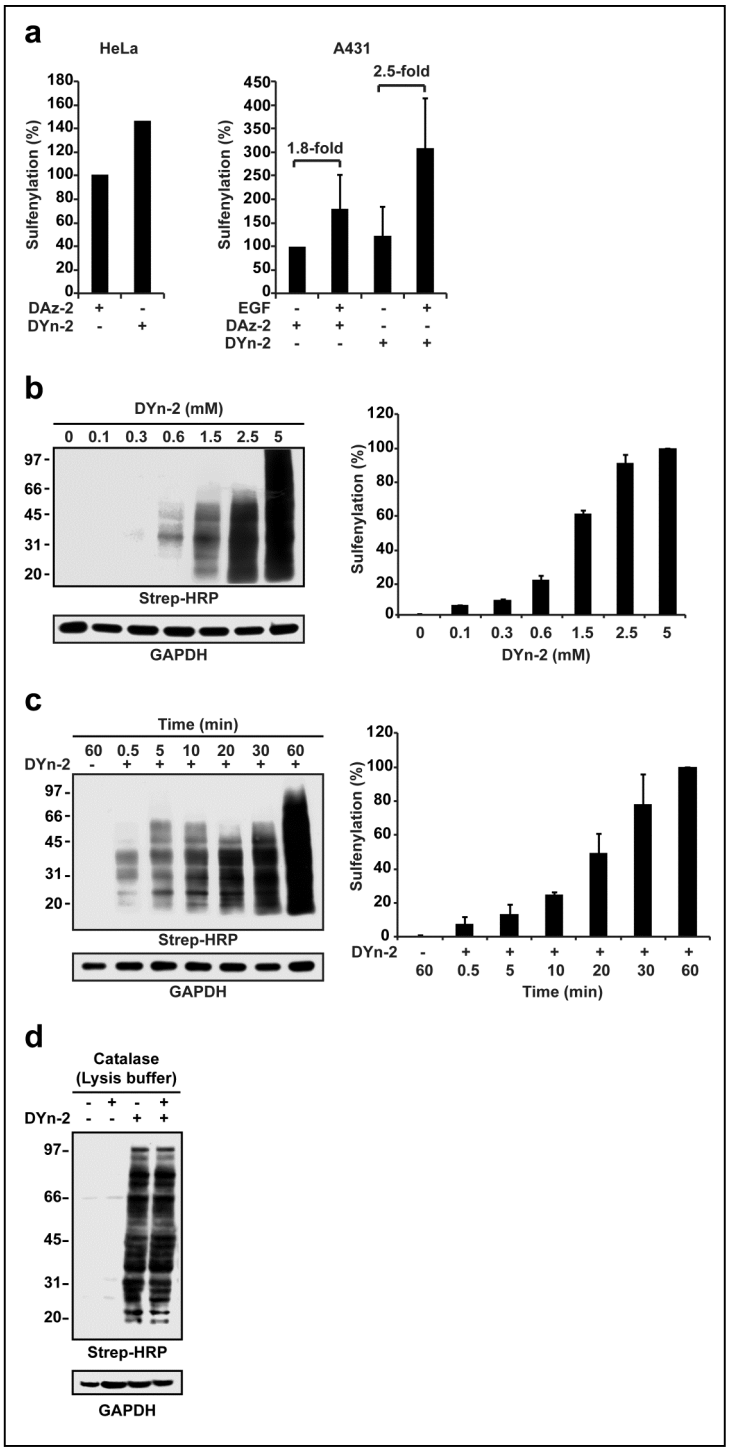

4.6.5 DYn-2 labeling of protein sulfenic acids in A431 cells. (**a**) Densitometric quantification of electrophoretic lanes from **Figure 4.2f** and **g**. Right graph: The numbers situated above indicate the fold-increase in sulfenylation signal between unstimulated and EGF-treated cells. (**b**,**c**) Western blot showing dose- and time-dependent detection of protein sulfenic acids in A431 cells and total GAPDH as loading controls. A431 cells were stimulated with 100 ng/ml EGF for 5 min, washed, lifted as described in Methods and then treated with vehicle or the indicated concentrations of DYn-2 for 1 h at 37 °C (**b**), or with 5 mM DYn-2 for the indicated times (**c**), and protein sulfenic acids were detected by streptavidin-HRP Western blot as in **Figure 4.2g**. Densitometric quantification of each electrophoretic lane from dose (**b**) and time (**c**) dependencies are shown at the right of their respective Western blots and data were normalized to the maximal signal

observed in each case. (**d**) A431 cells were treated with 5 mM DYn-2 or vehicle for 1 h at 37 °C, washed, harvested in the presence or absence of 200 U/ml catalase, and protein sulfenic acids were detected by streptavidin-HRP Western blot as in **Figure 4.2g**. For all graphs, error bars show ± s.e.m.

4.6.6 DYn-2 treatment of A431 cells does not trigger cell death or oxidative stress.

A431 cells were stimulated with 100 ng/ml EGF for 5 min, washed, and incubated with 5 mM DYn-2 or vehicle for 1 h at 37 °C as described in Methods. Following treatment: (**a**) A431 cell viability was evaluated by cell counting using trypan blue exclusion after DYn-2 or vehicle treatment and results were expressed as the percentage of viable cells. (**b**,**c**) Production of intracellular ROS was measured by DCF fluorescence as described in Methods. Where indicated, H_2O_2 was added at a final concentration of 400 μM. In (**c**), data were normalized to vehicle control as 100% DCF fluorescence. (**d**) Reduced glutathione (GSH) and oxidized glutathione (GSSG) levels were measured in DYn-2 and vehicle-treated samples as described in Methods. (**e**) GSH represented as a percentage of total glutathione pool. (**f**) Samples were resolved by SDS-PAGE and analyzed by anti-Prx-SO_3 Western blot (left). Comparable protein loading was confirmed by anti-GAPDH Western blot. Prx-SO_3 signal was quantified by densitometry, and normalized to the vehicle control (right). For all graphs, error bars show ± s.e.m.

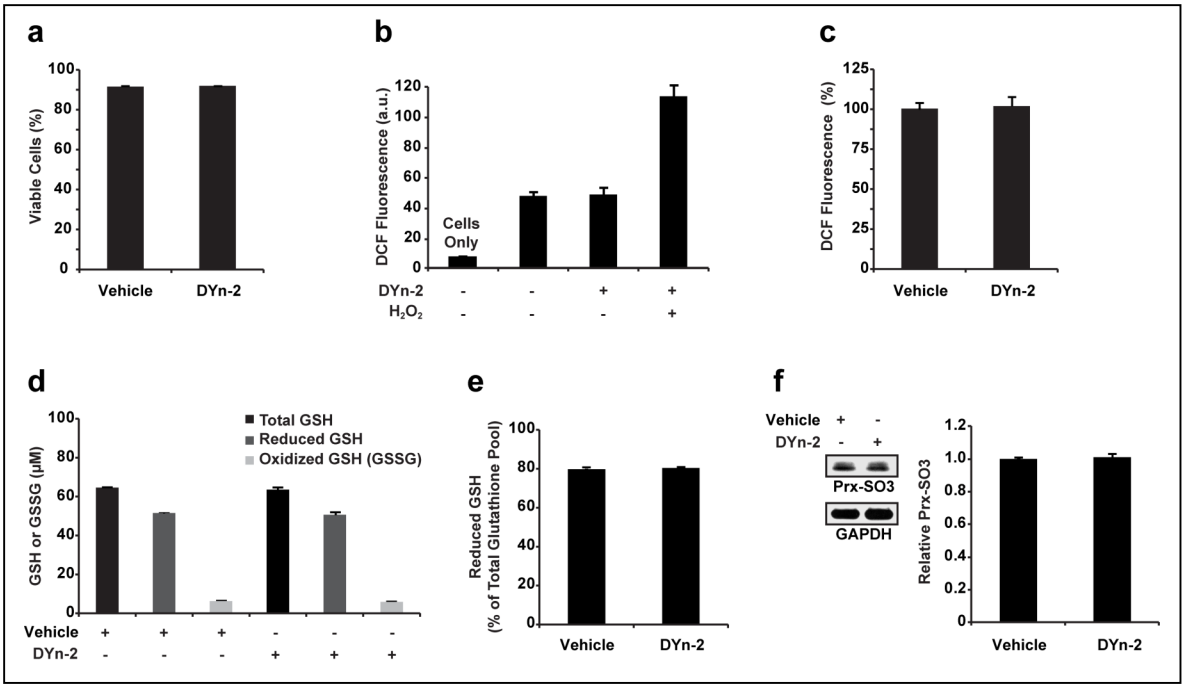

4.6.7 Secondary antibody only control and imaging of Nox2 in A431 cells that are not permeabilized. (**a**) Confocal fluorescence images of A431 cells labeled with secondary antibody only. Cells were fixed and stained as described in Methods with Alexa488-conjugated goat anti-rabbit secondary or Alexa594-conjugated (red) goat anti-rabbit secondary antibodies (1:1000). Nuclei were counterstained with DAPI (blue). (**b**) A431 cells were fixed but not permeabilized and stained with PE-

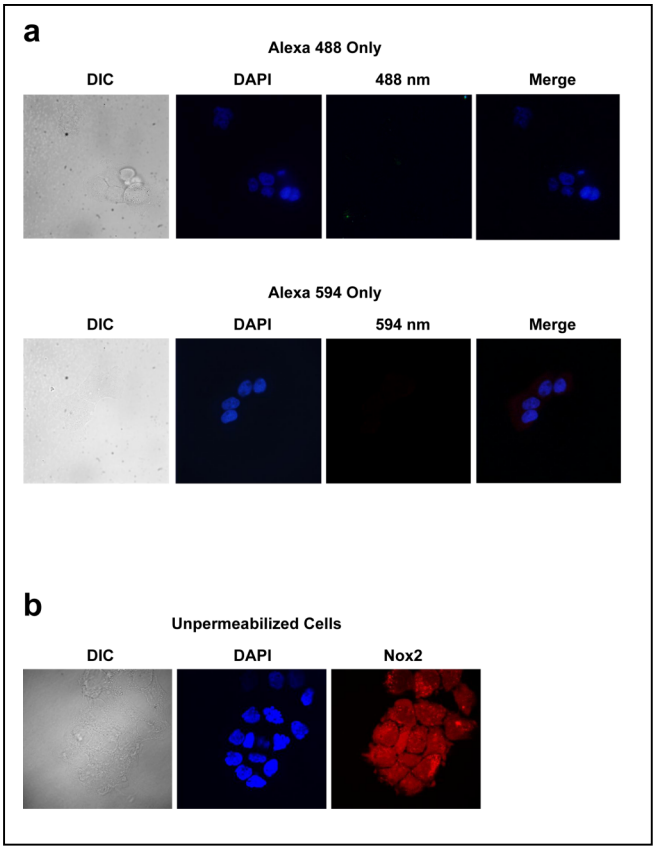

conjugated (red) mouse anti-Nox2 antibody. Nuclei were counterstained with DAPI (blue).

4.6.8 EGF-mediated sulfenylation requires EGFR activity and is modulated by cellular redox status in A431 cells. Western blots showing protein sulfenic acids in A431 cells and total GAPDH. (**a**) A431 cells were stimulated with 100 ng/ml EGF for 2 min after pretreatment with 10 μM gefitinib, 1 μM afatinib, 10 μM canertinib, 1 μM pelitinib, 100 μM apocynin, 100 μM wortmannin, 100 μM L-NAME or vehicle for 25 min. In (**b**), A431 cells were stimulated with 100 ng/ml EGF for 2 min after pretreatment with PEG-catalase at the indicated concentration for 5 min. In (**c**), A431 cells were stimulated with 100 ng/ml EGF for 5 min after pretreatment with NAC at the indicated concentration for 5 min. In (**d**), A431 cells were stimulated with 100 ng/ml EGF for 2 min after pretreatment with apocynin at the indicated concentration for 5 min (**d**). In (**e**) A431 cells were stimulated with 100 ng/ml EGF for 5 min after pretreatment with DPI at the indicated

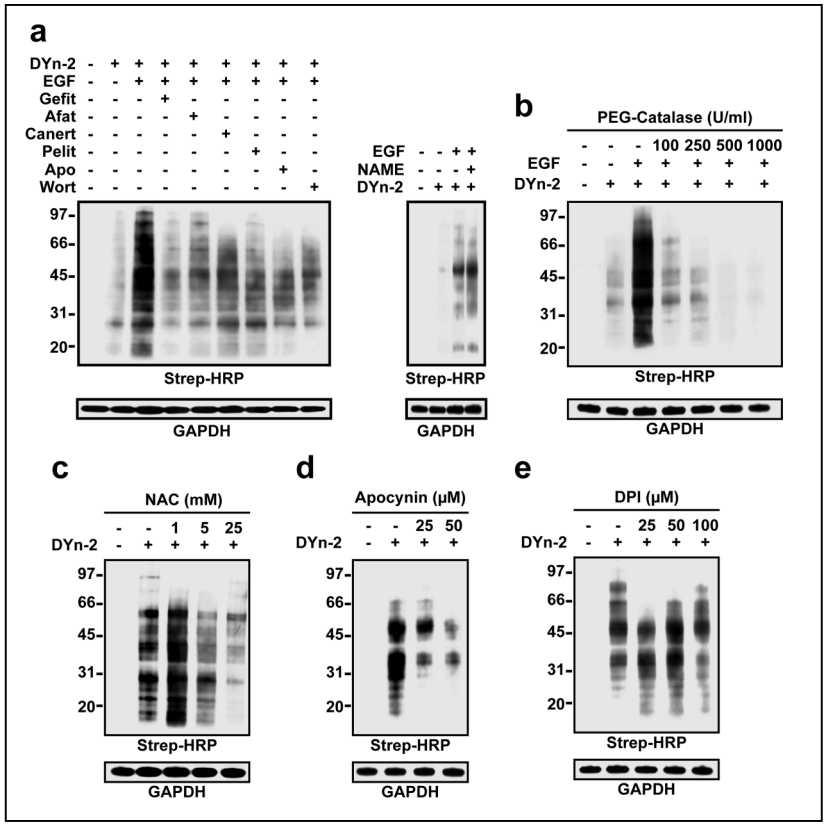

concentration for 5 min. Following treatment, cells were incubated with DYn-2 or vehicle for 1 h (**a**) or 15 min (**b**-**e**) at 37 °C and sulfenic acids were detected by streptavidin-HRP Western blot as in **Figure 4.2g**.

4.6.9 Nox2 expression, H_2O_2-mediated EGFR oxidation and modulation of recombinant EGFR tyrosine kinase activity. (**a, b**) Expression of Nox1 and Nox2 in A431 cells was analyzed by Western blot with rabbit anti-Nox1 and rabbit anti-Nox2, with GAPDH as a loading control (**a**) or immunofluorescence microscopy (**b**). In (**b**), cells were fixed and stained with rabbit anti-Nox1 or rabbit anti-Nox2 antibodies at 2 μg/ml, followed by Alexa594-conjugated goat anti-rabbit (red) secondary antibodies (1:1000). Nuclei were counterstained with DAPI (blue). (**c**) Western blot showing sulfenylated and total EGFR. A431 cells were stimulated with H_2O_2 at the indicated concentrations for 10 min and sulfenic acids were detected by streptavidin-HRP Western blot as in **Figure 4.5b**. (**d**) Western blot showing coimmunoprecipitation of SHP2, EGFR, and Nox2. A431 cells were stimulated with 100 ng/ml EGF or vehicle for the indicated times and samples were processed as in **Figure 4.5c**. The presence of SHP2 was evaluated using a rabbit anti-SHP2 antibody and comparable recovery of immunoprecipitated EGFR was confirmed by probing the Western blot with rabbit anti-EGFR antibody. IC, isotype control. (**e**-**g**,**i**) Measurement of EGFR tyrosine kinase activity *in vitro* as described in Methods. (**e**) Recombinant EGFR (rEGFR) kinase activity titration. (**f**,**g**) rEGFR was incubated with gefitinib (**f**) or afatinib (**g**) at the indicated concentrations and assayed for kinase activity. (**h**) rEGFR was incubated with H_2O_2 or vehicle for 15 min, and then 1 mM DTT or vehicle was added for an additional 10 min and assayed for kinase activity. Data were normalized to the untreated control and error bars show ± s.e.m. (**i**) The ATP-regenerating system from the EGFR kinase activity assay was

untreated or co-incubated with the indicated concentrations of H_2O_2 and assayed for kinase activity.

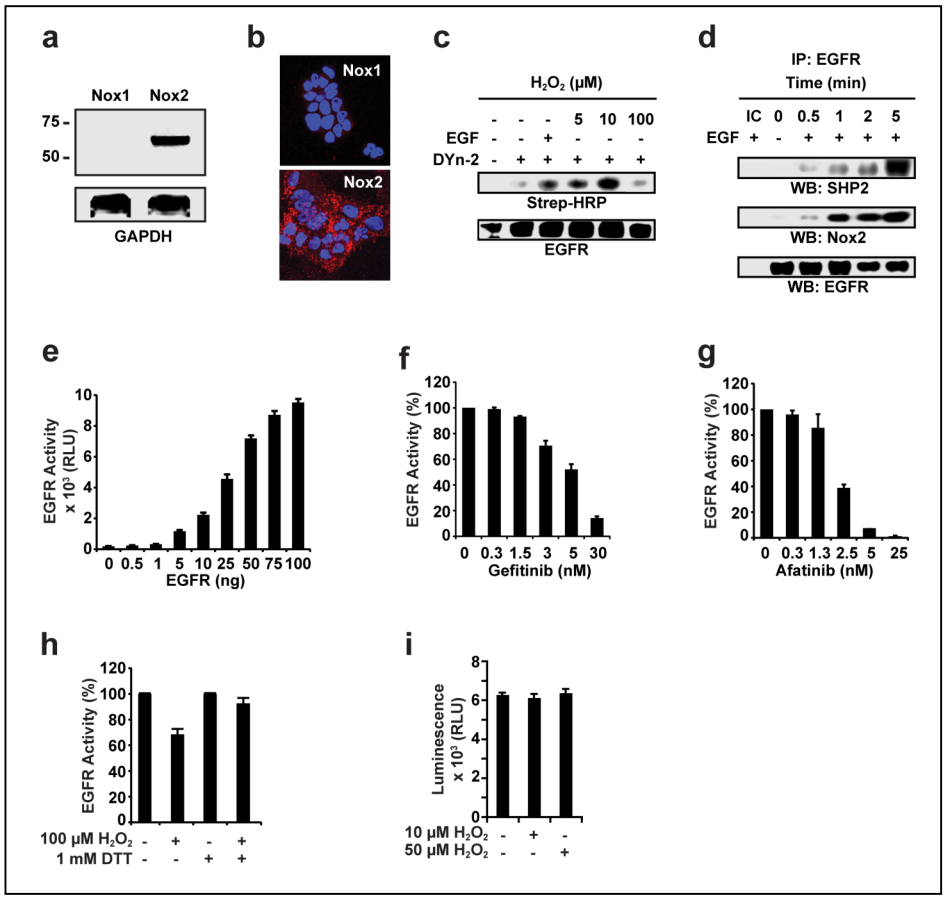

4.6.10 Indirect and direct chemical techniques to monitor cysteine oxidation and PTP oxidation/trapping scheme. (**a**) Loss of reactivity with thiol-modifying reagents indirectly monitors cysteine oxidation. ROS and RNS oxidize reactive protein thiols (red protein). Addition of a thiol-specific alkylating agent such as NEM or IAM derivatized with a detection handle covalently modifies free thiols. Increased cysteine oxidation exhibits a decrease in probe signal. (**b**) Restoration of thiol-labeling by reducing agents indirectly monitors cysteine oxidation. Initially samples are incubated with NEM or IAM to irreversibly alkylate free thiols. Next a reducing agent returns oxidized cysteines to free thiols. Addition of NEM or IAM derivatized with a detection handle covalently modifies nascent thiols. Increased cysteine oxidation exhibits an increase in probe

signal. (**c**) Direct detection of specific cysteine oxoforms. Samples are incubated with a chemoselective alkylating agent for a specific cysteine oxoform (*i.e.* nitrosothiols and sulfenic acids) derivatized with a detection handle. Visualization of probe incorporation results in an increase in signal with increased oxidation. (**d**) Reaction of H_2O_2 with the catalytic cysteine thiolate of PTPs generates sulfenic acid (second order reaction). Once formed, the sulfenic acid can condense with a backbone amide to form a sulfenamide in PTP1B, or with a second cysteine residue to form an intramolecular disulfide in PTEN and SHP2 (first order reaction). Alternatively, the sulfenic acid intermediate can be trapped by dimedone or DYn-2 (second order reaction). The amount of sulfenic acid detected is a function of the: (i) rate of oxidation (~2-10 $M^{-1}s^{-1}$)[75,76], (ii) rate of dimedone/DYn-2 trap (~10^3 $M^{-1}s^{-1}$)[90,91], and (iii) rate of intramolecular condensation (~10^{-3} s^{-1} for sulfenamide[78] and ~10 s^{-1} for intramolecular disulfide[77]). Note: the aforementioned rates were measured *in vitro* with recombinant proteins. In some cases, the sulfenic acid may be directly reduced back to the thiol.

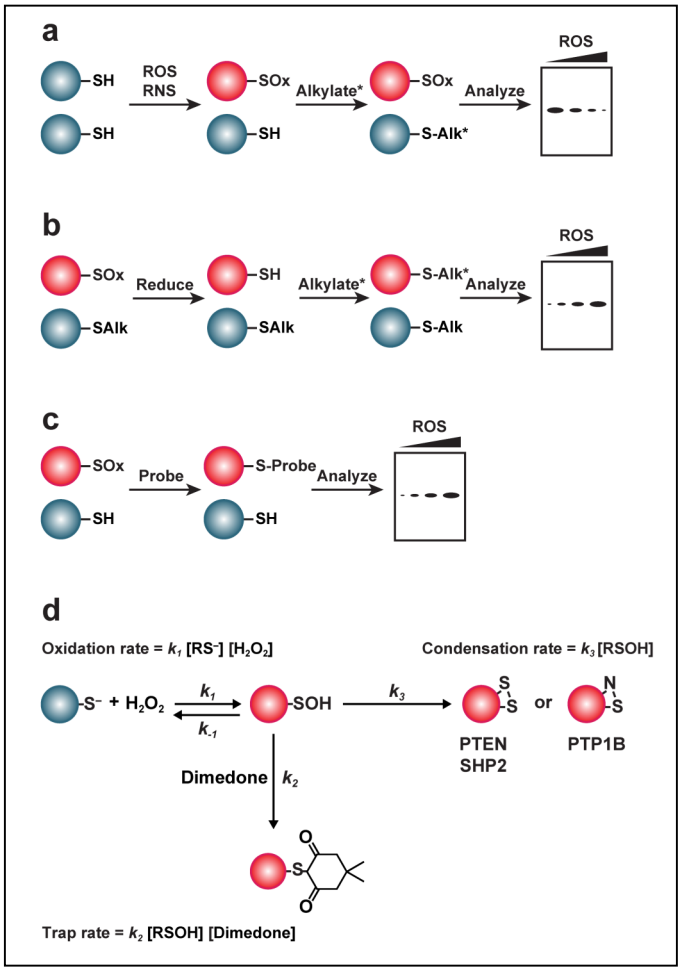

Acknowledgments

We apologize to the many authors of important primary research studies whose work could not be cited directly due to space limitations. The authors acknowledge funding from the Camille Henry Dreyfus Teacher Scholar Award (to K.S.C.) and the American Heart Association Scientist Development Award (0835419N to K.S.C.). The authors also wish to thank R. Peter and group members for support and helpful discussion.

Notes

This work has been submitted for publication in *Nature Chemical Biology* as Paulsen C.E., Truong T.H., Garcia F.G., Homann A., Gupta V., Leonard S.E., and Carroll K.S., "Protein sulfenylation goes global: Probing intracellular targets of hydrogen peroxide produced for growth factor signaling". Candice E. Paulsen, Thu H. Truong and Arne Homann performed all cell culture experiments. Francisco J. Garcia performed all mass spectrometry analysis. Vinayak Gupta and Stephen E. Leonard synthesized compounds in the paper and performed analytical measurements. All coauthors designed experimental strategies. Candice E. Paulsen and Kate S. Carroll wrote the paper with input from all coauthors.

4.7 References

1 Rhee, S. G. Cell signaling. H_2O_2, a necessary evil for cell signaling. *Science* **312**, 1882-1883 (2006).

2 Stone, J. R. & Yang, S. Hydrogen peroxide: a signaling messenger. *Antioxid. Redox Signal.* **8**, 243-270 (2006).

3 D'Autreaux, B. & Toledano, M. B. ROS as signalling molecules: mechanisms that generate specificity in ROS homeostasis. *Nat. Rev. Mol. Cell Biol.* **8**, 813-824 (2007).

4 Miller, E. W., Tulyathan, O., Isacoff, E. Y. & Chang, C. J. Molecular imaging of hydrogen peroxide produced for cell signaling. *Nat. Chem. Biol.* **3**, 263-267 (2007).

5 Woo, H. A. *et al.* Inactivation of peroxiredoxin I by phosphorylation allows localized H_2O_2 accumulation for cell signaling. *Cell* **140**, 517-528 (2010).

6 Dansen, T. B. *et al.* Redox-sensitive cysteines bridge p300/CBP-mediated acetylation and FoxO4 activity. *Nat Chem Biol* **5**, 664-672 (2009).

7 Fomenko, D. E. *et al.* Thiol peroxidases mediate specific genome-wide regulation of gene expression in response to hydrogen peroxide. *Proceedings of the National Academy of Sciences of the United States of America* **108**, 2729-2734 (2011).

8 Klomsiri, C., Karplus, P. A. & Poole, L. B. Cysteine-based redox switches in enzymes. *Antioxidants & redox signaling* **14**, 1065-1077 (2011).

9 Paulsen, C. E. & Carroll, K. S. Orchestrating redox signaling networks through regulatory cysteine switches. *ACS Chem Biol* **5**, 47-62 (2010).

10 Weerapana, E. *et al.* Quantitative reactivity profiling predicts functional cysteines in proteomes. *Nature* **468**, 790-795 (2010).

11 Winterbourn, C. C. & Hampton, M. B. Thiol chemistry and specificity in redox signaling. *Free Radic Biol Med* **45**, 549-561 (2008).

12 Poole, L. B. & Nelson, K. J. Discovering mechanisms of signaling-mediated cysteine oxidation. *Current Opinion in Chemical Biology* **12**, 18-24 (2008).

13 Reddie, K. G. & Carroll, K. S. Expanding the functional diversity of proteins through cysteine oxidation. *Current Opinion in Chemical Biology* **12**, 746-754 (2008).

14 Roos, G. & Messens, J. Protein sulfenic acid formation: From cellular damage to redox regulation. *Free Radic. Biol. Med.* (2011).

15 Charles, R. L. *et al.* Protein sulfenation as a redox sensor: proteomics studies using a novel biotinylated dimedone analogue. *Mol. Cell Proteomics* **6**, 1473-1484 (2007).

16 Leonard, S. E., Reddie, K. G. & Carroll, K. S. Mining the thiol proteome for sulfenic acid modifications reveals new targets for oxidation in cells. *ACS Chem. Biol.* **4**, 783-799 (2009).

17 Michalek, R. D. *et al.* The requirement of reversible cysteine sulfenic acid formation for T cell activation and function. *J. Immunol.* **179**, 6456-6467 (2007).

18 Paulsen, C. E. & Carroll, K. S. Chemical dissection of an essential redox switch in yeast. *Chem. Biol.* **16**, 217-225 (2009).

19 Salsbury, F. R., Jr., Knutson, S. T., Poole, L. B. & Fetrow, J. S. Functional site profiling and electrostatic analysis of cysteines modifiable to cysteine sulfenic acid. *Protein Science* **17**, 299-312 (2008).

20 Seo, Y. H. & Carroll, K. S. Profiling protein thiol oxidation in tumor cells using sulfenic acid-specific antibodies. *Proc. Natl. Acad. Sci. U.S.A.* **106**, 16163-16168 (2009).

21 Takanishi, C. L. & Wood, M. J. A Genetically Encoded Probe for the Identification of Proteins that Form Sulfenic Acid in Response to H_2O_2 in Saccharomyces cerevisiae. *J. Prot. Res.* **10**, 2715-2724 (2011).
22 Chinkers, M., McKanna, J. A. & Cohen, S. Rapid induction of morphological changes in human carcinoma cells A-431 by epidermal growth factors. *Journal of Cell Biology* **83**, 260-265 (1979).
23 Miller, K., Beardmore, J., Kanety, H., Schlessinger, J. & Hopkins, C. R. Localization of the epidermal growth factor (EGF) receptor within the endosome of EGF-stimulated epidermoid carcinoma (A431) cells. *Journal of Cell Biology* **102**, 500-509 (1986).
24 Bae, Y. S. *et al.* Epidermal growth factor (EGF)-induced generation of hydrogen peroxide. Role in EGF receptor-mediated tyrosine phosphorylation. *Journal of Biological Chemistry* **272**, 217-221 (1997).
25 Aslan, M. & Ozben, T. Oxidants in receptor tyrosine kinase signal transduction pathways. *Antioxid. Redox Signal.* **5**, 781-788 (2003).
26 Chen, K., Kirber, M. T., Xiao, H., Yang, Y. & Keaney, J. F., Jr. Regulation of ROS signal transduction by NADPH oxidase 4 localization. *Journal of Cell Biology* **181**, 1129-1139 (2008).
27 Dickinson, B. C., Peltier, J., Stone, D., Schaffer, D. V. & Chang, C. J. Nox2 redox signaling maintains essential cell populations in the brain. *Nat. Chem. Biol.* **7**, 106-112 (2011).
28 Rhee, S. G., Bae, Y. S., Lee, S. R. & Kwon, J. Hydrogen peroxide: a key messenger that modulates protein phosphorylation through cysteine oxidation. *Sci. STKE* **2000**, pe1 (2000).
29 Gamou, S. & Shimizu, N. Hydrogen peroxide preferentially enhances the tyrosine phosphorylation of epidermal growth factor receptor. *FEBS Letters* **357**, 161-164 (1995).
30 Goldkorn, T. *et al.* EGF-Receptor phosphorylation and signaling are targeted by H_2O_2 redox stress. *American Journal of Respiratory Cell and Molecular Biology* **19**, 786-798 (1998).
31 Benitez, L. V. & Allison, W. S. The inactivation of the acyl phosphatase activity catalyzed by the sulfenic acid form of glyceraldehyde 3-phosphate dehydrogenase by dimedone and olefins. *Journal of Biological Chemistry* **249**, 6234-6243 (1974).
32 Leonard, S. E. & Carroll, K. S. Chemical 'omics' approaches for understanding protein cysteine oxidation in biology. *Current Opinion in Chemical Biology* **15**, 88-102 (2011).
33 Nelson, K. J. *et al.* Use of dimedone-based chemical probes for sulfenic acid detection methods to visualize and identify labeled proteins. *Methods in Enzymology* **473**, 95-115 (2010).
34 Poole, L. B. *et al.* Fluorescent and affinity-based tools to detect cysteine sulfenic acid formation in proteins. *Bioconjug. Chem.* **18**, 2004-2017 (2007).
35 Reddie, K. G., Seo, Y. H., Muse III, W. B., Leonard, S. E. & Carroll, K. S. A chemical approach for detecting sulfenic acid-modified proteins in living cells. *Mol. Biosyst.* **4**, 521-531 (2008).
36 Seo, Y. H. & Carroll, K. S. Facile synthesis and biological evaluation of a cell-permeable probe to detect redox-regulated proteins. *Bioorganic & Medicinal Chemistry Letters* **19**, 356-359 (2009).
37 Go, Y. M. & Jones, D. P. Redox compartmentalization in eukaryotic cells. *Biochimica et Biophysica Acta* **1780**, 1273-1290 (2008).

38 Depuydt, M. *et al.* A periplasmic reducing system protects single cysteine residues from oxidation. *Science* **326**, 1109-1111 (2009).
39 Agard, N. J., Baskin, J. M., Prescher, J. A., Lo, A. & Bertozzi, C. R. A comparative study of bioorthogonal reactions with azides. *ACS Chem. Biol.* **1**, 644-648 (2006).
40 Charron, G. *et al.* Robust fluorescent detection of protein fatty-acylation with chemical reporters. *Journal of the American Chemical Society* **131**, 4967-4975 (2009).
41 Speers, A. E. & Cravatt, B. F. Profiling enzyme activities in vivo using click chemistry methods. *Chem. Biol.* **11**, 535-546 (2004).
42 Zaro, B. W., Yang, Y. Y., Hang, H. C. & Pratt, M. R. Chemical reporters for fluorescent detection and identification of O-GlcNAc-modified proteins reveal glycosylation of the ubiquitin ligase NEDD4-1. *Nat. Rev. Drug Dis.* **108**, 8146-8151 (2011).
43 Bedard, K. & Krause, K. H. The NOX family of ROS-generating NADPH oxidases: physiology and pathophysiology. *Physiol. Rev.* **87**, 245-313 (2007).
44 Oakley, F. D., Smith, R. L. & Engelhardt, J. F. Lipid rafts and caveolin-1 coordinate interleukin-1beta (IL-1beta)-dependent activation of NFkappaB by controlling endocytosis of Nox2 and IL-1beta receptor 1 from the plasma membrane. *Journal of Biological Chemistry* **284**, 33255-33264 (2009).
45 von Lohneysen, K., Noack, D., Wood, M. R., Friedman, J. S. & Knaus, U. G. Structural insights into Nox4 and Nox2: motifs involved in function and cellular localization. *Mol. Cell Biol.* **30**, 961-975 (2010).
46 Kwon, J. *et al.* Reversible oxidation and inactivation of the tumor suppressor PTEN in cells stimulated with peptide growth factors. *Proc. Natl. Acad. Sci. U.S.A.* **101**, 16419-16424 (2004).
47 Lee, S. R., Kwon, K. S., Kim, S. R. & Rhee, S. G. Reversible inactivation of protein-tyrosine phosphatase 1B in A431 cells stimulated with epidermal growth factor. *Journal of Biological Chemistry* **273**, 15366-15372 (1998).
48 Meng, T. C., Fukada, T. & Tonks, N. K. Reversible oxidation and inactivation of protein tyrosine phosphatases in vivo. *Mol. Cell* **9**, 387-399 (2002).
49 Tanner, J. J., Parsons, Z. D., Cummings, A. H., Zhou, H. & Gates, K. S. Redox Regulation of Protein Tyrosine Phosphatases: Structural and Chemical Aspects. *Antioxid. Redox Signal.* (2011).
50 Winterbourn, C. C. Reconciling the chemistry and biology of reactive oxygen species. *Nat. Chem. Biol.* **4**, 278-286 (2008).
51 Zhang, S. & Yu, D. PI(3)king apart PTEN's role in cancer. *Clin. Cancer Res.* **16**, 4325-4330 (2010).
52 Liu, F. & Chernoff, J. Protein tyrosine phosphatase 1B interacts with and is tyrosine phosphorylated by the epidermal growth factor receptor. *Biochem. J.* **327 (Pt 1)**, 139-145 (1997).
53 Agazie, Y. M. & Hayman, M. J. Molecular mechanism for a role of SHP2 in epidermal growth factor receptor signaling. *Mol. Cell Biol.* **23**, 7875-7886 (2003).
54 Singh, J., Petter, R. C., Baillie, T. A. & Whitty, A. The resurgence of covalent drugs. *Nat. Rev. Drug Disc.* **10**, 307-317 (2011).
55 Singh, J., Petter, R. C. & Kluge, A. F. Targeted covalent drugs of the kinase family. *Current Opinion in Chemical Biology* **14**, 475-480 (2010).
56 Cuddihy, S. L., Winterbourn, C. C. & Hampton, M. B. Assessment of Redox Changes to Hydrogen Peroxide-Sensitive Proteins During EGF Signaling. *Antioxid. Redox Signal.* (2011).

57 Miller, E. W. & Chang, C. J. Fluorescent probes for nitric oxide and hydrogen peroxide in cell signaling. *Current Opinion in Chemical Biology* **11**, 620-625 (2007).
58 Dickinson, B. C., Srikun, D. & Chang, C. J. Mitochondrial-targeted fluorescent probes for reactive oxygen species. *Current Opinion in Chemical Biology* **14**, 50-56 (2010).
59 Dickinson, B. C., Huynh, C. & Chang, C. J. A palette of fluorescent probes with varying emission colors for imaging hydrogen peroxide signaling in living cells. *Journal of the American Chemical Society* **132**, 5906-5915 (2010).
60 Juarez, J. C. *et al.* Superoxide dismutase 1 (SOD1) is essential for H_2O_2-mediated oxidation and inactivation of phosphatases in growth factor signaling. *Proc. Natl. Acad. Sci. U.S.A.* **105**, 7147-7152 (2008).
61 Sundaresan, M., Yu, Z. X., Ferrans, V. J., Irani, K. & Finkel, T. Requirement for generation of H_2O_2 for platelet-derived growth factor signal transduction. *Science* **270**, 296-299 (1995).
62 Irani, K. *et al.* Mitogenic signaling mediated by oxidants in Ras-transformed fibroblasts. *Science* **275**, 1649-1652 (1997).
63 Saunders, J. A., Rogers, L. C., Klomsiri, C., Poole, L. B. & Daniel, L. W. Reactive oxygen species mediate lysophosphatidic acid induced signaling in ovarian cancer cells. *Free Radic. Biol. Med.* **49**, 2058-2067 (2010).
64 Lambeth, J. D. NOX enzymes and the biology of reactive oxygen. *Nat. Rev. Immunol.* **4**, 181-189 (2004).
65 Petry, A., Weitnauer, M. & Gorlach, A. Receptor activation of NADPH oxidases. *Antioxid. Redox Signal.* **13**, 467-487 (2010).
66 Stolk, J., Hiltermann, T. J., Dijkman, J. H. & Verhoeven, A. J. Characteristics of the inhibition of NADPH oxidase activation in neutrophils by apocynin, a methoxy-substituted catechol. *American Journal of Respiratory Cell and Molecular Biology* **11**, 95-102 (1994).
67 Shao, M. X. & Nadel, J. A. Dual oxidase 1-dependent MUC5AC mucin expression in cultured human airway epithelial cells. *Proc. Natl. Acad. Sci. U.S.A.* **102**, 767-772 (2005).
68 Touyz, R. M. Apocynin, NADPH oxidase, and vascular cells: a complex matter. *Hypertension* **51**, 172-174 (2008).
69 Bae, Y. S. *et al.* Platelet-derived growth factor-induced H_2O_2 production requires the activation of phosphatidylinositol 3-kinase. *Journal of Biological Chemistry* **275**, 10527-10531 (2000).
70 Baumer, A. T. *et al.* Phosphatidylinositol 3-kinase-dependent membrane recruitment of Rac-1 and p47phox is critical for alpha-platelet-derived growth factor receptor-induced production of reactive oxygen species. *Journal of Biological Chemistry* **283**, 7864-7876 (2008).
71 Park, H. S. *et al.* Sequential activation of phosphatidylinositol 3-kinase, beta Pix, Rac1, and Nox1 in growth factor-induced production of H2O2. *Mol. Cell Biol.* **24**, 4384-4394 (2004).
72 Boivin, B., Yang, M. & Tonks, N. K. Targeting the reversibly oxidized protein tyrosine phosphatase superfamily. *Sci. Signal.* **3**, pl2 (2010).
73 Leichert, L. I. *et al.* Quantifying changes in the thiol redox proteome upon oxidative stress in vivo. *Proc. Natl. Acad. Sci. U.S.A.* **105**, 8197-8202 (2008).
74 Morazzani, M. *et al.* Monolayer versus aggregate balance in survival process for EGF-induced apoptosis in A431 carcinoma cells: Implication of ROS-P38 MAPK-integrin alpha2beta1 pathway. *Int. J. Cancer* **110**, 788-799 (2004).

75 Chen, C. Y., Willard, D. & Rudolph, J. Redox regulation of SH2-domain-containing protein tyrosine phosphatases by two backdoor cysteines. *Biochemistry* **48**, 1399-1409 (2009).
76 Denu, J. M. & Tanner, K. G. Specific and reversible inactivation of protein tyrosine phosphatases by hydrogen peroxide: evidence for a sulfenic acid intermediate and implications for redox regulation. *Biochemistry* **37**, 5633-5642 (1998).
77 Lee, C. *et al.* Redox regulation of OxyR requires specific disulfide bond formation involving a rapid kinetic reaction path. *Nat. Struct. Mol. Biol.* **11**, 1179-1185 (2004).
78 Lee, J. W., Soonsanga, S. & Helmann, J. D. A complex thiolate switch regulates the Bacillus subtilis organic peroxide sensor OhrR. *Proc. Natl. Acad. Sci. U.S.A.* **104**, 8743-8748 (2007).
79 Yazdanpanah, B. *et al.* Riboflavin kinase couples TNF receptor 1 to NADPH oxidase. *Nature* **460**, 1159-1163 (2009).
80 Godin-Heymann, N. *et al.* The T790M "gatekeeper" mutation in EGFR mediates resistance to low concentrations of an irreversible EGFR inhibitor. *Mol. Cancer Ther.* **7**, 874-879 (2008).
81 Giannoni, E., Buricchi, F., Raugei, G., Ramponi, G. & Chiarugi, P. Intracellular reactive oxygen species activate Src tyrosine kinase during cell adhesion and anchorage-dependent cell growth. *Mol. Cell Biol.* **25**, 6391-6403 (2005).
82 Tang, H., Hao, Q., Rutherford, S. A., Low, B. & Zhao, Z. J. Inactivation of SRC family tyrosine kinases by reactive oxygen species in vivo. *Journal of Biological Chemistry* **280**, 23918-23925 (2005).
83 Cunnick, J. M. *et al.* Role of tyrosine kinase activity of epidermal growth factor receptor in the lysophosphatidic acid-stimulated mitogen-activated protein kinase pathway. *Journal of Biological Chemistry* **273**, 14468-14475 (1998).
84 Kemble, D. J. & Sun, G. Direct and specific inactivation of protein tyrosine kinases in the Src and FGFR families by reversible cysteine oxidation. *Proc. Natl. Acad. Sci. U.S.A.* **106**, 5070-5075 (2009).
85 Jackson, P. M., Moody, C. J. & Shah, P. Preparation and Diels-Alter reactivity of thieno[2,3-c]-and thioeno[3,2-c]-pyran-3-one. Stale 2,30dimethylenethiophene derivatives: synthesis of benzothiophenes *J Chem Soc, Perkin Trans 1* **11**, 2909-2918 (1990).
86 Zhao, X. Z. *et al.* Biotinylated biphenyl ketone-containing 2,4-dioxobutanoic acids designed as HIV-1 integrase photoaffinity ligands. *Bioorg Med Chem* **14**, 7816-7825 (2006).
87 Lin, P. C. *et al.* Site-specific protein modification through Cu(I)-catalyzed 1,2,3-triazole formation and its implementation in protein microarray fabrication. *Angew Chem Int Ed Engl* **45**, 4286-4290 (2006).
88 Leonard, S. E., Reddie, K. G. & Carroll, K. S. Mining the thiol proteome for sulfenic acid modifications reveals new targets for oxidation in cells. *ACS Chem Biol* **4**, 783-799 (2009).
89 Paulsen, C. E. & Carroll, K. S. Chemical dissection of an essential redox switch in yeast. *Chem Biol* **16**, 217-225, (2009).
90 Klomsiri, C. *et al.* Use of dimedone-based chemical probes for sulfenic acid detection evaluation of conditions affecting probe incorporation into redox-sensitive proteins. *Methods Enzymol* **473**, 77-94 (2010).
91 Poole, L. B. *et al.* Fluorescent and affinity-based tools to detect cysteine sulfenic acid formation in proteins. *Bioconjug Chem* **18**, 2004-2017, (2007).

Chapter 5

Conclusions and future directions

5.1 Abstract

The data presented in the previous chapters provide the first direct evidence for the role of sulfenylation in regulating the function of proteins involved in vital eukaryotic signaling pathways and the design and development of a new probe for selective sulfenic acid detection. The present chapter summarizes these findings and the significance of this work. Moreover, we discuss future directions aimed at the discovery of additional novel targets of growth factor-derived hydrogen peroxide (H_2O_2), development of novel irreversible inhibitors for epidermal growth factor receptor (EGFR) and the continued investigation of redox regulation of protein tyrosine kinases (PTKs).

5.2 Conclusions: Elucidating the role of protein sulfenylation in eukaryotic signal transduction

H_2O_2 acts as a second messenger that can modulate intracellular signal transduction *via* chemoselective oxidation of cysteine residues in signaling proteins. Unfortunately, the protein targets of H_2O_2, as well as how oxidation influences protein activity has remained largely unknown. The overall goal of this thesis was to use chemical tools developed in our lab that are chemoselective for sulfenic acid to shed light on how protein sulfenylation can regulate activity within the context of cellular signaling. Mechanistic insights into signal-mediated H_2O_2 production, an overview of techniques used to detect

reactive oxygen species (ROS) and reversible cysteine oxidation, and diverse examples of how H_2O_2 can regulate protein function was provided in Chapter 1.

In Chapter 2, we used our first generation sulfenic acid probe, DAz-1, to uncover an essential role for sulfenic acid modification of Gpx3 in its communication of conditions of oxidative stress to the transcription factor Yap1 in *S. cerevisiae*. This study constituted the first direct evidence that cysteine oxidation to sulfenic acid in Gpx3 was essential for yeast to sense oxidative stress and, more broadly, shed light on the growing roles of sulfenic acid modifications in biology. From a chemical perspective, this study also highlighted the utility of our sulfenic acid probes to investigate redox signaling in living cells.

In addition to regulating signal transduction in healthy cells, ROS production and cysteine oxidation are also implicated in a number of pathologies including neurodegenerative disorders. In Chapter 3, we used our second generation sulfenic acid probe, DAz-2, which exhibits enhanced reactivity in comparison to DAz-1[1] to develop a method to globally profile protein sulfenylation in *S. cerevisiae*. We intended to use this methodology to investigate the correlation between mutant huntingtin (Ht) aggregation, ROS production, and cysteine oxidation using a yeast model of Huntington's disease (HD). Unfortunately, our methodology suffered from low sensitivity, likely due to low permeability of the yeast cell membrane, and irreproducibility and the study was ultimately discontinued.

Finally, in Chapter 4, we present the design and characterization of an alkyne-based sulfenic acid probe, DYn-2. DYn-2 is used to reveal, for the first time, dynamic changes in global protein sulfenylation in response to epidermal growth factor (EGF) signaling in

the human epidermoid carcinoma A431 cell line. We additionally identified three protein tyrosine phosphatases (PTPs) and EGFR as direct protein targets of H_2O_2 produced for EGF signaling. Moreover, we demonstrated that each of these enzymes exhibits differential sensitivities to oxidation and rationalized these sensitivities based on proximity to the H_2O_2 source. Lastly, we provided the first evidence that H_2O_2 can directly regulate receptor tyrosine kinase function. The results of this study shed new light on the molecular mechanisms underlying redox signaling pathways and have broad therapeutic implications.

5.3 Future directions in the exploration and exploitation of redox signaling

5.3.1 Proteomic identification and quantification of proteins oxidized in response to EGF signaling

The results in Chapter 4 demonstrate, for the first time in cells, that EGF signaling stimulates dynamic changes in global protein sulfenylation. These results, in combination with the recent publication of additional studies that demonstrate increased protein sulfenylation in response to peptide growth factors,[2,3] motivate a proteomics study to broadly identify protein targets of H_2O_2 produced for EGF signaling. Indeed, our sulfenic acid probe, DAz-2, was previously used to identify nearly 200 oxidized proteins in HeLa cells [1]. A limitation to current proteomics methodology, however, is that while a substantial number of proteins can be identified, no functional significance for oxidative modifications is provided. One approach to identify potentially significant protein targets of redox signaling is to quantify the extent of cysteine oxidation in response to different cellular conditions. For such studies, however, methods would be required that eliminate the contribution of fluctuation in protein expression to differences in protein oxidation such that relative differences could be revealed. Herein, the expectation is that

proteins that exhibit larger changes in cysteine oxidation after EGF stimulation are more likely to be significant targets of redox regulation. Towards this end, our lab has developed a ratiometric method that permits relative quantification of cysteine oxidation of a sample between two conditions [4]. This method, isotope-coded dimedone and 2-iododimedone (ICDID), utilizes deuterium-labeled dimedone (d6-dimedone) to label protein sulfenic acids and 2-iododimedone to label reduced protein thiols [4]. The resulting covalent adduct generated by each reaction is the same, differing in mass by 6 Da that can be readily detected by mass spectrometry and the relative amount of oxidized protein in a given sample can be quantified from the ratio of heavy/light isotype peak intensities. This relative quantification can then be used to compare the extent of protein oxidation between conditions. To apply this methodology more broadly to redox proteomics, our lab is in the process of generating d6-DYn-2 and 2-iodoDYn-2 that can be used in conjunction with alkyne-biotin reagents containing an acid-cleavable linker[5] to facilitate enrichment and enhanced recovery of modified proteins. Quantification of protein oxidation in response to EGF signaling will help to prioritize protein targets of signal-derived H_2O_2 for further biochemical characterization of redox regulation.

5.3.2 Development of irreversible redox-based inhibitors for EGFR

The findings in Chapter 4 mark the first demonstration that EGFR is susceptible to redox regulation, which has broad implications for therapeutic intervention. EGFR is mutated or amplified in a number of human cancers including breast[6] and lung[7] cancer, which has motivated the development of selective irreversible inhibitors that covalently modify Cys797 in this receptor tyrosine kinase (RTK) (**Figure 5.1a**). These inhibitors compete with ATP, which is present at millimolar concentrations in the cell, for binding to EGFR and thus high concentrations must be used to achieve desired pharmacological effects. Unfortunately, these inhibitors cannot discriminate between “cancerous” and “normal”

cells and their use is associated with numerous undesirable side effects [8]. Interestingly, overexpression of EGFR in breast cancer cell lines correlated with increased global protein sulfenylation [9]. We have demonstrated that EGFR Cys797 is susceptible to oxidation, which necessitates the consideration of the oxidation state of this residue in irreversible drug development. While the acrylamide warhead of irreversible EGFR kinase inhibitors reacts with the thiol form of Cys797, these inhibitors would not be expected to react with the sulfenic acid or disulfide oxoforms. In this way, oxidation of Cys797 might impact the efficacy of the irreversible EGFR kinase inhibitors, particularly in states of high stress as is associated with cancer [10,11]. Sulfenylation of Cys797 could be exploited, however, to develop redox-based inhibitors akin to probes recently developed for PTPs [12]. Towards this end, our lab is currently synthesizing derivatives of the irreversible inhibitors shown in **Figure 5.1a** that are equipped with a 1,3-cyclopentadione moiety for selective reaction with oxidized receptor (**Figure 5.1b**). These redox-based inhibitors will be examined for their ability to inhibit recombinant EGFR kinase activity subsequent to H_2O_2 treatment. Importantly, these redox-based inhibitors, if successful, would be expected to exhibit enhanced selectivity for cancer

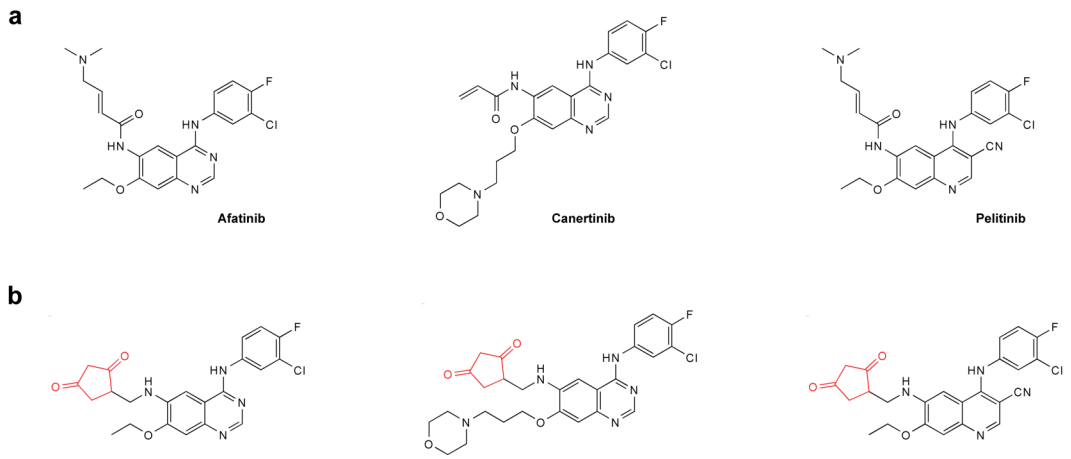

Figure 5.1. Structures of irreversible EGFR kinase inhibitors. a) Structures of acrylamide-based irreversible EGFR kinase inhibitors in clinical trials. b) Structures of redox-based irreversible EGFR kinase inhibitors. These inhibitors are based on the structures in (a), but incorporate a 1,3-cyclopentadione moiety (red) to facilitate reaction with the sulfenylated receptor.

cells due to their association with oxidative stress[10,11] and may therefore reduce the toxicity observed with acrylamide-based inhibitors.

5.3.3 Investigation of redox regulation of additional receptor and protein tyrosine kinases

Of the 96 known human protein tyrosine kinases (PTKs), 9 additional kinases, including Her2 and Her4, share a cysteine that structurally corresponds to EGFR Cys797 (**Figure 5.2**) [13]. The presence of a structurally homologous cysteine residue in these additional PTKs entertains the possibility that they may be similarly regulated by oxidation. Cys797 and its structural analogues serve as the N-terminal end of an alpha helix, deemed the N_{cap} position. Interestingly, cysteine is the most sparsely occurring N_{cap} residue in natural proteins, comprising less than 1% of all of these positions [14]. Interaction of a cysteine residue with the helical dipole in an N_{cap} context reduces the pKa of the thiol under physiological conditions, which would increase the reactivity of that residue [15]. Indeed, this N_{cap} effect has been attributed to the reactivity of the human peroxiredoxin I peroxidatic cysteine [16]. Therefore, localization of Cys797 and its structural analogues to the N_{cap} position may influence their reactivity making them more susceptible to redox regulation, though continued experiments are required to investigate oxidative modification of these PTKs. Interestingly, one of these PTKs, Btk, which is involved in the proliferation, development, differentiation, and survival of B-cells is also targeted by irreversible kinase inhibitors and thus, if redox regulated akin to EGFR, would have the same therapeutic implications.

Kinase										
BKL	E	Y	M	A	R	G	C	L	L	D
BMX	E	Y	I	S	N	G	C	L	L	N
BTK	E	Y	M	A	N	G	C	L	L	N
EGFR	Q	L	M	P	F	G	C	L	L	D
HER2	Q	L	M	P	Y	G	C	L	L	D
HER4	Q	L	M	P	H	G	C	L	L	E
ITK	E	F	M	E	H	G	C	L	S	D
JAK3	E	Y	L	P	S	G	C	L	R	D
TEC	E	F	M	E	R	G	C	L	L	N
TXK	E	F	M	E	N	G	C	L	L	N

Figure 5.2. Ten kinases unified by sequence alignment of cysteine in EGFR.

A second set of PTKs including Src, which interacts with EGFR, and FGFR1 have a cysteine residue in the glycine loop, a conserved structural motif in kinases that contributes to catalysis by interacting with the γ-phosphate of ATP. Interestingly, cellular studies indicate a role for cysteines in Src activity [17-19] and a recent study with purified Src implicated the glycine loop-residing cysteine as the site of redox regulation[20]. In addition, DTT was found to activate recombinant FGFR1, indicating that this class of RTK may be regulated differently than EGFR[20]. To date, however, neither Src nor FGFR1 have been confirmed as direct targets of signaling-derived H_2O_2 in cells and the cellular significance of their oxidation remains unknown. These combined observations open the door to the possibility of diverse mechanisms for redox regulation of key enzymes involved in eukaryotic signal transduction and underscore the extensive cross-talk that occurs between cysteine oxidation and protein phosphorylation.

5.4 Concluding remarks

Prior to the commencement of this work, the role of protein sulfenylation in eukaryotic redox signaling was highly speculative and had only been considered within the context of oxidant metabolism and oxidative stress responses. By utilizing the sulfenic acid-specific probes developed in the Carroll lab, we have provided the first direct demonstrations of functional roles for sulfenylation in regulating protein function in cells. Moreover, the work outlined in this thesis has uncovered EGFR as a novel target of H_2O_2 produced for growth factor signaling, which has broad implications for redox regulation of vital signaling pathways and provides new avenues for therapeutic intervention. Implementation of quantitative proteomics will expedite the discovery of additional novel protein targets of growth factor-mediated H_2O_2 that will expand upon our current understanding of the mechanisms through which sulfenylation regulates protein activity and cellular signaling in normal and diseased states.

5.5 References

1 Leonard, S. E., Reddie, K. G. & Carroll, K. S. Mining the thiol proteome for sulfenic acid modifications reveals new targets for oxidation in cells. *ACS Chem Biol* 4, 783-799 (2009).

2 Wani, R. *et al.* Isoform-specific regulation of Akt by PDGF-induced reactive oxygen species. *Proc Natl Acad Sci U S A* 108, 10550-10555 (2011).

3 Kaplan, N. *et al.* Localized cysteine sulfenic acid formation by vascular endothelial growth factor: role in endothelial cell migration and angiogenesis. *Free Radic Res* (2011).

4 Seo, Y. H. & Carroll, K. S. Quantification of Protein Sulfenic Acid Modifications Using Isotope-Coded Dimedone and Iododimedone. *Angew Chem Int Ed Engl* (2011).

5 Truong, T. H., Garcia, F. J., Seo, Y. H. & Carroll, K. S. Isotope-coded chemical reporter and acid-cleavable affinity reagents for monitoring protein sulfenic acids. *Bioorg Med Chem Lett* (2011).

6 Bhargava, R. *et al.* EGFR gene amplification in breast cancer: correlation with epidermal growth factor receptor mRNA and protein expression and HER-2 status and absence of EGFR-activating mutations. *Mod Pathol* 18, 1027-1033 (2005).

7 Yoshida, T., Zhang, G. & Haura, E. B. Targeting epidermal growth factor receptor: central signaling kinase in lung cancer. *Biochem Pharmacol* 80, 613-623 (2010).

8 Zhou, W. *et al.* Novel mutant-selective EGFR kinase inhibitors against EGFR T790M. *Nature* 462, 1070-1074 (2009).

9 Seo, Y. H. & Carroll, K. S. Profiling protein thiol oxidation in tumor cells using sulfenic acid-specific antibodies. *Proc Natl Acad Sci U S A* 106, 16163-16168 (2009).

10 Halliwell, B. Oxidative stress and cancer: have we moved forward? *Biochem J* 401, 1-11 (2007).

11 Klaunig, J. E. & Kamendulis, L. M. The role of oxidative stress in carcinogenesis. *Annu Rev Pharmacol Toxicol* 44, 239-267 (2004).

12 Leonard, S. E., Garcia, F. J., Goodsell, D. S. & Carroll, K. S. Redox-based probes for protein tyrosine phosphatases. *Angew Chem Int Ed Engl* 50, 4423-4427 (2011).

13 Singh, J., Petter, R. C. & Kluge, A. F. Targeted covalent drugs of the kinase family. *Curr Opin Chem Biol* 14, 475-480 (2010).

14 Penel, S., Hughes, E. & Doig, A. J. Side-chain structures in the first turn of the alpha-helix. *J Mol Biol* 287, 127-143 (1999).

15 Anderson, T. A. & Sauer, R. T. Role of an N(cap) residue in determining the stability and operator-binding affinity of Arc repressor. *Biophys Chem* 100, 341-350 (2003).

16 Woo, H. A. *et al.* Inactivation of peroxiredoxin I by phosphorylation allows localized H(2)O(2) accumulation for cell signaling. *Cell* 140, 517-528 (2010).

17 Giannoni, E., Buricchi, F., Raugei, G., Ramponi, G. & Chiarugi, P. Intracellular reactive oxygen species activate Src tyrosine kinase during cell adhesion and anchorage-dependent cell growth. *Mol Cell Biol* 25, 6391-6403 (2005).

18 Tang, H., Hao, Q., Rutherford, S. A., Low, B. & Zhao, Z. J. Inactivation of SRC family tyrosine kinases by reactive oxygen species in vivo. *J Biol Chem* 280, 23918-23925 (2005).

19 Cunnick, J. M. *et al.* Role of tyrosine kinase activity of epidermal growth factor receptor in the lysophosphatidic acid-stimulated mitogen-activated protein kinase pathway. *J Biol Chem* 273, 14468-14475 (1998).
20 Kemble, D. J. & Sun, G. Direct and specific inactivation of protein tyrosine kinases in the Src and FGFR families by reversible cysteine oxidation. *Proc Natl Acad Sci U S A* 106, 5070-5075 (2009).